Diffusion in the pore water of compacted crushed salt

GRS - 421

Gesellschaft für Anlagen-
und Reaktorsicherheit
(GRS) gGmbH

Diffusion in the pore water of compacted crushed salt

Judith Flügge
Sebastian Herr
Thomas Lauke
Artur Meleshyn
Rüdiger Miehe
André Rübel

July 2016

Remark:

This report was prepared unter the contract no. 02 E 10951 with the Federal Ministry for Economic Affairs and Energy (BMWi).

The work was conducted by the Gesellschaft für Anlagen- und Reaktorsicherheit (GRS) gGmbH.

The authors are responsible for the content of this report.

GRS - 421
ISBN 978-3-946607-03-8

Key words:

Compacted crushed salt, caesium, diffusion, diffusion experiment, nuclear waste disposal, pore water, salt, tracer

Abstract

Diffusion of dissolved radionuclides in the pore water of compacted crushed salt in the long-term is the most relevant process for the release of radionuclides from a dedicated repository for high-level waste in a salt formation as has been shown in latest safety assessments and research projects /BUH 16/.

So far, diffusion coefficients for free water have been applied for the diffusion in pore water in models for long-term safety assessments. This conservative assumption was used, because data on the diffusion coefficient of dissolved substances in crushed salt have been missing. Furthermore, the diffusion coefficient in the pore water was assumed to be constant and independent from the degree of compaction of the crushed salt. The work presented in this report was intended to contribute to fill this gap of knowledge about how the diffusion of radionuclides takes place in the compacted backfill of a repository in salt. For the first time, the pore diffusion coefficient as well as its dependence on the porosity of the crushed salt was determined experimentally by means of through-diffusion experiments using caesium as tracer.

The results achieved in this project suggest that the diffusion in compacted crushed salt is not fully comparable to that in a homogeneous, temporally stable porous medium like sand or clay. The results obtained from four diffusion experiments show a remarkably different behaviour and all yield unique concentration versus time plots which includes highly temporal variable tracer fluxes with even full interruptions of the flux for longer periods of time. This effect cannot be explained by assuming a tracer transport by diffusion in a temporarily invariant pore space and / or under temporally invariant experimental conditions. From our point of view, a restructuring of the pore space seems to lead to closed areas of pore water in the sample which may open up again after some time, leading to a variable pore space and hence variable diffusive fluxes.

No reduction of the pore diffusion coefficient could be observed down to a sample porosity of 2 %, and diffusion of caesium in the pore space of the compacted crushed salt occurs with the same diffusion coefficient as in free water. Therefore, the approach used in the long-term safety assessment so far, to apply the diffusion coefficient in free water remains valid. However, the temporal change of the pore space in the crushed salt might lead to a variation or reduction of the resulting diffusive tracer flux. To confirm this effect however, more experiments would be necessary.

Zusammenfassung

Die Ergebnissen neuerer Sicherheitsanalysen und Forschungsprojekte zeigen, dass die Diffusion gelöster Radionuklide im Porenwasser von kompaktiertem Salzgrus über große Zeiträume der wichtigste Ausbreitungspfad der Radionuklide aus einem Endlager für hochradioaktive Abfälle in einer Salzformation ist /BUH 16/.

Bis heute wurden in den Modellen zur Langzeitsicherheitsanalyse bei der Betrachtung der Diffusion im Porenwasser die Diffusionskoeffizienten entsprechend jenen im freien Wasser gewählt. Diese abdeckende Annahme wurde getroffen, weil bisher keine Daten für Diffusionskoeffizienten von gelösten Stoffen im Porenwasser von Salzgrus vorlagen. Weiterhin wurde bisher angenommen, dass der Porendiffusionskoeffizient unabhängig vom Kompaktionsgrad und somit von der Porosität des Salzgruses ist. Die in diesem Bericht präsentierten Arbeiten wurden durchgeführt, um die Wissenslücke über die Diffusion im Porenwasser von Salzgrus zu verringern. Zum ersten Mal wurde dabei der Diffusionskoeffizient von Cäsium im Porenwasser, sowie seine Abhängigkeit von der Porosität mit Hilfe von Diffusionsexperimenten bestimmt.

Die in diesem Projekt erzielten Ergebnisse deuten darauf hin, dass die Diffusion in kompaktiertem Salzgrus nicht vergleichbar abläuft zu jener in typischen porösen Medien wie Sand oder Tongestein. Die Ergebnisse von vier durchgeführten Diffusionsexperimenten zeigen ein deutlich unterschiedliches Verhalten und weisen alle deutlich unterschiedliche zeitliche Konzentrationsverläufe auf, was auf einen zeitlich variablen Fluss des Tracer schließen lässt. Dabei kommt es teilweise sogar zu einem völligen Erliegen des diffusiven Flusses durch die Probe. Dieser Effekt kann nicht mit einem zeitlich unveränderlichen Porenraum, bzw. zeitlich unveränderlichen experimentellen Randbedingungen erklärt werden. Eine mögliche plausible Erklärung ist die Restrukturierung des Porenraums in dem Probekörper zu abgeschlossenen Bereichen in der Probe, die sich dann nach einer Zeit unter Umständen wieder öffnen.

Es konnte in den Experimenten bis zu einer minimalen Porosität von 2 % keine Reduktion des Diffusionskoeffizienten gegenüber jenem im freien Wasser beobachtet werden. Somit bleibt der bisher angewendete Ansatz in den Modellen der Langzeitsicherheitsanalyse gültig, nämlich die Verwendung des Diffusionskoeffizienten in freiem Wasser. Es ist allerdings nicht auszuschließen, dass die zeitliche Veränderung des Porenraums zu einer Verringerung des diffusiven Schadstoffstroms führt. Für einen Beleg dieses Effekts wären jedoch weitere Experimente notwendig.

Table of contents

1 Introduction 1

2 Theoretical background of diffusion 5

3 State-of-the-art of science and technology 9

4 Methods 15

4.1 Gravimetric water content 15

4.2 Grain size analyses 15

4.3 Mineralogical analyses 16

4.4 Permeability 16

4.5 Grain density of the salt samples 17

4.6 Porosity and density of the salt samples 17

4.7 Density of the brines 18

4.8 Main and trace elements of the brines 18

4.9 Temperature in the laboratory room 20

5 Materials 21

5.1 Diffusion cells 21

5.2 Crushed salt 26

5.3 Salt brine 28

5.4 Tracers 31

6 Diffusion experiments 37

6.1 Orienting calculations 37

6.2 Sample preparation 39

6.3 Experiment execution 44

6.4 Uncertainty analysis 48

6.5 Results 51

6.6 Conclusions from the experiments 57

7 Integration of the results in a safety assessment code 63

7.1 Analysis of the influence of the diffusion coefficient 64

7.2 Analysis of the LOPOS code 67

8 Résumé 71

9 References 75

List of figures 81

List of tables 85

A. Construction design of the diffusion cells 87

1 Introduction

During the last four decades, the strategy in safety assessments for high-level radioactive waste repositories in salt formations has significantly changed. In the 1980s and 1990s, it was commonly assumed that a brine intrusion would take place during the early stages after repository closure, when the convergence of the openings has not yet reached the final state. In this case the advancing convergence in the salt formation would lead to the squeezing of brine out of the repository. The advective transport of brine, caused by the convergence, dominates the transport of contaminants in the safety assessments, thus they focused on the exact description of the contaminant transport by advection.

The concept of safety assessments for high-level waste repositories has changed to that effect, that the safe enclosure of the waste within the containment providing rock zone (CRZ) is to be proven /DBE 08/. This includes the proof of the integrity of the rock salt barrier and of the geotechnical barrier, preventing a brine intrusion into those parts of the repository, where the waste is to be disposed of. Newer safety analyses in the course of the preliminary safety assessment for Gorleben (VSG) and the project ISIBEL have shown, that in the reference case, with the proven integrity of the barriers, a contact of significant volumes of brine with the waste is generally to be expected only at such a point in time, when the convergence of the openings has already reached its final state /LAR 13/, /BUH 08/ and /BUH 16/. In this case, no flow of brines out of the repository by displacement due to convergence occurs. Consequently, no advective transport of radionuclides in the brine occurs either and diffusion is the only remaining transport process for dissolved radionuclides expected evolution of the repository system.

Even in less likely alternative evolutions of the repository system assuming the brine intrusion to take place due to a shaft failure, the influent brine will not necessarily fill all open volumes within the repository, but at most only single emplacement fields, that are located closest to the shaft. The relevance of advective transport of solution in the repository caused by the convergence of the formation decreases subsequently and the diffusion of dissolved radionuclides in the brine becomes more important with time /BUH 16/.

Very long time frames are regarded in long-term safety assessments. During such time frames, diffusive transport processes may dominate the radionuclide release from the

CRZ. After the failure of the containers, diffusive transport of dissolved radionuclides is possible as soon as a continuous pathway of at least partly saturated connected pore space exists in the backfill reaching from the waste through the drifts and the shaft up to the biosphere – even in a repository mine, where the openings are already closed with backfill and the convergence has reached its final state.

In models for long-term safety assessments, the diffusive transport is usually described by Fick's law. Accordingly, the transported amount of substance is directly proportional to the macroscopic diffusion coefficient, which is the averaged value of the free diffusion over a defined volume. This macroscopic diffusion coefficient takes into account that the transport path of diffusion is not linear but has to follow an enforced longer path around the grains of the material due to the warped pore space (tortuosity). In case of a repository in a salt formation, the porous medium, through which the diffusive transport takes place, is the crushed salt in its drifts and shafts, which is at least partially filled with solution.

So far, diffusion coefficients for the free water have been applied for the diffusion in pore water in models for long-term safety assessments. This assumption was used, because data on the diffusion coefficient of dissolved substances in crushed salt have been missing. Furthermore, the diffusion coefficient in the pore water was assumed to be constant and independent from the degree of compaction of the crushed salt. For other porous media like clays, it is well known that the pore diffusion coefficient is decreasing with porosity (e. g. /NAG 02/).

The dependence of the pore diffusion coefficient on the porosity of crushed salt was not investigated in detail before. In case the pore diffusion coefficient turns out to be dependent on the porosity, as has been proven for other porous media, it could be possible, that the pore diffusion coefficient is reduced by a factor of one to two orders of magnitude by compaction of the crushed salt, which would significantly lower potential releases of radionuclides from a radioactive waste repository in salt.

The diffusion coefficient of pollutants in the pore water of porous materials can be determined experimentally e. g. by means of through-diffusion experiments /SHA 91/, which is a well-tested procedure for different types of porous media. Main goal of the project presented in this report was to determine for the first time diffusion coefficients of pollutants in the pore water of compacted crushed salt with the aim to achieve a quantitatively less conservative description of the diffusion coefficient of radionuclides

through compacted crushed salt with differing porosities in a repository in a salt formation.

This report presents the results for the diffusion experiments performed. It first gives the theoretical background of diffusion and the state of the art of diffusion experiments in the chapters two and three. Chapters four and five than describe the methods and materials used in the diffusion experiments. Chapter six finally describes the execution and the results of the experiments. The final two chapters deal with consequences for safety assessment and conclusions.

2 Theoretical background of diffusion

Diffusion is the movement of molecules as a consequence of their thermal energy. If regarded on a molecular level, the movement of molecules in a fluid (liquid or gas) by their thermal energy is described by Einstein's theory of Brownian movement. If a concentration gradient of different types of molecules exists in a fluid, this movement results in a reduction of the concentration gradient until the fluid is perfectly mixed. Although the thermal movement of the molecules continues after that point in time, the net flux of molecules is zero /JOS 60/.

The net flux of transported molecules can be described by the phenomenological Fick's law of diffusion. According to that, the flux per surface area j is directly proportional to the gradient of the concentration c. The proportionality factor D is called diffusion coefficient and hast the unit m^2/s. The resulting equation is called Fick's first law:

$$j = -D \cdot \nabla c \tag{2.1}$$

Due to the nature of the diffusion as thermal Brownian motion, the diffusion coefficient is depending on the temperature, the properties of the fluid and the diffusing molecule. The diffusion coefficients for different chemical species are generally experimentally determined for free water and the according diffusion coefficient is labelled D_0 in the following. At 25 °C most species have a diffusion coefficient in free water in the order of magnitude of 10^{-9} m^2/s.

In a porous medium, diffusion of contaminants dissolved in the pore water actually takes place only in the pore water itself, not in the solid matter. Therefore, the net diffusive flux in a porous medium is reduced in comparison to the one in free water to the diffusion-accessible porosity n_{diff}. In many materials it is observed that the diffusion-accessible porosity is smaller than the total porosity n_0 of the porous medium, which denotes the fraction of the pore water volume in the total volume of the rock /PEA 99/. An example for the reduction of diffusion-accessible porosity compared to the total porosity is the well-known anion exclusion effect for the diffusion of anions in the pore water of clay-rich media. In the case of clays, this is due to the interaction of the negatively charged clay surface with the anions, which are consequently repelled from the surface and reside preferably in the central part of the pores. Hence, the Fick's first law in a porous media therefore can be written as

$$j = -n_{diff} D_0 \nabla c \,. \tag{2.2}$$

An additional effect is the following: The diffusing contaminants in a porous medium are typically not able to propagate straightforward through the medium due to the geometry of the pore space. This effect is usually dependent on the porosity /BOV 01/, /LOO 15/. Hence, the diffusion coefficient in the pore water which is called pore diffusion coefficient D_p is further reduced by a geometrical factor G compared to that for free water D_0:

$$D_P = G \cdot D_0 \,. \tag{2.3}$$

The geometrical factor, which is depending on the diffusing contaminant, takes two effects into account which are often mentioned in the literature; the so called tortuosity and the constrictivity /GRA 98/. The geometry factor is always smaller than unity and was e.g. determined to be about $6 \cdot 10^{-3}$ for Helium in the Opalinus Clay /RUE 02/. Typically, the geometry factor is not explicitly specified, but the pore diffusion coefficient is used instead.

To use Fick's first law in its form given in equation 2.1, an effective diffusion coefficient is often defined taking into account all effects mentioned above related to the diffusion in a porous medium:

$$D_{eff} = n_{diff} \cdot D_p \,. \tag{2.4}$$

A retardation of dissolved contaminants may occur by sorption processes as a consequence of their interaction with the rock matrix, e.g. surface complexation or ion exchange. Different models exist to describe sorption processes. These models either describe the sorption in a phenomenological way or they try to depict the sorption in a mechanistic way. Isotherms are a phenomenological way to describe the sorption. The so called Henry isotherm or equilibrium sorption model assumes a linear relationship between the concentration of the sorbed and the dissolved contaminants. The quotient of both concentrations is called distribution coefficient or for short K_d-value in this model and the retardation factor R_f is determined by

$$R_f = 1 + \frac{1-n}{n} \rho K_d \,, \tag{2.5}$$

where n denotes the porosity and ρ the bulk density of the rock. R_f characterises the retardation effect of the sorption on the radionuclide transport. The so called apparent diffusion coefficient D_a finally includes the retardation factor

$$D_a = \frac{D_{eff}}{R_f} \tag{2.6}$$

and this is the type of diffusion coefficient usually determined in laboratory diffusion experiments in rock and soil samples. For non-sorbing contaminants, the apparent diffusion coefficient is equal to the effective diffusion coefficient.

As discussed above, the diffusive flux is inevitably reduced proportionally to the porosity of the rock. This effect is expected for any type of rock. Further reduction might apply from the pore structure or an interaction of the contaminants with the rock matrix. To separate these effects, a rock specific coefficient α is defined in the following by

$$\alpha = \frac{D_a}{n_0 \cdot D_0}. \tag{2.7}$$

Accordingly, α is less or equal one and gives the reduction of the diffusive flux by rock specific effects. For α = 1, the diffusion is found to occur as expected with negligible influence on the diffusion process by rock-contaminant interaction or particular properties of the pore space.

3 State-of-the-art of science and technology

The way how to determine diffusion coefficients can be directly derived from Fick's first law. The application of a concentration gradient results in a diffusive flux. By measuring concentration gradients and mass fluxes, the apparent diffusion coefficient can be calculated if an adequate experimental setup is used. The two most common diffusion experiment setups are the so called through-diffusion and the in-diffusion experiments /SHA 91/. Through-diffusion experiments regard the diffusion of a substance through a porous medium and record the mass flux of the regarded substance at the sink. In-diffusion experiments regard the diffusion into the medium and record the decrease of the concentration at the source.

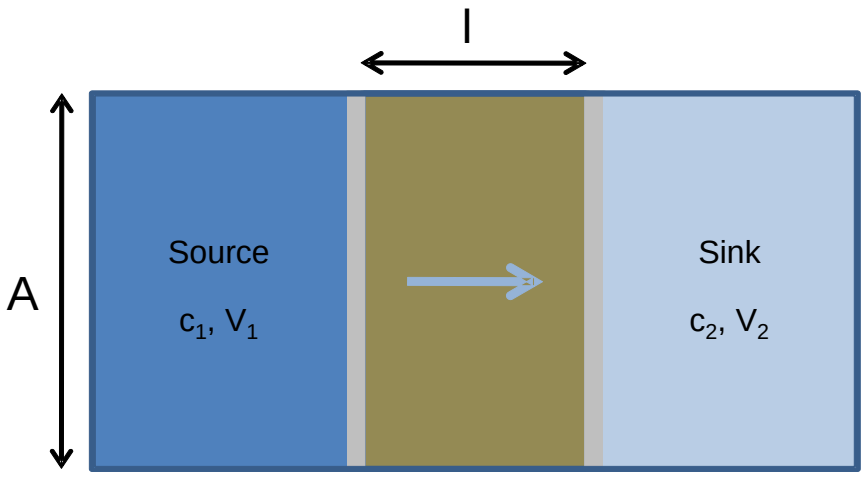

Fig. 3.1 Schematic illustration of a through-diffusion experiment

A schematic illustration of such a through-diffusion experiment is shown in figure 3.1. A sample of a porous medium is placed within a diffusion cell between two reservoirs of fluid. The source reservoir is containing a fluid with a tracer substance of an initial concentration c_1. The initial concentration c_0 of the tracer in the sample is zero. The tracer concentration in the sink reservoir c_2 is also initially zero. The concentrations in the sample and in the sink reservoir are evolving with time due to the tracer flux through the sample. Different types of through-diffusion experiment setups are used. In the dynamic setup, the concentration in the source and the sink reservoirs are allowed to change with time. In the static setup, the tracer concentration c_1 in the source reservoir is kept at a constant level. This is guaranteed by pumping and circulating the fluid in the source reservoir from a larger reservoir. The tracer concentration in the sink reservoir c_2 is kept at zero by constantly replacing and collecting the fluid.

As a result of the concentration gradient between both reservoirs, a diffusive flux is evolving with time. Equations to calculate the concentration profile in the sample and the diffusive flux into the sink reservoir are given in the literature for the static as well as for the dynamic setup (e.g. /CRA 79/). The solution for the concentration $c(x,t)$ in the sample at time t and position x is given for the static setup by:

$$c(x,t) = c_1 - \frac{x}{l}c_1 + \frac{2}{\pi}\sum_{n=1}^{\infty} -\frac{c_1}{n}\sin\frac{n\pi x}{l}\exp\frac{-D_a n^2\pi^2 t}{l^2}, \tag{3.1}$$

where l denotes the length of the sample. For long times, this equation is converging against the linear concentration profile of the steady-state:

$$c(x) = c_1 - \frac{x}{l}c_1 . \tag{3.2}$$

The time dependent tracer flux per second q at the sink boundary of the sample can be calculated using the following analytical solution:

$$q(t) = \frac{D_a c_1}{l} + \frac{2D_a c_1}{l}\sum_{n=1}^{\infty}(-1)^n \exp\left(\frac{-D_a n^2\pi^2 t}{l^2}\right). \tag{3.3}$$

For $t \to \infty$ the flux is converging against

$$q = \frac{D_a c_1}{l} . \tag{3.4}$$

For the dynamic setup the situation is different. In case the concentrations in the sink and the source reservoirs are not influenced by external conditions during the experiment, the steady-state conditions finally result in an equal mean concentration in both reservoirs and in the pore water and the diffusive flux is zero. Therefore, the diffusion coefficient in this case can only be determined during the pre-steady-state phase by fitting modelling results to the experimental results. In the static case, the diffusion coefficients can be directly determined from the flux to the sink reservoir in the stead state according to equation 3.4.

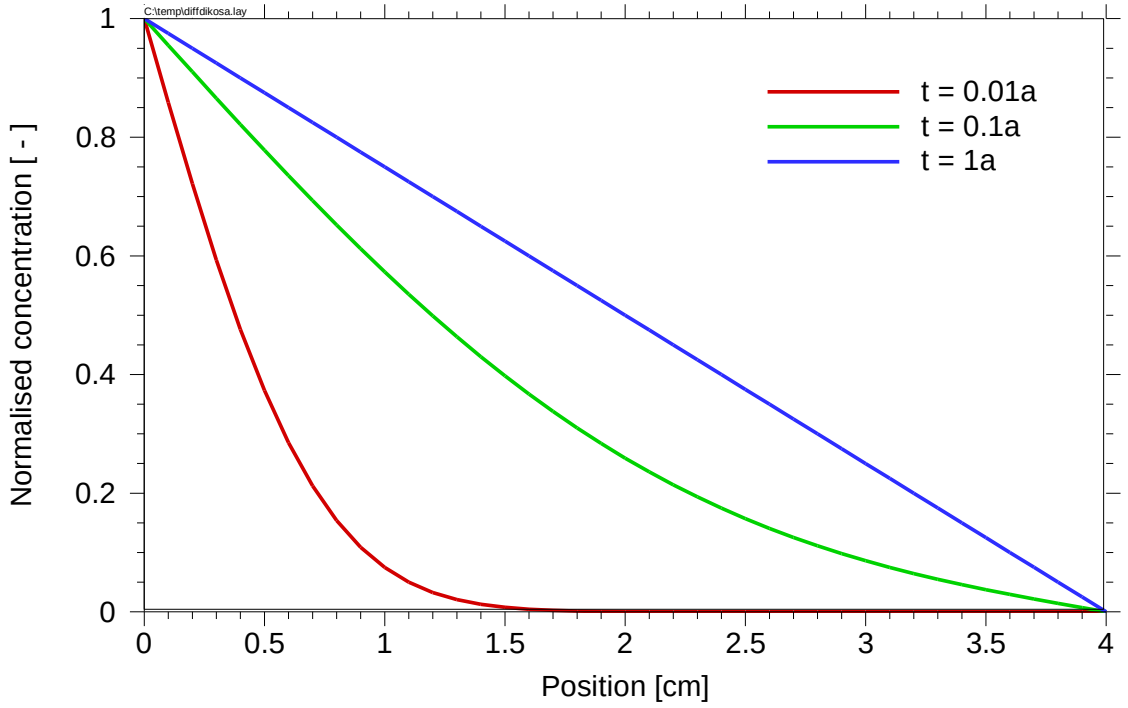

Fig. 3.2 Normalised concentration in a sample of 4 cm length for different times of a through-diffusion experiment ($D_a = 5 \cdot 10^{-11}$ m^2/s)

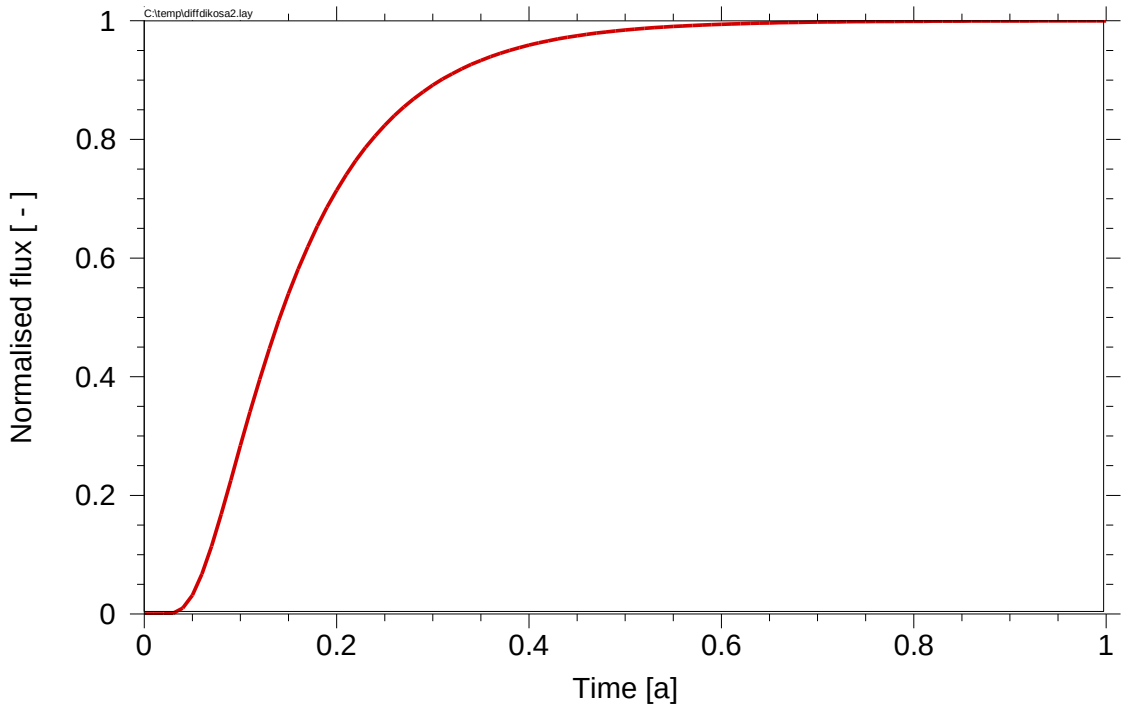

Fig. 3.3 Normalised flux out of a sample of 4 cm length of a through-diffusion experiment ($D_a = 5 \cdot 10^{-11}$ m^2/s)

To illustrate equations 3.1 to 3.4, an example for the concentration profile in the sample and the tracer flux from the sample into the sink reservoir of a through-diffusion experiment is shown in the Figures 3.2 and 3.3. A sample length of 4 cm and a diffusion coefficient of $D_a = 5 \cdot 10^{-11}$ m^2/s is regarded in this example. The plotted concentration is normalised by the concentration of the solution in the source reservoir, while the flux into the sink reservoir is normalised by the flux at equilibrium as given in equation 3.4. It can be seen how the tracer propagates into the sample. After 0.01 years, the concentration reaches about 1.5 cm into the sample. The tracer front has not reached the end of the sample, yet. Consequently, the flux from the sample is zero. After 0.1 years, the tracer has already reached the end of the sample and the flux from the sample is about 30 % of the steady-state value. After one year, the experiment is in steady-state. The tracer flux from the sample is constant and the concentration profile in the sample is linear. According to Figure 3.3, the flux from the sample has reached 99 % of the steady-state flux after 200 days. This is regarded as the minimum experimental duration of the experiment for the assumed boundary conditions.

As noted before, the advantage of the method of static through-diffusion experiments is that after reaching the steady-state of the experiment, the diffusion flux can be determined by just measuring concentrations in solution, which is usually quite easy to achieve. No additional modelling is needed. Additionally, the diffusion coefficient can be measured repeatedly by continuing the experiment after reaching the steady-state phase. This results in a reduction of the experimental error. The drawback of this method is that the time needed to reach steady-state can be very long depending on the diffusion coefficient and even exceed feasible periods for experiments by far, if sorbing tracers are used. In this case, dynamic methods like the in-diffusion experiments have to be used. Dynamic experiments can only be evaluated by fitting modelling results to the experimental results. In-diffusion experiments additionally require the measurement of the concentration profile in the rock. A much higher experimental and analytical effort is needed in this case and the experimental error might be larger.

Pre-existing knowledge on diffusion experiments is quite common, especially in the context of radioactive waste disposal. Through-diffusion experiments are an established method for measuring diffusion coefficients in porous rocks, like clay rock, e.g. /LOO 03/, /ZHA 04/. Some experiments have also been conducted in granitic rocks of very low porosity, e.g. /PAR 09/. In-diffusion techniques are less common because of their higher experimental effort, but they are preferable for sorbing tracers e.g. /LOO 05/, /CHU 14/. Care has to be taken in both types of diffusion experiments of the

boundary conditions at the reservoir-sample interfaces, especially if filters are used in the experiment which are often affecting the experimental results e.g. /ALD 14/, /GLA 15/.

For crushed salt, no sorption of the tracer was expected, so it was decided to start the experimental program with through-diffusion experiments. However, no pre-existing knowledge exists on through-diffusion experiments using samples of intact rock salt or compacted crushed salt. In comparison to the studies on clay rock or granitic rock mentioned before, this introduces two major challenges to be handled: The use of a sample material which is soluble in water and the resulting need for the use of saturated solutions, which are usually difficult to handle in the experiment and during measurement. Therefore, to carry out through-diffusion experiments with samples of compacted crushed salt, the existing methods have to be adapted, and new strategies have to be developed.

4 Methods

Analytical methods for the determination of necessary data to characterize the crushed salt samples, brine solutions, tracers, and boundary conditions of the performed experiments, are described in this chapter. This comprises the generic description of analytical methods for lithological, mineralogical, chemical, physicochemical and physical parameters.

4.1 Gravimetric water content

The gravimetric water content of the crushed salt was determined via oven drying according to DIN 18121-1 /DIN 98/. Therefore, crushed salt was placed in a muffle furnace (BINDER, APT. Line ED(E2)) and dried at 110 °C until constant weight is reached according to the instructions. Usually, 2 to 3 kg of the crushed salt was left in the muffle furnace until the start of the experiments to prevent any hygroscopic water absorption at contact with the atmosphere.

The gravimetric water content is calculated by

$$w = \frac{m_w}{m_d} \cdot 100, \tag{4.1}$$

where w is the gravimetric water content [%], m_w the mass of the water [kg] and m_d the mass of the dry sample [kg].

4.2 Grain size analyses

The crushed salt was analysed for its grain size via granulometric sieve analyses according to DIN 18123 /DIN 83/. Representative samples (chapter 6.2) were used. It was decided not to wash the samples before analysis to avoid salt dissolution. Approximately 1.5 kg of crushed salt was used for each grain size analysis. The crushed salt samples were placed in a sieve stack with eight sieves with the mesh sizes 0.063 mm, 0.125 mm, 0.25 mm, 0.5 mm, 1 mm, 2 mm, 4 mm, and 8 mm. The sieve stack was placed on a shaking device (Retsch AS200 control ‘g’) for 30 minutes. The single sieves were weighed using a METTLER PM30000-K scale. Results were plotted on a logarithmic scale depicting the through fraction of each sieve (chapter 5.2).

4.3 Mineralogical analyses

The crushed salt was analysed by X-ray diffraction for its mineralogical composition. This was done with the X' Pert MPD PRO by PANalytical which is equipped with an X-ray tube with molybdenum or copper anode. The primary ray has a characteristic wavelength K of 0.71 A° for molybdenium, and 1.54 A° for copper. The x-radiation passes a monochromator and a collimator. A monocrystal is placed and fine adjusted in the primary ray. A detector records the position and intensity of each reflex. The X' Pert MPD/MRD diffractometer runs as a closed system with integrated sample change. For evaluation of the resulting diffractograms, the software X'Pert HighScore Plus by PANalytical with the PANalytical ICSD Database (Inorganic Crystal Structure Database) from 2009 was used.

4.4 Permeability

The permeability of the crushed and compacted salt samples was determined after saturation of the samples with saturated brine directly in the diffusion cells. Therefore the diffusion cells with the compacted samples were connected with tubes to a storage reservoir with saturated brine. At each side of the diffusion cell, one of the two connectors was closed using a stainless steel blind plug. The diffusion cell with the compacted crushed salt sample was flushed with saturated brine by applying a slight excess pressure of nitrogen of ca. 0.5 bar to the reservoir container, resulting in a flow of brine through the sample from one side to the other. The collected brine at the outflow of the diffusion cell was weighed using a scale (METTLER PM6100 by METTLER TOLEDO). The permeability was calculated via

$$K = \frac{Q\,\eta\,l}{A\,p}, \tag{4.2}$$

where K is the permeability [m^2], Q the flow rate [$m^3\ s^{-1}$], η the dynamic viscosity [Pas], l the length of the sample [m], A the cross section area of the sample [m^2] and p the excess pressure [Pa] applied to the brine storage reservoir.

4.5 Grain density of the salt samples

The grain density of the salt samples was determined with the pycnometer method according to DIN 66137-2 /DIN 04/. The measuring principle is based on the displacement of gas in a pycnometer container. The empty pycnometer and the pycnometer, filled entirely with a defined gas, are weighed. After cleaning and drying the container, the object of investigation is added to the same container, the container is filled entirely with gas and then weighed again. The grain density is calculated via

$$\rho_0 = \frac{m_2 - m_0}{(m_1 - m_0) - (m_3 - m_2)} \cdot \rho_s , \tag{4.3}$$

where ρ_0 the grain density of the salt [kg m^{-3}], m_0.the mass of the empty pycnometer container [kg m^{-3}], m_1.the mass of the pycnometer container filled with solution [kg m^{-3}], m_2 the mass of the pycnometer container with the object of investigation [kg m^{-3}], m_3 the mass of the pycnometer container with the object of investigation filled with solution [kg m^{-3}], and where ρ_s the density of the solution [kg m^{-3}].

4.6 Porosity and density of the salt samples

The porosity of the compacted crushed salt sample was determined by means of geometric calculation. The porosity is

$$n = 1 - \frac{\rho}{\rho_0} , \tag{4.4}$$

where n is the porosity [-], ρ the bulk density of the sample [kg m^{-3}] and ρ_0 the grain density of the salt [kg m^{-3}].

The bulk density of the sample ρ is calculated by

$$\rho = \frac{m}{V} , \tag{4.5}$$

where m is the mass of salt used to prepare the compacted salt sample [kg] and V the volume of the compacted crushed salt [m^3].

The uncertainty of the calculated sample porosity is quite large due the measurement uncertainty of the sample properties. While the mass of the sample is measured before compaction with the high accuracy of the scales, the sample length has to be measured after compaction which results in a significant uncertainty. The measurement of the sample length is uncertain by at least 0.05 mm because of the rough and bent sample surfaces resulting from the imprint of the surfaces of the sample holder during the compaction process. The grain density of the sample was determined to be 2.182 g/cm³ from the mean value from seven measurements with an uncertainty of 0.002 g/cm³. The uncertainty of the porosity resulting from the error of the given sample parameters is calculated from

$$\Delta n = \frac{\partial n}{\partial m}\Delta m + \frac{\partial n}{\partial \rho_0}\Delta \rho_0 + \frac{\partial n}{\partial L}\Delta L = \frac{1}{AL\rho_0}\Delta m + \frac{m}{AL}\frac{1}{\rho_0^2}\Delta \rho_0 + \frac{m}{A\rho_0}\frac{1}{L^2}\Delta L\,, \quad (4.6)$$

where A is the sample surface area. An uncertainty of the porosity of 1.3 % is calculated for typical values for the mass, surface and length of the sample.

4.7 Density of the brines

The density of the brines was determined using a density oscillator by Anton Paar (Density Meter DMA 5000M). The density oscillator measures the eigenfrequency of a flexural resonator filled with the regarded sample. The samples were injected to the device using nozzles by Braun (Inject-F, 1 ml). The density of the sample is calculated and displayed automatically by the oscillator.

4.8 Main and trace elements of the brines

Chemical analyses of the saturated brines are challenging due to their high salt concentration. Different dilutions of the samples were necessary to be able to measure main as well as trace elements. For chemical analyses, inductively coupled plasma optical emission spectrometry (ICP-OES), inductively coupled plasma mass spectrometry (ICP-MS) and potentiometric titration were used.

4.8.1 ICP

Inductively coupled plasma optical emission spectrometry (ICP-OES) was used for the quantitative and qualitative determination of principal elements and element traces. The utilised ICP-OES spectrometer IRIS Intrepid II XUV is equipped with a low-noise CID detector, features a radial or plasma-duo view, a 2000 W HF generator at 27.12 MHz and covers a wavelength range of 130 – 1050 nm. The ICP-OES was used to measure sodium (dilution 1:31.5), potassium, magnesium and calcium (dilution 1:2,500), and sulphur (dilution 1:2,500; the corresponding sulphate concentration is calculated automatically by the ICP-OES' software).

Inductively coupled plasma mass spectrometry (ICP-MS) was used for the quantitative and qualitative determination of traces and ultra-traces. The available ICP-MS spectrometer Thermo X Series has an integrated 1600 W "solid state" quartz-controlled 27 MHz ICP generator, works with the plasma screen plus technique, an "off-axis" high performance quadrupole with abundance sensitivity and peak form mass filter and the CCT technique. The mass range is 2 – 255 AMU.

ICP-MS was used to measure the concentrations of the tracers iodide and caesium (chapter 5.4). The dilution of the samples varied between 1:200 and 1:200,000. The minimum dilution of 1:200 is necessary to meet the acceptable limit of the measuring system regarding the chlorine concentration of the brine. The diffusion experiments were designed in a way that at the minimum dilution factor, the expected caesium concentrations in the sink reservoir are in the optimum measuring range of the ICP.

4.8.2 Potentiometric titration

The potentiometric titration was performed with a titration device Titrando 857. It is equipped with a sample exchanger, a control and data unit, an automatic electrode identification for the ion selective electrodes. The potentiometric titration was used here to quantitatively determine the anions chloride and bromide in solution. Measurements were conducted without a prior dilution of the samples.

4.9 Temperature in the laboratory room

The temperature is a crucial aspect for running diffusion experiments with saturated brines and salt samples. An increasing temperature leads to an increasing solubility of salt, which has to be avoided in order not to alter the compacted salt samples. On the other hand, a decreasing temperature could result in the precipitation of salt, as well leading to an alteration of the compacted crushed salt sample. In the worst case, precipitation of salt crystals could cause clogging of tubings and fittings leading to the abortion of the experiment.

In order to run the experiments under constant temperature conditions, the temperature in the laboratory room, where the diffusion experiments were run, was controlled by air-condition and monitored. This was done using a portable temperature measuring instrument ALMEMO 2290-8 by Ahlborn. The constant recording and evaluation of the temperature data was performed using the AMR Win Control 6 software.

5 Materials

Employed materials are the diffusion cells, the crushed salt used to prepare the compacted crushed salt samples, the salt brine and the applied tracers. These materials are described in the following.

5.1 Diffusion cells

The general design and setup of the diffusion experiments was already tested and applied during the project *Fe-Bentonite* on clay samples /HER 11/. According to the requirements of the experiments in this project, such as the different grain size of the infill material and the different targeted porosities, the diffusion cells built and used in the previous project could not be reused, but new diffusion cells had to be designed and constructed. The company *InfraServ Wiesbaden Technik GmbH & Co.KG* manufactured five diffusion cells as shown in figure 5.1. The original technical drawings provided by InfraServ are shown in Appendix A.

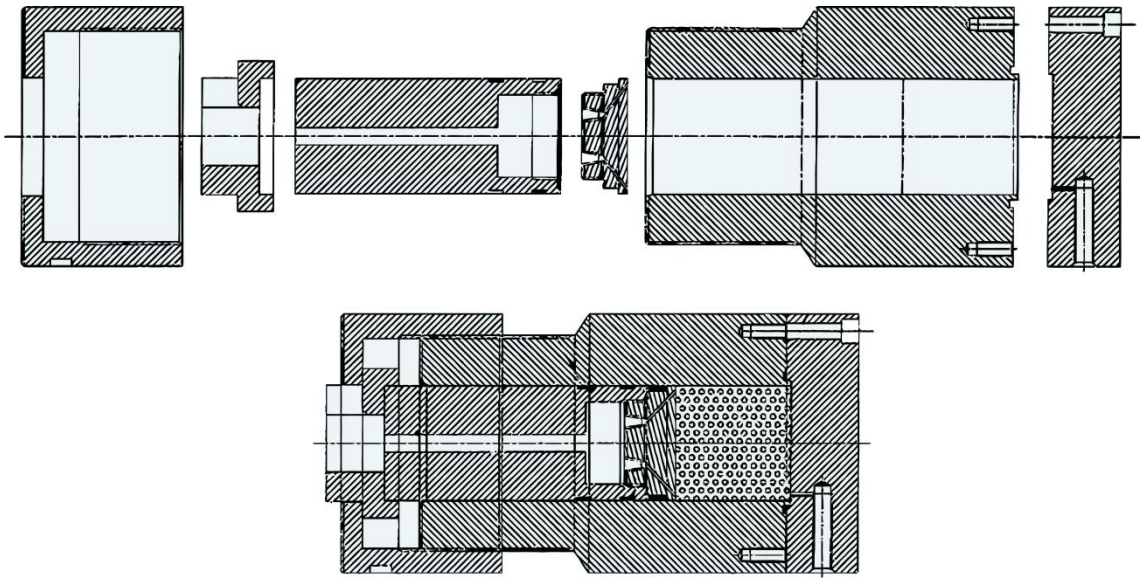

Fig. 5.1 Construction design of the diffusion cells: General assembly drawing and exploded view, after /INF 11/

In the following, the decisions for dimensioning and material selection of the cell are described. The sample diameter and therefore the inner diameter of the cells have to be chosen according to the grain size of the respective porous media. The Landesumweltamt Nordrhein-Westfalen /LUA 00/ recommends that the maximum grain size of a porous medium used for column experiments should not exceed the one-fifth of the in-

ner diameter of the column. This recommendation is targeted at column experiments, where a homogeneous advective flow is a prerequisite for representative experimental results. Here, the advective flow is to be prevented a priori. A homogenous distribution of the grains in the cells can be ensured by setting the inner diameter of the cells to the decuple of the largest grain /KRO 09/. To be able to relate the results of the diffusion experiments to the experiences gained within the *REPOPERM Phase 1* /KRO 09/ and *DEBORA* /ROT 99/ projects, it was intended to use a grain size range of 0.06 to 8 mm. Therefore the inner diameter of the cells was set to 8 cm.

The sample length is one important boundary condition of the diffusion experiments. On the one hand it has to be large enough to ensure the development of a representative pore network. On the other hand, the length has to be small enough to reduce the required time for the diffusion experiments to a reasonable extent. Preliminary calculations concerning the required time for the diffusion experiments revealed that a reduction of the sample length by half leads to a reduction the experiment duration by a factor of four. This is due to the fact that the distance of the tracer travelled through the sample by diffusion is proportional to the square of the sample length. Valkiainen et al. /VAL 96/ studied the effect of length in through-diffusion experiments on Rapakivi granite. They state that the effect of length on the results of the diffusion experiment shows that the connectivity of the pores decreases with decreasing sample length. The decrease as reflected in the diffusion coefficient was only minor and for their purpose, a sample length of 2 cm was regarded as sufficient. Other authors performed diffusion experiments on different granites with samples of length between 0.5 cm and 3 cm (/HU 08/, /TAC 15/, /HAR 96/, /SKA 83/).

Another crucial aspect in choosing the proper sample length is the required initial inner volume of the cell, i. e. the initial sample length before compaction. Depending on the targeted porosity of the compacted salt sample, the initial filling height of the cell with the loose crushed salt can be calculated assuming an initial porosity of the loose material of approx. 40 %. Experiences with compaction of porous media in diffusion cells at GRS show that the length of the cell has to be twice the length of the desired sample length to reach the required compaction of the sample.

During compaction of the samples, the pressure is applied to the sample from one side. This may lead to an inhomogeneous grain distribution and compaction along the direction of the sample compaction. We have not investigated the dependence of the homogeneity of the sample on the sample length, but visual inspections of compacted

crushed salt samples suggested that minimizing the sample length leads to an increase of the homogeneity of the sample.

Taking all above arguments into account and balancing between (i) the required homogeneity of the sample and the representative pore network within it and (ii) the resulting experimental time, a sample length of 4 cm was chosen for the diffusion experiments.

In the course of the project *Fe-Bentonite* /HER 11/ diffusion experiments were conducted using 90 % saturated salt brine. For these experiments, the inner diameter of tubing and fittings was set to 1/8". To avoid clogging of the tubes and connectors due to precipitation of salt while working with saturated salt brine, the inner diameter of the tubings was set to 1/4" where possible. Those tubings which could not be changed to the inner diameter of 1/4" were those within the peristaltic pump (cf. experimental execution in chapter 6). These had an inner diameter of 1/16". Also, the diameters of some of the inner boreholes of the diffusion cell were initially set to 1/8", which proved to be insufficient during first diffusion experiments. The small diameters of these boreholes were weak points of the construction, where only small salt crystals sometimes led to a complete clogging of the flow path. Thus, it was decided to widen the diameter of the inner boreholes of Pos. 5 and Pos. 10 (figure A.1) to 6 mm during the project. Simultaneously, connecting threads were widened to 1/4" and the milled surface of the flange and the connection plunger (Pos. 5 in figure A.1) were deepened to 2 mm.

The diffusion cells are constructed in such a way, that the entire sample preparation as well as the experiment itself can be carried out using them. This means, they are robust enough to withstand the compaction pressure. The loose salt sample is filled into the void volume constituted by the flange (Pos. 1 in figure A.1) and the cover flange (bottom panel, Pos. 10 in figure A.1). For some experiments, a spacer was placed at the bottom of the diffusion cell during compaction. This spacer has a thickness of 0.5 cm and is made of Teflon. The sample is compacted in the diffusion cell by applying pressure to the main plunger (Pos. 2 and Pos. 10 in figure A.1).

The main parts of the cell including its body were manufactured from titanium to be corrosion resistant against the saturated brines, to withstand the high pressures during compaction and to have an acceptable weight to be handled. Accessory components of the diffusion cells are different rings (Pos. 6 to Pos. 9 in figure A.1): Two guide rings (Pos. 6) made of fine cotton fabric, one lip ring (Pos. 7) made of 90P (Polyurethan), and two O-rings (Pos. 8 and Pos. 9) made of Nitrile Butadiene Rubber. Screw connec-

tions between the diffusion cell and connected tubes are made of titanium, while connectors and reducing connectors and made of Teflon. During assembly of the cells, threads are lubricated with copper paste. Tubing used in the peristaltic pump (chapter 6) are made of Tygon®, while all other tubes are made of Polyvinyl chloride.

Fig. 5.2 Photos of the different parts of the diffusion cell
Left row from top to bottom: top flange, body, sleeve nut
Right row from top to bottom: plunger, centering ring

The cells that have been constructed according to these requirements are shown in figure 5.1 as technical drawing and in figure 5.2, 5.3 and 5.4 as pictures of the individual parts. To withstand the load during compaction of the samples, the cell has a wall thickness of up to 5 cm. The length of the assembled cell is about 37 cm and the total weight is around 35 kg.

Fig. 5.3 Detail view of the sleeve nut

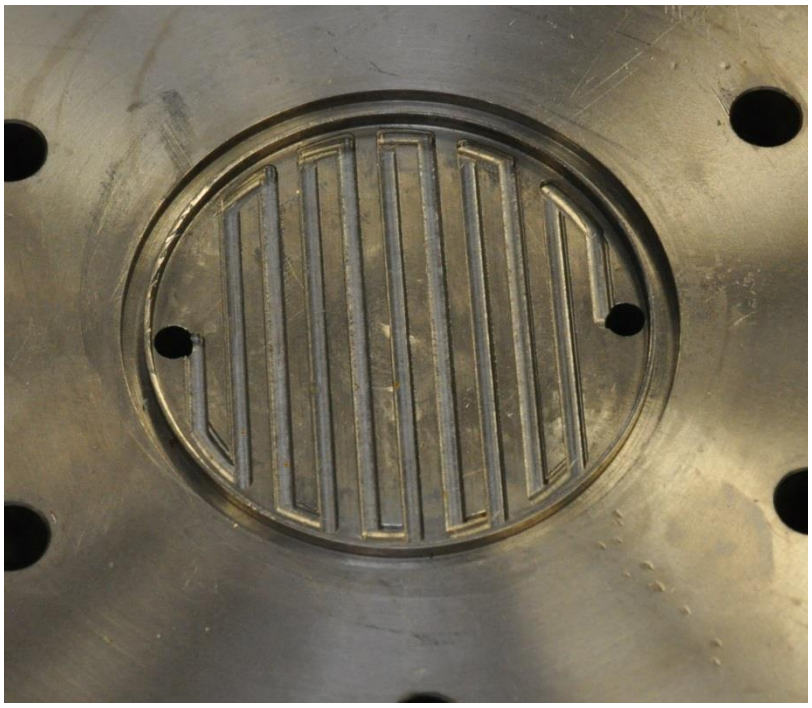

Fig. 5.4 Detail view of milled surface in the top flange

5.2 Crushed salt

Former projects investigated different aspects of crushed salt, including its suitability as a sealing material for borehole seals in repositories for high-level waste (*DEBORA* project /ROT 99/) and the relation between porosity and permeability (*REPOPERM Phase 1* project /KRO 09/). The investigated crushed salt used in the projects *DEBORA* and *REPOPERM Phase 1* was extracted from the former Asse salt mine and is referred to as Asse salt in the following. It is classified as the Hauptsalz of the Stassfurt-Folge (z2HS).

For the diffusion experiments discussed here, crushed salt from the Hauptsalz of the Stassfurt-Folge from the Grasleben mine could be obtained by courtesy of the *european salt company GmbH & Co. KG (esco), Werk Braunschweig-Lüneburg,* and is referred to as Grasleben salt in the following. It originates from the same stratigraphic formation as the Asse salt (z2HS) and the sampling location in the salt mine was carefully documented by the samplers of the *esco* company. In the course of blasting operations, heaps of debris normally accrue in a mine. Debris boulders of crushed salt are approximately fist-sized. Still underground, the crushed salt was filled into wide-necked barrels, made of polyethylene with a rubber seal and delivered to GRS.

Additionally, crushed salt from the Gorleben exploration mine could be obtained by courtesy of the *Deutsche Gesellschaft zum Bau und Betrieb von Endlagern für Abfallstoffe mbH* (DBE) and is refered to as Gorleben salt in the following. The material originates from the same formation as the Grasleben salt (z2HS). In a first step, a niche was faced at the sampling site using a mill. The removed loose material was also transferred to wide-necked barrels, made of polyethylene with a rubber seal, after a few hours. To avoid interaction with air and possible water uptake due to the contact with air moisture, this was performed still being underground. A jaw crusher was deployed to reduce the particle size of the crushed salt to less than 200 mm. The content of each barrel was processed separately.

For some of the pretests (chapter 5.4.5), synthetic NaCl salt was used instead of the Grasleben or Gorleben salt. This salt was provided by the company *Sigma-Aldrich* and is referred to as Aldrich salt in the following. According to the product specification sheet, the salt is 99.8 % NaCl (product number 31434).

5.2.1 Grain size

The green line in Fig. 5.5 shows the grain size distribution of crushed Asse salt (data from /KRO 09/). The grain size ranges from 0.063 to 8 mm. Accordingly, the Grasleben and Gorleben crushed salt were sieved to the same grain size range (chapter 4.2). As shown in Fig. 5.5 the grain size distributions of the three different salt samples are in good agreement with each other. Thus it was decided not to adjust the crushed salt sampled used in this work to the same grain size as determined for the Asse crushed salt. All used samples of crushed salt were sieved and only the grain size fraction between 0.063 to 8 mm was used for further experiments.

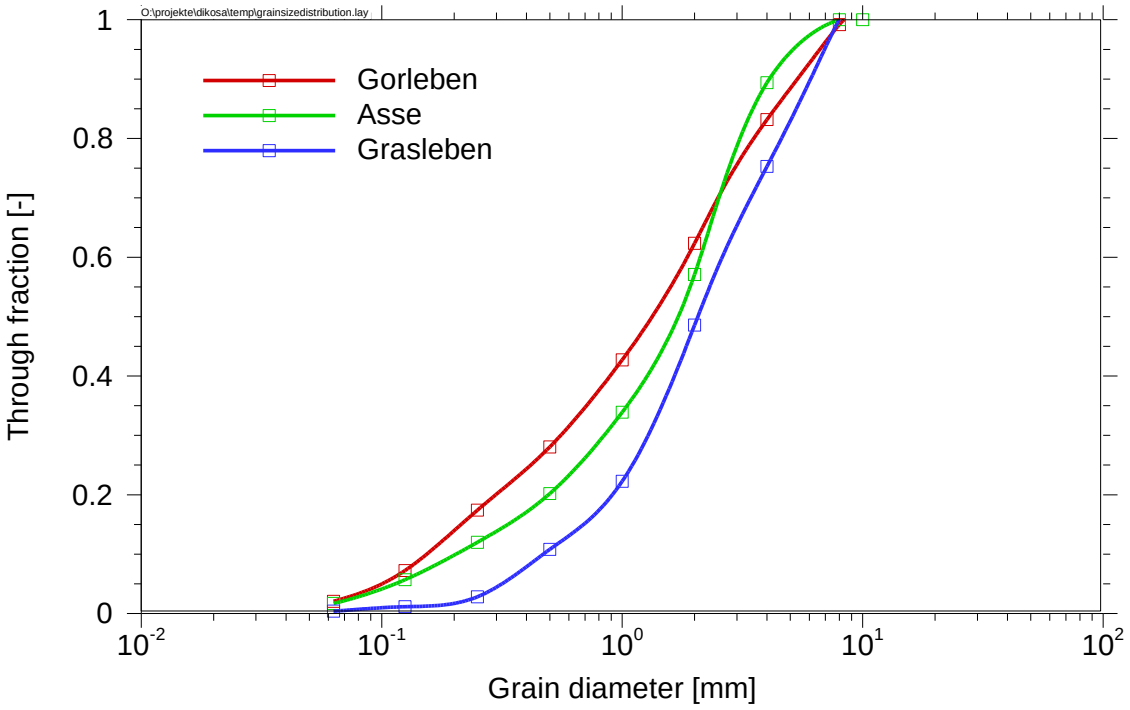

Fig. 5.5 Grain size distribution of the Grasleben and Gorleben crushed salt used in this project compared to the grain size distribution of the Asse crushed salt used in /KRO 09/

5.2.2 Mineralogy

The mineralogical composition of the Grasleben crushed salt was analysed by means of X-ray diffraction (chapter 4.3). Main component is halite, minor components are anhydrite, gypsum, quartz and clay minerals. Equally, the Gorleben crushed salt was analysed for its main and minor components. In the Gorleben crushed salt, only halite and anhydrite were detected with 84 % halite and 16 % anhydrite (see figure 5.6).

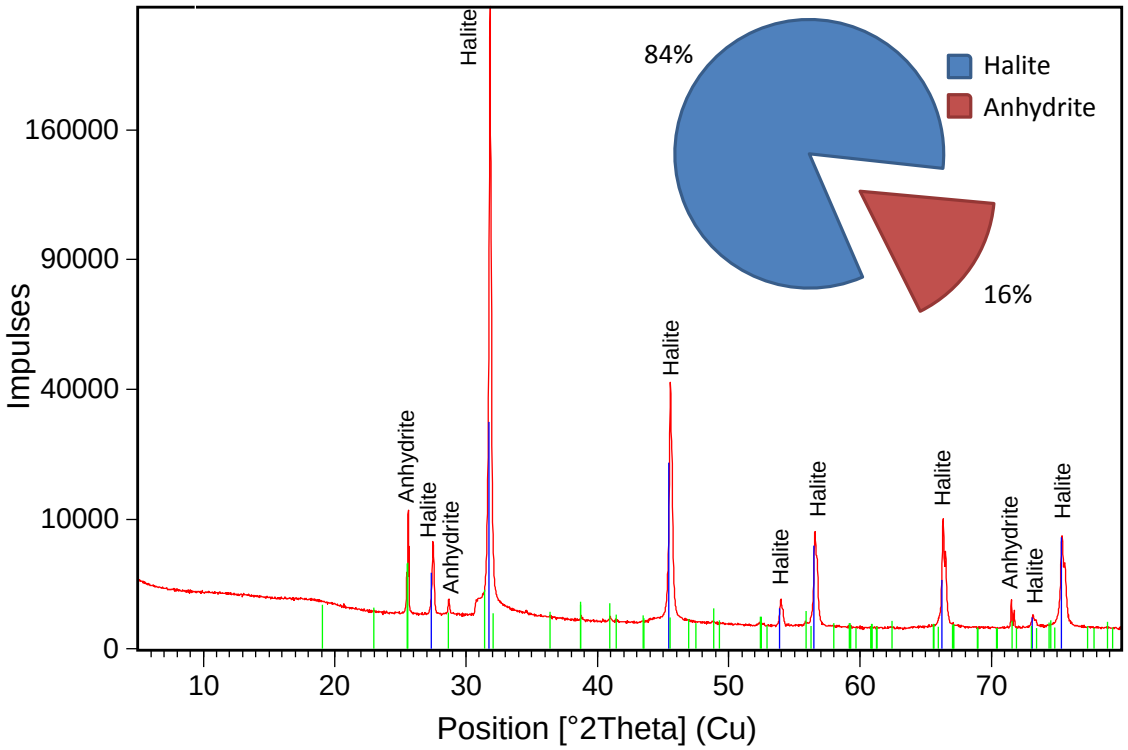

Fig. 5.6 XRD spectrum of the Gorleben crushed salt

5.2.3 Gravimetric water content

The gravimetric water content w of the Gorleben crushed salt upon delivery was determined gravimetrically to be 0.05 %. It was again determined exemplarily for two samples one year later. Both samples showed a water content w of 0.06 %. It can be concluded from the constant water that the storage containers were hermetically sealed and the samples did not absorb moisture from the air.

5.3 Salt brine

Three different types of saturated salt brines were produced by dissolving salts in pure water and applied in pretests and diffusion experiments: Grasleben, Gorleben and Aldrich ones. In pretests and diffusion experiments applied salt brine was prepared from the same crushed salt that was to be used in the respective experiment.

5.3.1 Preparation

All brines were produced in the same laboratory room, where the pretests and diffusion experiments were conducted, i. e. with the same boundary conditions in order to avoid a later precipitation or dissolution of salt during the experiments as a result of changing boundary conditions, such as the temperature.

For brine preparation, the grain size fraction of > 8 mm was used, i. e. the excess grain size fraction from sieving (section 5.2.1), assuming the mineralogical composition remains the same for all fractions. In a first step, the grains were milled using a jaw breaker type Pulverisette 01.503 by Fritsch at the finest level. Salt brines were either prepared in 5 l or 10 l silica glass containers by SCHOTT DURAN or in 120 l plastic drums according to DIN EN ISO 20848-1 by MAUSER. For the small volume containers, salt was added to pure water in the container and then placed on a roller shaker by Multifix for three days. For the large volume containers, salt and pure water were filled into the container and then stirred well using a paddle stirrer type RW28W by IKA Labortechnik Janke & Kunkel for three days. In any way, it was taken care to always have a residuum amount of salt remaining in the containers to ensure a complete saturation of the brine with the different minerals of the respective salt.

Before utilizing the brines in any of the pretests or diffusion experiments, they were filtered using general purpose filter paper with medium retention and flow rate, which is routinely used for clarifying liquids. This way, insoluble components of the salt samples (e. g. clay minerals, cf. chapter 5.2.2) as well as salt minerals remaining solid after a complete saturation of the brines were removed from the brines.

Tracers (chapter 5.4) were added to the saturated brines after preparation and filtration. Here, only the silica glass containers by SCHOTT DURAN with 5 l or 10 l volume were used. The solution was stirred well with an IKA magnetic stirrer C-MAGHS4 (without active heating) until a complete dissolution of the respective tracer.

5.3.2 Characterisation of the salt brine

Results of a chemical analysis of saturated Grasleben brine are given in Tab. 5.1. As it was expected, main elements are sodium and chloride; minor elements are potassium, magnesium, calcium, and sulphate. Bromide and iodide concentrations were below the detection limit.

Tab. 5.1 Results of the chemical analysis of the saturated Grasleben brine (<DL = below detection limit)

Element	Concentration [mg l^{-1}]	Concentration [mol l^{-1}]
Sodium, Na^+	116.500	5.07
Potassium, K^+	146.3	$3.74 \cdot 10^{-3}$
Magnesium, Mg^{2+}	169.5	$6.97 \cdot 10^{-3}$
Calcium, Ca^{2+}	1.556	$3.88 \cdot 10^{-2}$
Chloride, Cl^-	175.650	4.95
Bromide, Br^-	<DL	<DL
Iodide, I^-	<DL	<DL
Sulphate, SO_4^{2-}	4.207	$4.29 \cdot 10^{-2}$

The chemical composition of the Gorleben brine shows a higher concentration of sodium, but lower concentrations of potassium, magnesium and calcium (Tab. 5.2). Also, the chloride concentration of the Gorleben brine is higher than that of the Grasleben brine, while bromide, iodide and sulphate concentrations are all at a very low level or not detectable. This shows that the Gorleben salt has a higher content of halite than the Grasleben salt compared to other salt minerals, such as anhydrite and gypsum. The chemical analyses of the Grasleben and Gorleben salts are also plotted in figure 5.7.

Tab. 5.2 Results of the chemical analysis of the saturated Gorleben brine

Element	Concentration [mg l^{-1}]	Concentration [mol l^{-1}]
Sodium, Na^+	123.667	5.38
Potassium, K^+	58.4	$1.49 \cdot 10^{-3}$
Magnesium, Mg^{2+}	7.272	$2.99 \cdot 10^{-4}$
Calcium, Ca^{2+}	1.193	$2.98 \cdot 10^{-2}$
Chloride, Cl^-	196.633	5.55
Bromide, Br^-	46.9	$5.87 \cdot 10^{-4}$
Iodide, I^-	0.02	$5.87 \cdot 10^{-7}$
Sulphate, SO_4^{2-}	2.904	$3.02 \cdot 10^{-2}$

The Aldrich salt is a synthetic pure salt. Because the provider indicates a pureness of the NaCl salt of 99.8 % (section 5.2.2), it was decided not to analyse the salt brine and it was assumed that it features only concentrations of sodium and chloride in a saturated state.

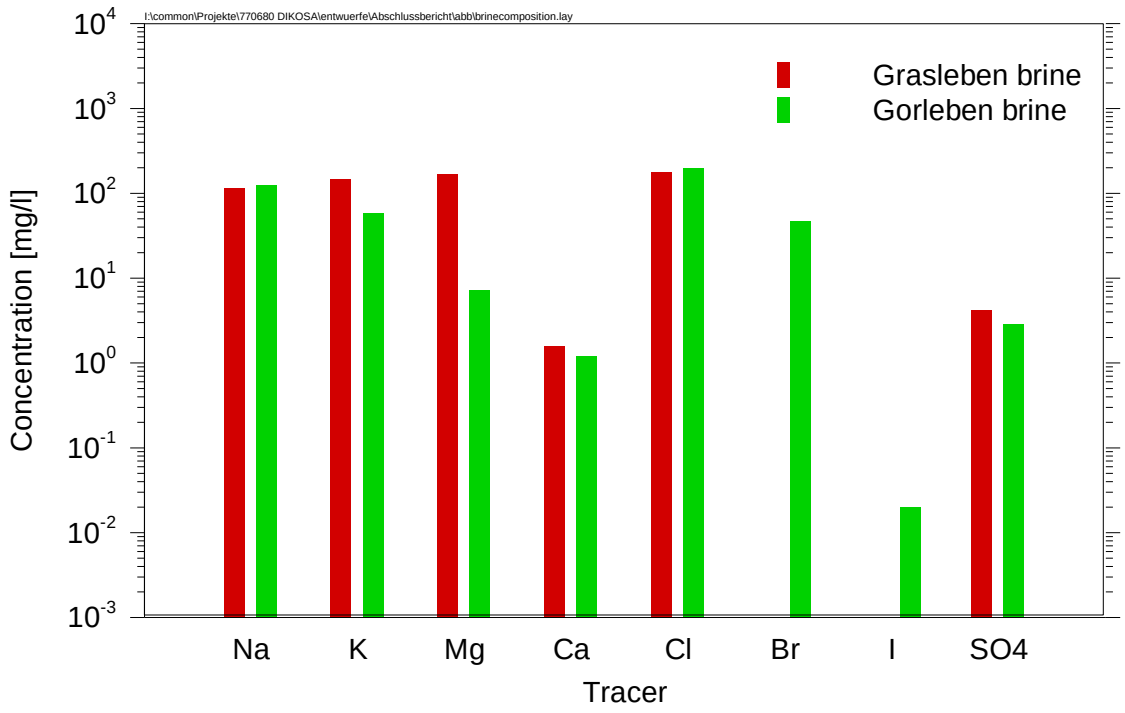

Fig. 5.7 Chemical analysis of Grasleben and Gorleben brines

5.4 Tracers

Initially, it was aimed at using three different tracers in the diffusion experiment. Ideally, those tracers would have chemically different characteristics. This way interactions between the tracers and the salt matrix can be observed and studied. Different chemical characteristics are for example the chemical charge, the ionic radius and the hydration number of the tracers. Additionally, interactions between the tracers have to be excluded in order to apply all considered tracers in the same experiments. In the first place, it was intended to use the three tracers: iodide, caesium and uranine.

After conducting some pretests concerning the potential tracers to be applied, their possible concentration and their detectability in salt brines, as well as concerning the interactions between the tracers, only caesium was used in most of the experiments. Additionally, iodide, selenium and neodymium were used in one other successful diffusion experiment. In this chapter, the tracers that were actually applied in the diffusion experiments presented in chapter 6 are described including their chemical characteristics. Other tracers that were considered during the planning phase but were finally not applied in the presented diffusion experiments.

5.4.1 Caesium

The choice of caesium as a monovalent cationic tracer ion for the diffusion experiments, which was made during the planning period of the project, was proven to work well concerning the necessary experimental time. In order to work with a high caesium concentration, and to avoid any interactions between different tracers, it was decided to only use caesium as a tracer in most of the experiments. Only one other experiment was run using the additional tracers iodide, selenium and neodymium.

Cs^+ was decided to be added to the source reservoir at a concentration of $1 \cdot 10^{-2}$ mol l^{-1}, which is below the high solubility limit of caesium-chloride in the tested saturated brines /LID 05/. A diffusion coefficients of 20.7 10^{-10} m^2 s^{-1} for Cs^+ at infinite dilution in water and a temperature of 25 °C is given in the literature /LI 74/. For the quasi steady-state of the diffusion experiments, the concentration of Cs^+ in the sink reservoir was predicted to be well above the respective detection limits. For the experiment with the tracer cocktail, caesium was used at a concentration of $8.73 \cdot 10^{-4}$ mol l^{-1}. At this initial concentration a steady-state concentration of $5.44 \cdot 10^{-6}$ mol l^{-1} to be observed in the sink reservoir.

Caesium was added to the source reservoir as Caesium chloride (CsCl).

5.4.2 Iodide

The halogenide iodide was also considered as a possible tracer during the planning phase. One successful diffusion experiment was run using the tracer iodide beside the discussed tracer caesium and the two other tracers selenium and neodymium. Monovalent anionic iodide (I^-) is stable over almost the entire pH spectrum and has a high solubility /LID 05/. The sorption of iodine on sediments is generally very low and there is no complexiation of iodine, thus its environmental mobility is very high.

Iodide was used at a concentration of $1.98 \cdot 10^{-3}$ mol l^{-1} in the experiment. A diffusion coefficient for iodide of $20.0 \cdot 10^{-10}$ m^2 s^{-1} at infinite dilution and a temperature of 25 °C is given in the literature /LI 74/.

Iodide was added to the source reservoir as Sodium iodide (NaI).

5.4.3 Selenium

As divalent tracer anion for the diffusion experiments, selenium was chosen, which is as ^{79}Se of relevance in long-term safety analyses of radioactive waste repositories and is present in solution as selenite, SeO_3^{2-}, or selenate, SeO_4^{2-}, depending on redox potential and pH. A source reservoir concentration of $1.30 \cdot 10^{-3}$ mol l^{-1} was used for diffusion experiments. Upon reaching the steady-state breakthrough, the corresponding selenium sink reservoir concentrations are predicted by calculations to be at $3.72 \cdot 10^{-6}$ mol l^{-1} assuming a sample length of 4 cm and a porosity of 4 %. A diffusion coefficient of $9.5 \cdot 10^{-10}$ m^2 s^{-1} for selenate at infinite dilution and a temperature of 25 °C is given in the literature /LI 74/.

Selenium was added to the source reservoir as Sodium selenate (Na_2SeO_4).

5.4.4 Neodymium

In experimental studies related to long-term performance assessments of radioactive waste repositories in rock salt, Nd(III), as a representative element of the lanthanides is used as a redox-invariant analogue for americium(III) and plutonium(III), which account e.g. for over 80 % of the potential release from the U.S. Department of Energy Waste Isolation Pilot Plant (WIPP) through the dissolved-brine-release mechanism, based on current assumptions of WIPP performance assessment /BOR 08/. Neodymium(III) solubility was measured in the latter study to lie above about $1 \cdot 10^{-6}$ mol l^{-1} in a 5 mol l^{-1} NaCl brine for values of the negative logarithm of the hydrogen ion concentration, pC_{H+}, below about 8. A Nd(III) concentration $2.99 \cdot 10^{-4}$ mol l^{-1} was used in the diffusion experiments. A diffusion coefficient for neodymium of $6.2 \cdot 10^{-10}$ m^2 s^{-1} for La(III) at infinite dilution and a temperature of 25 °C is given in the literature /LI 74/.

Neodymium was added to the source reservoir as Neodymium(III) chloride hydrate ($NdCl_3 \cdot xH_2O$).

5.4.5 Pretests

Several pretests were conducted concerning the characterisation of the sample material and the boundary conditions of the diffusion experiments. More precisely, these experiments were related to the solubility of the tracers in saturated brine, possible inter-

actions of the tracers with the brine and/or the crushed salt and the compaction of the crushed salt.

Both the Grasleben brine and a synthetic NaCl brine (prepared from NaCl salt obtained from the *Sigma-Aldrich Co. LLC* company, chapter 5.2) were analysed for their contents of the three potential tracers iodide and caesium. The concentrations were below the detection limits, which are given in Tab. 5.3. Thus, the tracer concentrations in the brine will not be measurably increased by dissolution of the salt.

Tab. 5.3 Limits of determination for selected tracers (ICP-MS)

Isotope	**Detection limit [mg l^{-1}]**	**Detection limit [mol l^{-1}]**
Iodide	0.01	$8 \cdot 10^{-8}$
Caesium	0.001	$8 \cdot 10^{-9}$

To exclude sorption or precipitation during the experiments, a concentration of $1 \cdot 10^{-3}$ mol l^{-1} of each tracer was added to both the Grasleben brine and the synthetic brine. Samples were taken immediately (t = 0 days) and after two weeks' time (t = 14 days). Results are given in Tab. 5.4, Tab. 5.5 and Fig. 5.8.Tab. 5.5 and are visualized in Fig. 5.8. Differences in the tracer concentration after two weeks amount to ca. 1%, which is below the relative standard deviation of the analyses. No interaction of the tracers with the salt and/or the brine could be observed for the Grasleben and the synthetic brine in this pretest.

Furthermore, the pretests showed that a concentration of 10^{-3} mol l^{-1} is measurable using ICP methods even after a dilution of 1:10,000. In the following, the concentration to be aimed at in the experiments will be defined for each tracer with respect to the pumping rate and the detection limits.

Tab. 5.4 Results of the tracer interaction pretest with the Grasleben brine

Element	**Grasleben brine, t = 0 days**		**Grasleben brine, t = 14 days**	
	Concentration [mg l^{-1}]	**Concentration [mol l^{-1}]**	**Concentration [mg l^{-1}]**	**Concentration [mol l^{-1}]**
Iodide	125.5	$9.89 \cdot 10^{-4}$	124.9	$9.84 \cdot 10^{-4}$
Caesium	132.2	$9.89 \cdot 10^{-4}$	132.4	$9.96 \cdot 10^{-4}$

Tab. 5.5 Results of the tracer interaction pretest with the synthetic brine

Element	Synthetic brine, t = 0 days		Synthetic brine, t = 14 days	
	Concentration [mg l^{-1}]	Concentration [mol l^{-1}]	Concentration [mg l^{-1}]	Concentration [mol l^{-1}]
Iodide	123.3	$9.72 \cdot 10^{-4}$	123.6	$9.74 \cdot 10^{-4}$
Caesium	131.9	$9.92 \cdot 10^{-4}$	131.5	$9.89 \cdot 10^{-4}$

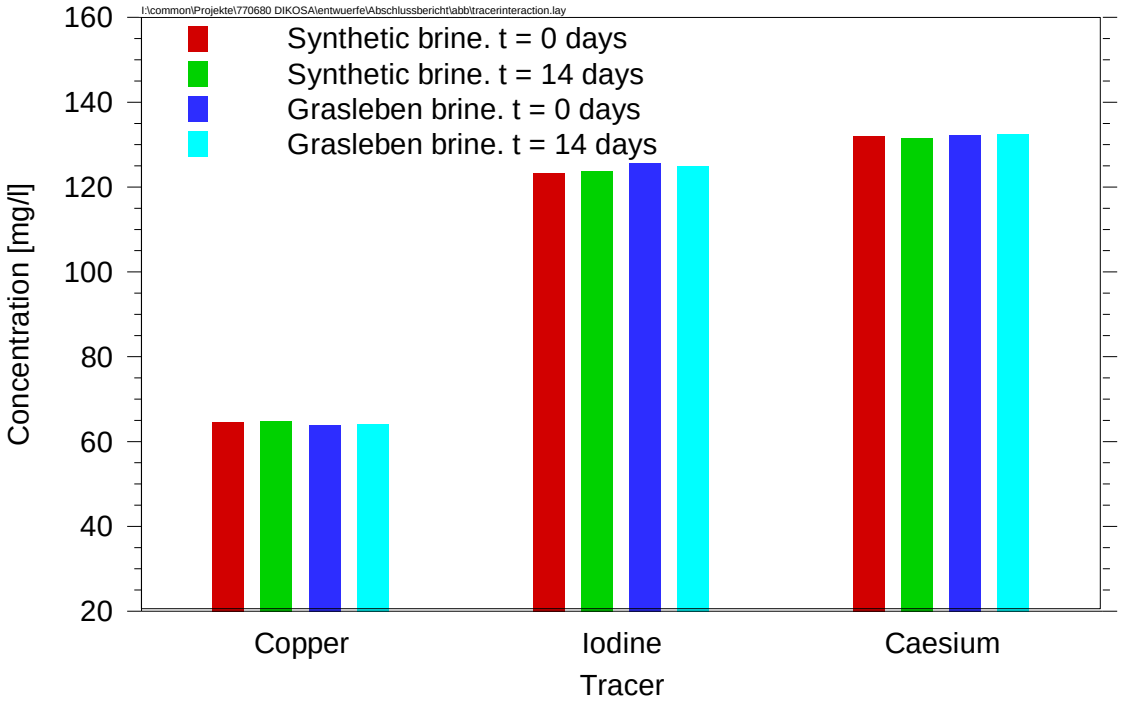

Fig. 5.8 Results of the tracer interaction pretests with the Grasleben brine and the synthetic brine

6 Diffusion experiments

6.1 Orienting calculations

To estimate the boundary conditions of the diffusion experiments with regard to sample length, experimental duration and time intervals of the sampling, orienting diffusion calculations have been performed. The tracer flux to the sink reservoir q has been calculated using equation 3.3 assuming a fixed hypothetical tracer concentration in the source reservoir of c_1 = 10 mol/m^3. A different concentration would scale the calculated flux linearly. The concentration in the sink reservoir has been calculated from the tracer flux q from

$$c_2 = \frac{q \cdot A \cdot n}{q_p} \tag{6.1}$$

assuming a porosity n of the sample of 4 %, a cross section of the sample A of $2 \cdot 10^{-4}$ m^2 corresponding to a diameter of the sample of 8 cm and a pumping rate q_p of the brine at the sink side of the diffusion cell of $2.8 \cdot 10^{-5}$ ml/min. All three values are realistic values for the actual experiment. Differences in those values would scale the calculated concentration in the tracer sink reservoir linearly.

Calculations first were performed regarding for a sample length of 8 cm, which was the preferred length at the planning stage of the experiments. Diffusion coefficients considered for the tracer in the pore water ranged from $1 \cdot 10^{-10}$ m^2/s down to $1 \cdot 10^{-11}$ m^2/s. Even for the highest diffusion coefficient considered, the time to establish steady-state conditions for the concentration in the sink reservoir was estimated to be about one year increasing to values of even several years for lower diffusion coefficients. As a result of these calculations, it was decided to reduce the sample length to only 4 cm. In this case, the steady-state of the tracer concentration in the sink reservoir is expected to be obtained after several months which is a more reasonable time span compared to the project duration.

The calculated flux and expected concentration c_2 in the brine of the sink reservoir assuming three different diffusion coefficients and sample lengths of 0.04 m and 0.08 m are plotted in Fig. 6.1. Since the tracer concentration in the sink reservoir is rising rapidly during the early phase it was decided to use a short sampling interval of two to

three days during the early phase of the experiment which optionally can be extended at a later stage of the experiment, when close to the steady-state.

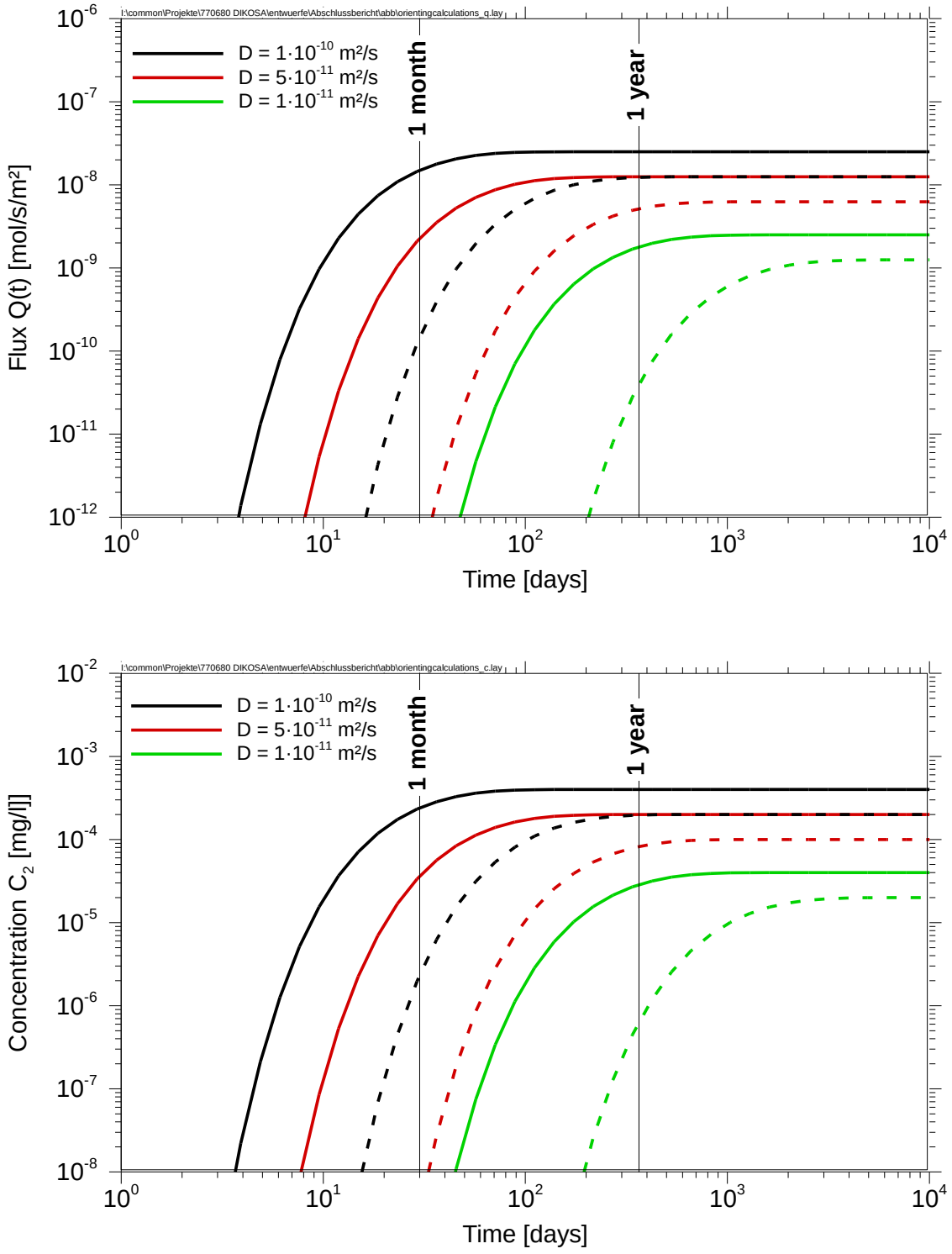

Fig. 6.1 Time-dependent flux (upper figure) and concentration of the tracer in the sink reservoir (lower figure) for sample lengths of 0.04 m (solid lines) and 0.08 m (dashed lines) for three different diffusion coefficients

6.2 Sample preparation

Crushed salt was delivered in wide-necked drums, made of polyethylene with a rubber seal. The drums have a volume of 42 l or 55 l and are filled with ca. 50 - 60 kg of crushed salt each.

Samples of the Grasleben crushed salt were taken using a sample divider type PT with vibrating chute type DR by RETSCH. Samples of the Gorleben salt were taken without a sample divider. Before taking samples from the drums, they were homogenized by removing half of the content from one drum and filling it into a new drum. Both drums were then stirred well until visual homogeneity and afterwards merged in one drum, from which salt samples were then taken.

The mass of crushed salt m needed to produce the compacted salt sample is given by

$$m = (1-n) \cdot \pi \cdot r^2 \cdot l \cdot \rho_0 , \tag{6.2}$$

where n is the targeted final porosity of the compacted sample (e.g. n = 0.04) for the diffusion experiment, r is the radius of the experimental cell (r = 4 cm), l is the preferred final length of the compacted sample (l = 4 cm) and ρ_0 is the grain density of the salt (ρ_0 = 2.170 g/cm^3 /GEV 81/). Accordingly, a mass of about 420 grams of crushed salt is used to produce a sample of a targeted porosity of 4 %. To enhance the compaction process, 1% by weight of saturated brine is added to the crushed salt. The mass of salt included in the saturated brine is added to the salt sample weight and is given by 27 % by weight of the brine.

The loose crushed salt material is filled into the diffusion cell. During the compaction of the sample of experiment number 12 it was tested to add a spacer between the bottom plate of the cell and the crushed salt during the compaction process. The spacer was again removed after the compaction was finished. This was done to obtain a void space for the brine circulation during the diffusion experiment. The crushed salt sample is compacted in the cell by applying pressure to the main plunger using a uniaxial Amsler hydraulic press (see figure 6.2). In the first phase of the compaction process, the force is automatically controlled and a constant force of 100 kN is applied to the sample. In the second phase of the compaction process, the position of the plunger is automatically controlled to obtain the targeted sample height. During the second phase, the force is consequently lowered continuously. Exemplary data from the compaction

process of sample number 6 is shown in figure 6.3 for the applied load and the calculated porosity of the sample. After the targeted sample height is reached, the sample is kept at constant conditions for about one week to achieve constant conditions in the sample.

After compaction of the sample, the cell is opened and the actually achieved length of the sample is measured at different points using a caliper. In case the targeted final length and porosity of the sample has not yet been reached, the compaction process is continued.

In case the targeted porosity has been achieved, the crushed salt sample is saturated with brine. Therefore, saturated brine is injected in one side of the cell under a constant pressure of about 50 kPa supplied by a nitrogen gas bottle (see figure 6.5). The gas bottle is connected to the headspace of a reservoir with brine which is again connected to the cell. The outflow of brine from the other side of the cell sample is captured and its mass is measured. The sample is regarded as being saturated as soon as the brine outflow has reached a constant rate. The permeability k_w of the sample is measured using the same setup. The permeability of the sample can be calculated from the mass of the captured brine outflow q_b using

$$k_w = \frac{q_b \cdot \mu_w \cdot h}{\pi \cdot r^2 \cdot \Delta p} \tag{6.3}$$

where μ_w is the viscosity of the brine and Δp is the applied pressure gradient. An example for the data received for pressure and brine flux is shown in figure 6.4.

Fig. 6.2 Amsler hydraulic press for compaction of the samples

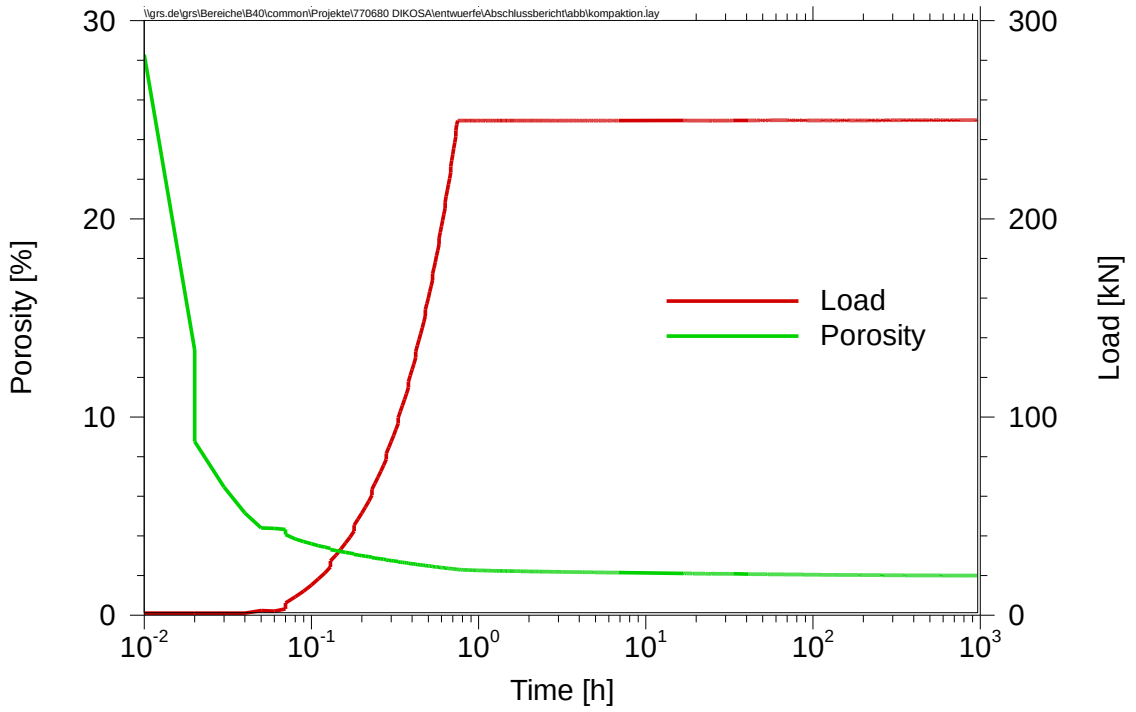

Fig. 6.3 Temporal evolution of the applied load of the uniaxial press and the calculated sample porosity for sample 6

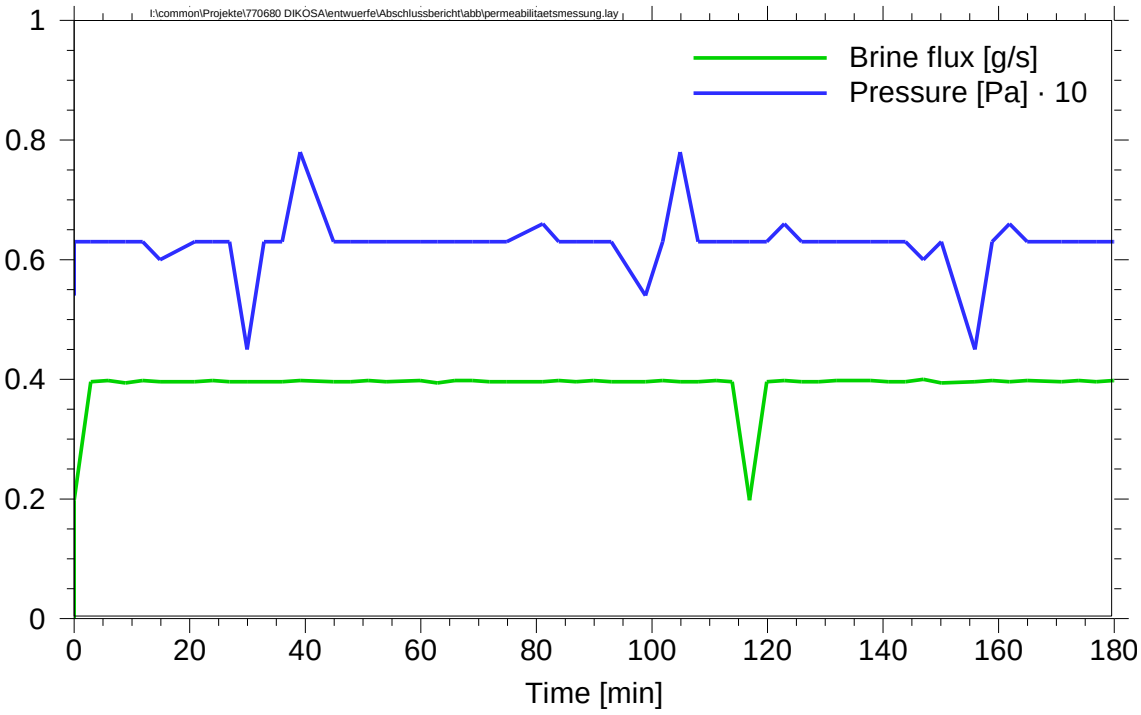

Fig. 6.4 Exemplary curves for pressure and brine flux during permeability measurement

Fig. 6.5 Experimental setup during sample saturation and permeability measurement

6.3 Experiment execution

The diffusion experiments were conducted as through-diffusion experiments according to /SHA 91/. A schematic illustration of the experimental setup is given in figure 6.6. Photos of the actual experimental setup in the lab are shown in figure 6.7.

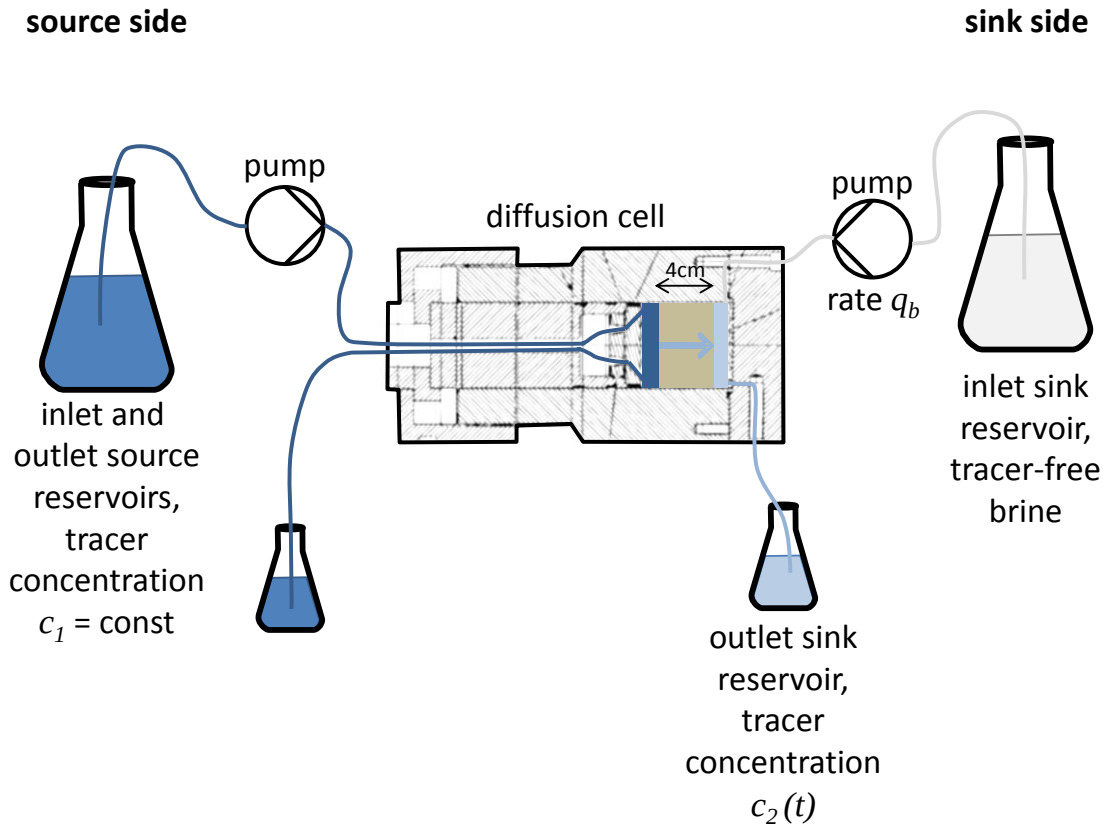

Fig. 6.6 Schematic illustration of the diffusion experiment setup (not to scale)

The experiments were conducted in a temperature controlled laboratory at a constant temperature of about 25 °C. All brines used in the experiments described in the following were saturated with Gorleben salt (see chapter 5.2) at 25 °C. The room temperature was kept at a constant value of ± 2 °C to avoid dissolution or precipitation of salts during the experiment (see figure 6.8). The diffusion cell features four connectors; two at the source and two at the sink side. On both sides of the cell, brine was pumped from reservoirs from the inlet to the outlet connectors. The diffusion cell was placed in horizontal direction during the diffusion experiment to avoid advective fluxes through the sample due to pressure differences.

The brine at the inlet source reservoir was spiked with the tracer. All experiments reported used caesium as tracer. For experiment 6 a concentration of about c_1 = 110 mg/l was used and for all other experiments reported a concentration of about c_1 = 1,500 mg/l was used. Experiment 6 additionally used selenium and iodine as tracers. The brine is pumped from the inlet source reservoir to the outlet source reservoir at a constant rate of about 0.1 cm^3/min. See figure 6.9 for the temporal evolution of the pumping rate as determined from weighing of the sample bottles. The brine in the storage vessel of the inlet sink reservoir is free of tracer. The brine is pumped from the inlet sink reservoir to the outlet sink reservoir at the same rate as on the source side of the experiment. The pumping rate was chosen identically at both sides of the cell to avoid pressure differences and resulting advective fluxes from the source to the sink side of the cell. This was achieved by using the same multichannel peristaltic pump for both sides of the cell.

Due to the diffusive flux of the tracer through the compacted crushed salt sample from the source side of the experiment to the sink side, the tracer concentration in the outlet sink reservoir was increasing with time. The brine at the outlet sink reservoir was sampled each two to three days (see figure 6.10). The actual brine flux at the sink side of the cell was determined by weighing the amount of brine sampled and the brine was analysed for the tracer concentration. The diffusive mass flux through the compacted salt sample j_t per area A can be calculated from

$$j_t = \frac{q_b \cdot c_2}{A} \tag{6.4}$$

Where c_2 is the measured tracer concentration in the sink outlet reservoir and q_b is brine flux.

Fig. 6.7 Photos of the diffusion experiment setup from front and above
The large bottles are the inlet reservoirs, while the small bottles are the outlet reservoirs

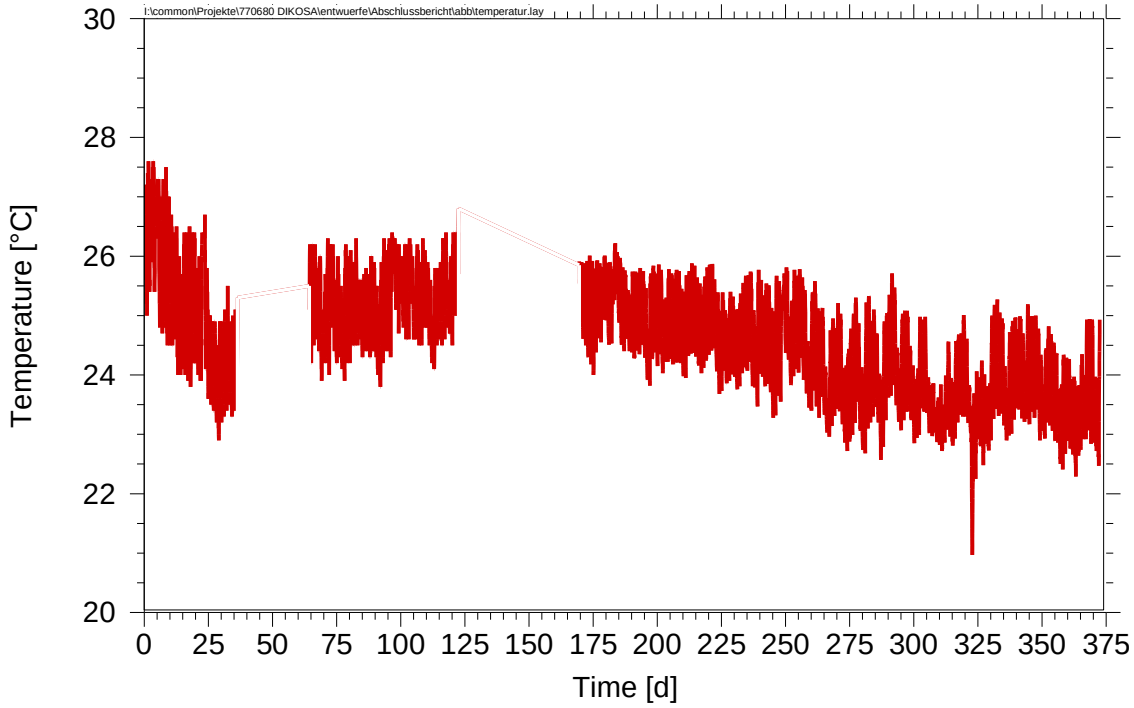

Fig. 6.8 Temporal evolution of the room temperature of the lab for a one-year time period starting at 01.03.2015

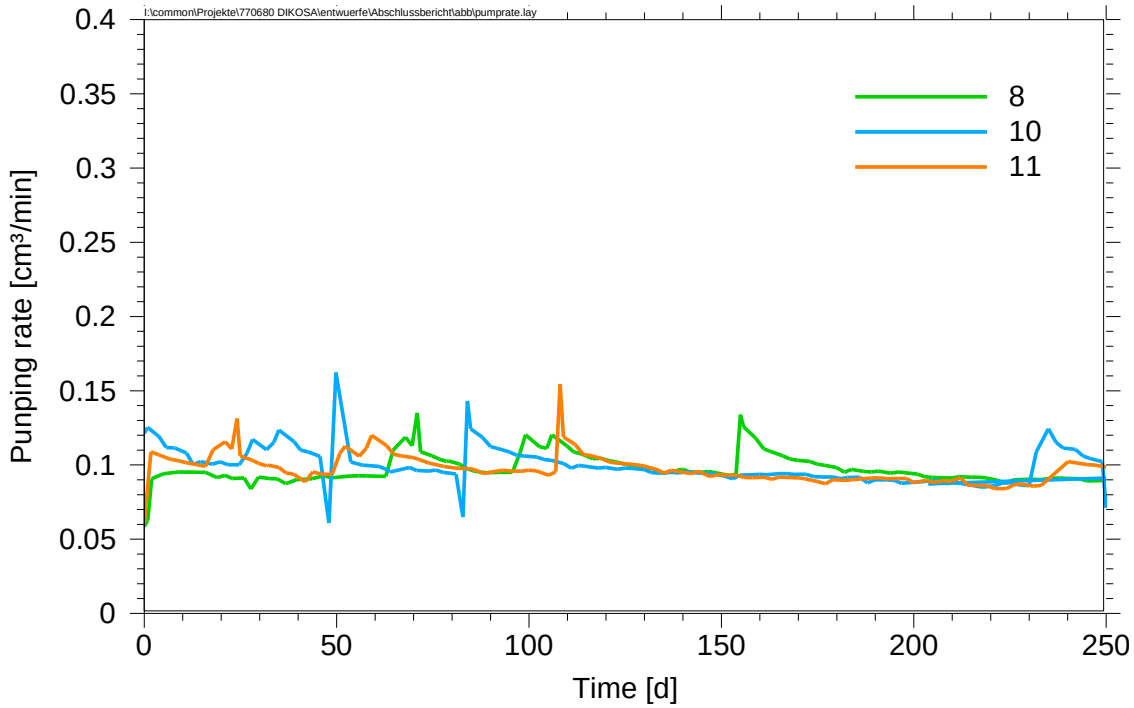

Fig. 6.9 Temporal evolution of the pumping rate for the experiments 8, 10 and 11

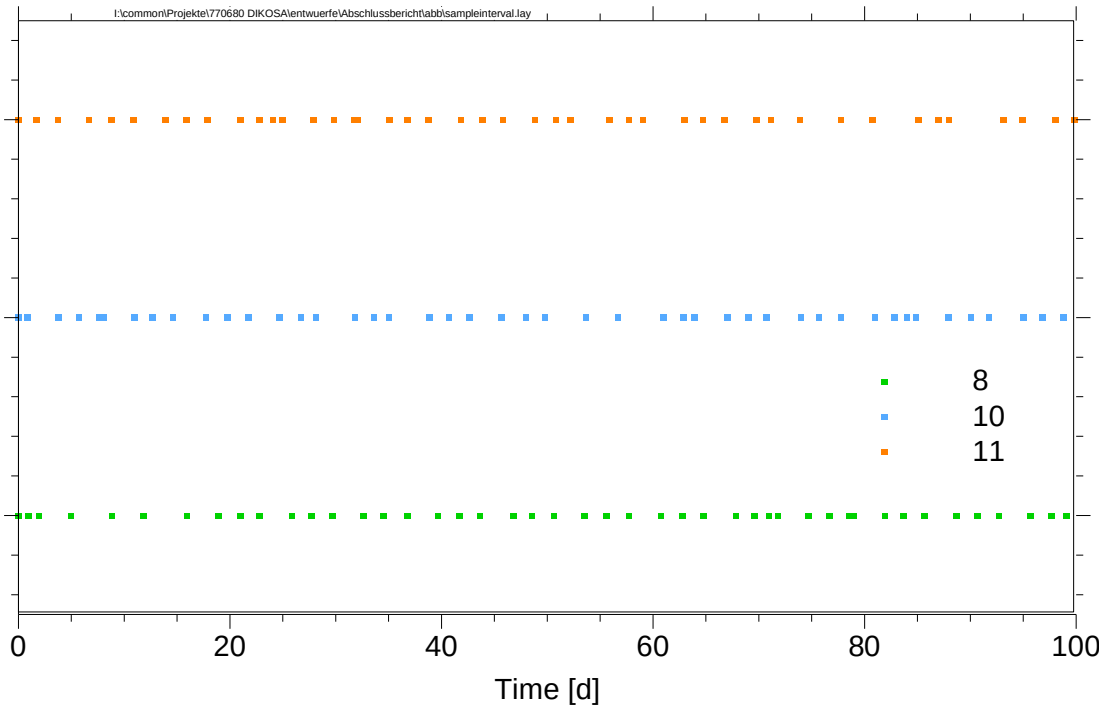

Fig. 6.10 Sampling density for the experiments 8, 10 and 11

6.4 Uncertainty analysis

For non-sorbing species, the diffusion coefficient D_{eff} is determined in the steady-state of the experiment (see chapter 2) from

$$D_{eff} = D_a = \frac{l}{c_1} q = \frac{l}{c_1} \frac{m_b c_b}{At\rho_b}, \tag{6.5}$$

where m_b, c_b and ρ_b are the measured mass, concentration and density of the brine captured at the outlet of the experiment during the period of sampling time interval t. Additionally l and A are the sample length and surface area, while c_1 is the concentration in the source reservoir of the experiment. The error of the measured diffusion coefficient can be estimated from

$$\Delta D = \sum_i \frac{\partial x_i}{\partial x_i} \Delta x_i = \frac{m_b c_b}{c_1 At\rho_b} \Delta l + \frac{l c_b}{c_1 At\rho_b} \Delta m_b + \frac{l m_b}{c_1 At\rho_b} \Delta c_b + \frac{m_b c_b}{c_1^2 At\rho_b} \Delta c_1 + \frac{m_b c_b}{c_1 A^2 t\rho_b} \Delta A + \frac{m_b c_b}{c_1 At^2 \rho_b} \Delta t + \frac{m_b c_b}{c_1 At\rho_b^2} \Delta\rho_b \tag{6.6}$$

The measurements uncertainties of the time interval, the mass of the collected brine and the surface area of the sample are regarded to be small due to the high accuracy of dedicated measuring process. The remaining contributors to the measurement uncertainty of the diffusion coefficient are determined therefore by those of the length of the sample (see also section 4.6), the measured concentrations and the density of the brine. The error of the measurement of the tracer concentrations in the brine and the brine density were both determined by repetitive measurement of a reference solution – i.e. the reproducibility of the measurement – to be less than 1 per mil for the measurement of the brine density, which is negligible, and about 10 % for the measurement of the tracer concentration of Cs in the brine (figures 6.12 and 6.11). This is larger than the actual accuracy expected for the ICP because of the high dilution of the brine samples of 1:200 to up to 1:200 000 before measurement to meet the acceptable limit of chlorine and tracer concentrations of the measuring system (see also section 4.8.1). The reference solution had to be diluted with a high factor at the upper end of the given range, while the solutions from the sink reservoir are diluted with a factor of only 1:200. Since the uncertainty is expected to increase with the dilution factor, the uncertainty is expected to be less for the samples from the sink reservoir.

For typical values determined for the mentioned parameters and the given values of the parameter uncertainties, a relative uncertainty of a single diffusion experiment and the resulting effective diffusion coefficient of 200 % are estimated. The uncertainty can be somewhat reduced by averaging repetitive measurements of the diffusion coefficient during the steady-state of the same experiment.

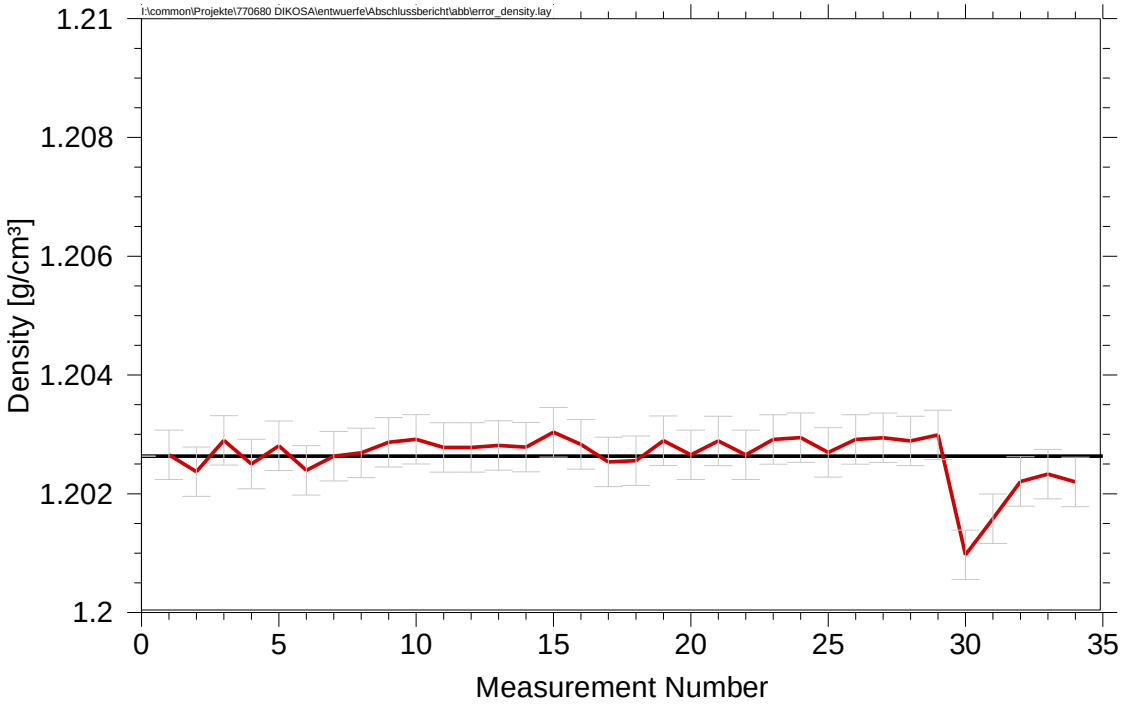

Fig. 6.11 Reproducibility of brine density measurement

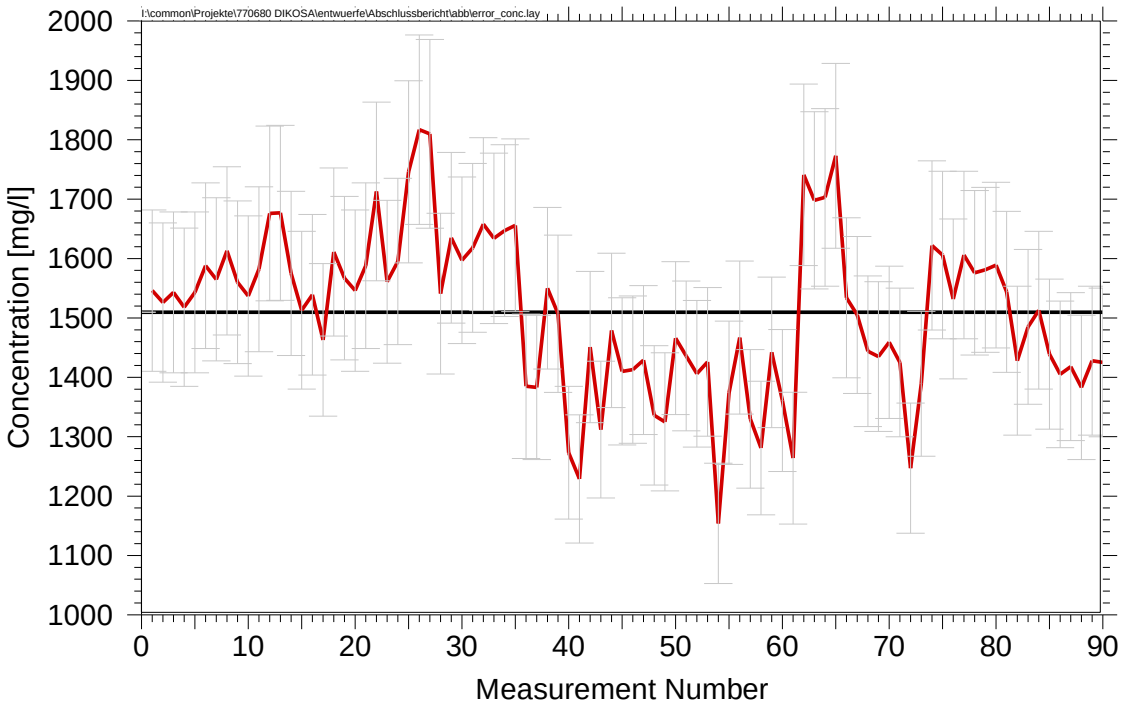

Fig. 6.12 Reproducibility of concentration measurement

6.5 Results

Four diffusion experiments were successfully performed in a way that information on the diffusion coefficient could be derived. Those four experiments were carried out using crushed salt from the Gorleben salt mine. The other salt types were only used for preliminary experiments. For every sample, its length, porosity and brine permeability were determined. An overview of the main sample properties is given in table 6.1. The determined brine permeabilities are in the range expected according to /KRO 09/ as is shown in figure 6.18.

In the following, the results of the experiments are presented as plots of the normalised tracer flux from the sample to the sink reservoir versus experiment duration. The normalised flux is derived by dividing the measured tracer flux through the sample – given in milligrams of tracer per area of the sample in square meters and second of time – by the concentration of the tracer in the source reservoir – given in milligrams per litre. The normalised flux therefore has a unit of meters per second. The pore water diffusion coefficient is directly proportional to the normalized flux. The proportional constant is only depending on the geometrical parameters length and porosity of the sample, which are expected to be temporally invariant for each of the experiments.

In addition to the measured data, one or more temporal evolutions of the expected flux are presented in the figures as they are calculated for different diffusion coefficients in the pore water according to Fick's law /CRA 79/. The highest effective diffusion coefficient regarded in these calculations represents the one of Cs^+ in free water at infinite dilution of D_0 = $2.1 \cdot 10^{-9}$ m^2/s as given in /LI 74/ multiplied by the porosity of the sample; the area above the associated line is shaded in grey in all figures. Data points plotting in the grey area would either indicate an influence of advective flow in the experiment, and therefore a malfunction of the experiment, or a discrepancy of the diffusion coefficient in the free water given in the literature to the one observed in the presented experiments.

The uncertainty of the data plotted was estimated to be about 200 % by error propagation calculation of the contributing uncertainties. The most relevant uncertainty contributing to the overall uncertainty of the flux is resulting from the concentration measurement. The uncertainty of the concentration measurement was determined as reproducibility by repetitive measurement of a reference solution to be about 10 %. This is considerably larger than the analytical accuracy of the ICP measurement and is due to the

high dilution of the brine samples of 1:200 to 1:200.000 before measurement to meet the acceptable range of chlorine and tracer concentrations of the measuring system.

Tab. 6.1 Overview of main sample properties

Number	Length [mm]	Porosity [%]	Permeability [m²]
6	40.6	2	$3 \cdot 10^{-17}$
8	40.8	2	$1 \cdot 10^{-16}$
10	40.0	4	$5 \cdot 10^{-16}$
11	40.0	4	$1 \cdot 10^{-16}$

6.5.1 Experiment 6

The experiment number 6 was started on the 24th of September 2013 using caesium, iodine, selenium and neodymium as tracers. The crushed salt sample was compacted down to a porosity of about 2 %. There are 47 measurements available for the tracer concentrations in the sink reservoir for an experimental duration of 110 days. The experiment was terminated prematurely on 13th of January 2014. The reason was that one of the inflow tubes was disconnected from the cell due to crystallization of salt which resulted in a clogging. As a consequence, the sample was not in contact with tracer solution for a few days. It was not possible to remove the clogging without opening the cell and therefore terminating the experiment. The last brine samples taken from the sink reservoir showed that an advective flow of brine from through the cell from the source to the sink reservoir must have occurred. It is most likely that the beginning clogging had led to a pressure increase in the system that consequently led to the advective flow through the sample. For this reason the last measurements of tracer in the sink reservoir were discarded.

The results of the tracer measurements before this incident are shown for caesium in figure 6.13 and for iodine and selenium in figure 6.14. The tracer concentrations of neodymium were too low to be reasonably evaluated.

This experiment within the uncertainty of the measurement shows a caesium flux into the sink reservoir which indicates a diffusion coefficient in the pore water which is in good agreement with the diffusion coefficient in the free water (see section 5.4.1). The same tendency can be seen for iodine and selenium, however the fluctuation in the values are quite high, which at least partly can be attributed to analytical uncertainties.

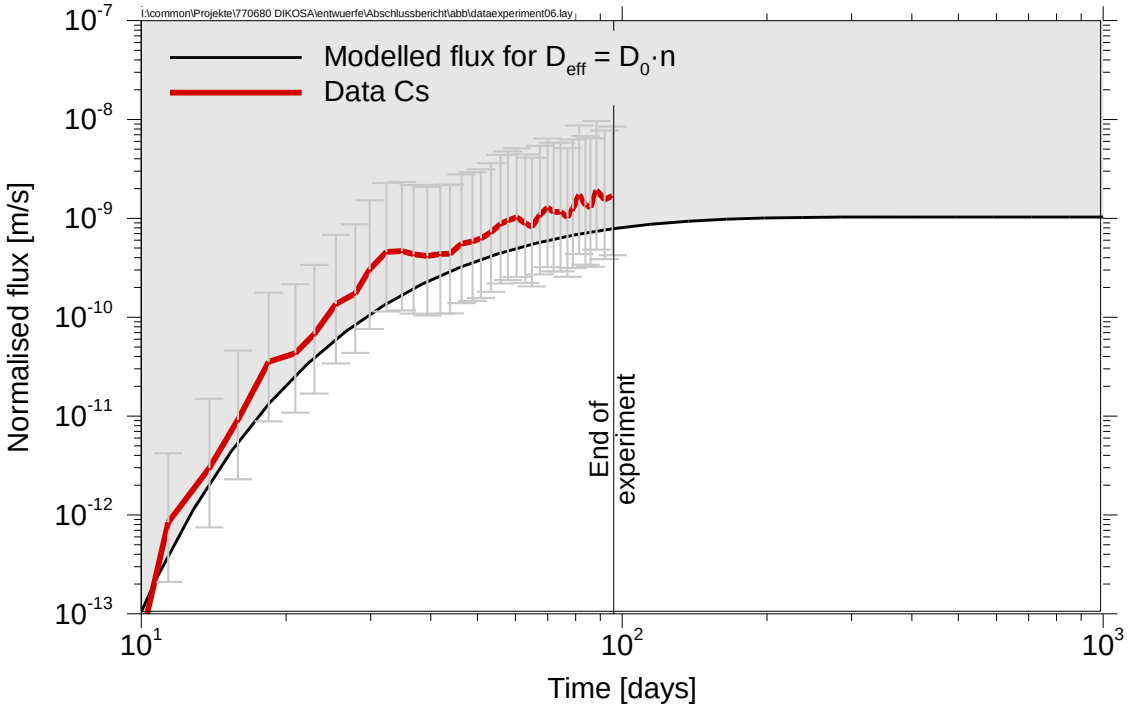

Fig. 6.13 Normalised Cs-flux measured for experiment number 6 together with modelled data

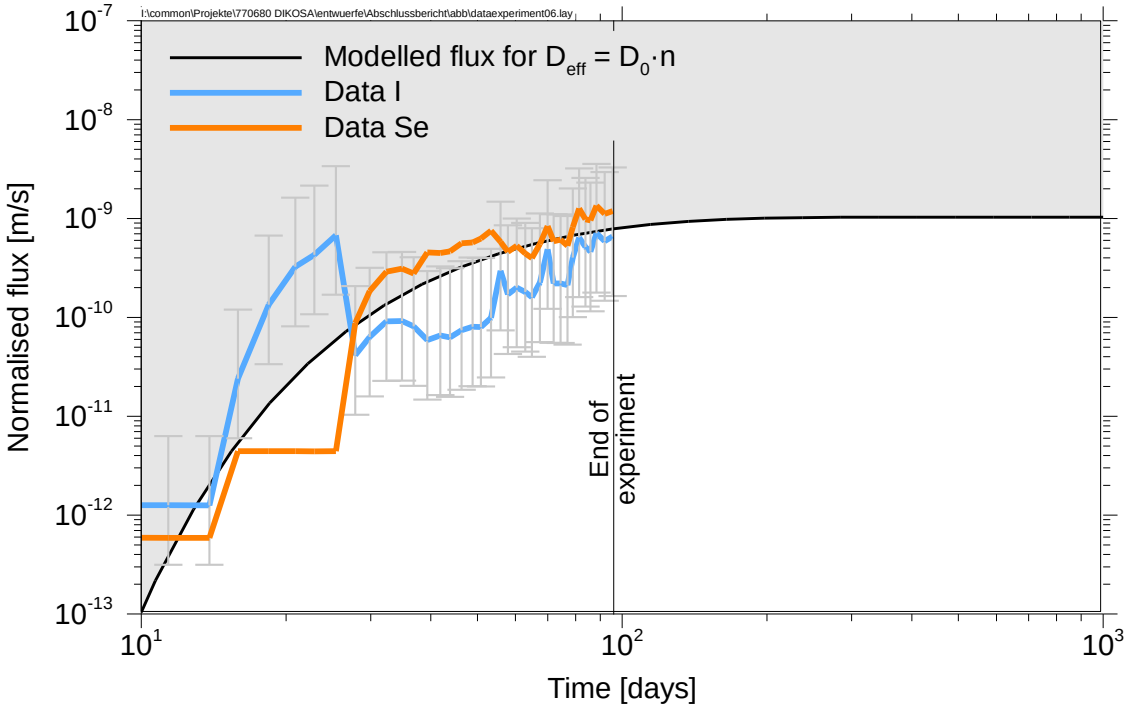

Fig. 6.14 Normalised iodine and selenium fluxes measured for experiment number 6 together with modelled data

6.5.2 Experiment 8

The experiment number 8 was started on the 17th of December 2014 using caesium as tracer. The crushed salt sample was compacted down to a porosity of about 2 %. There are measurements available for the tracer concentration in the sink reservoir for an experimental time of 340 days until the project ended. The results are shown in figure 6.15. The tracer concentrations in the sink reservoir reached measureable values for some time, but stayed below the detection limit for most of the time of the experimental procedure. This behaviour clearly contradicts the expected result for the diffusion of a tracer in a porous medium and also is in contrast to the result of experiment number 6.

This effect cannot be explained by assuming a tracer transport by diffusion in a temporary invariant pore space and / or under temporally invariant experimental conditions. Quite the contrary, this behaviour indicates that the pore space is not interconnected over the full time span of the experiment and consequently not allowing for an undisturbed diffusion of the tracer. Still, the rapid increases and decreases of the tracer concentration in the reservoir are hard to explain.

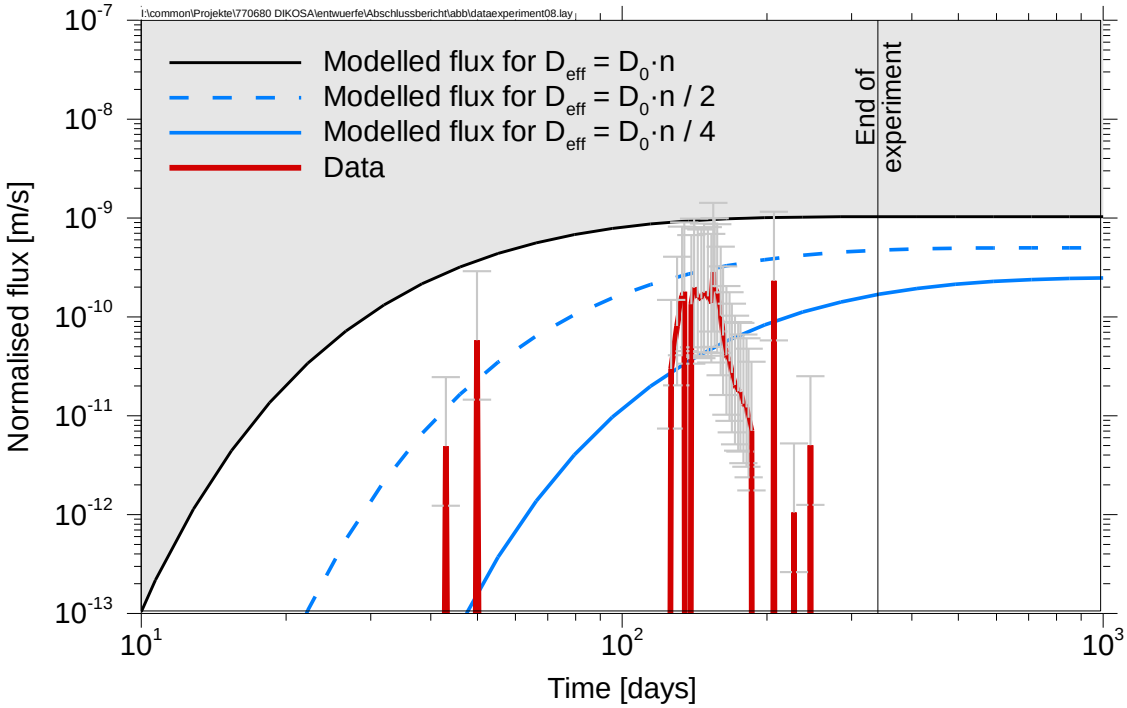

Fig. 6.15 Normalised flux measured for experiment number 8 together with modelled data

6.5.3 Experiment 10

The experiment number 10 was started on the 25th of February 2015 using caesium as tracer. The crushed salt sample was compacted down to a porosity of about 4 %. There are measurements available for the tracer concentration in the sink reservoir for an experimental time of 300 days until the project ended. The results are shown in figure 6.16. The tracer concentrations in the sink reservoir reached measureable values for a short time after 40 days and then again after 60 days. With some smaller interruptions, the tracer concentration in the sink reservoir is detectable between 60 days until about 240 days of the experiment and shows rather constant values during that time, but then stops again until the end of the experiment.

Like the experiment number 8, this experiment also shows a behaviour which deviates from the expected behaviour as observed in diffusion experiments with other porous media like clay.

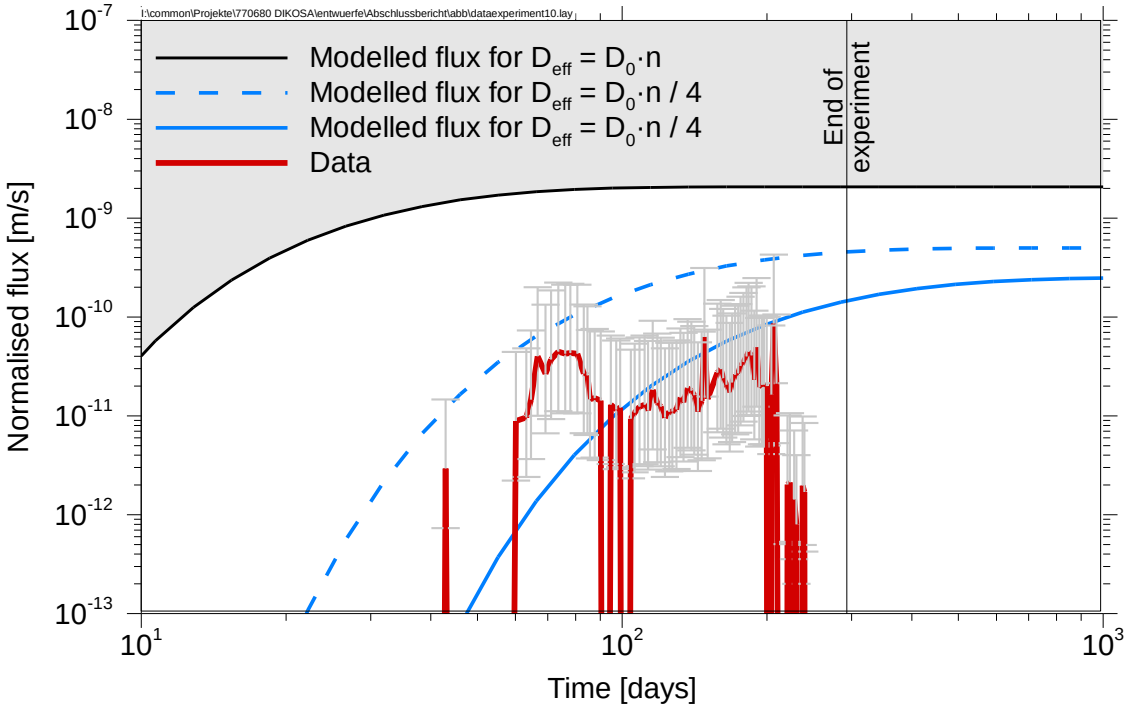

Fig. 6.16 Normalised flux measured for experiment number 10 together with modelled data

6.5.4 Experiment 11

The experiment number 11 was started on the 30th of January 2015 using caesium as tracer. The crushed salt sample was compacted down to porosity of about 4 %. There are measurements available for the tracer concentration in the sink reservoir for an experimental time of 320 days until the project ended. The results are shown in figure 6.17. The tracer concentrations in the sink reservoir reached measureable values for some time after only 18 days and with some smaller interruptions continued to show measurable concentrations until the end of the project. The diffusion process seems to be in steady-state after a bit more than 100 days.

This experiment has similarities to both, experiment 6 with a rather expected behaviour and experiments 8 and 10 with an unexpected behaviour. Like for experiment number 6, this experiment within the measurement uncertainty shows a caesium flux into the sink reservoir which indicates a diffusion coefficient in the pore water which is in agreement with a diffusion coefficient in the free water. However, this experiment like the ones number 8 to 10 also shows some gaps in the tracer flux which is not in agreement with this finding.

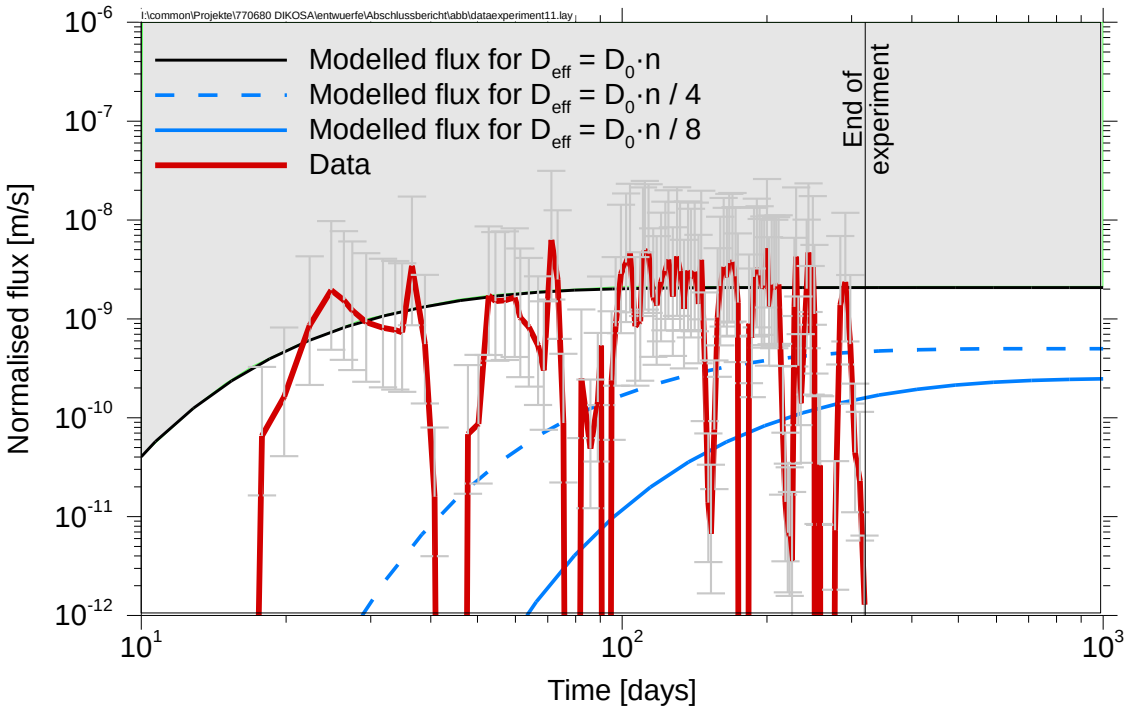

Fig. 6.17 Normalised flux measured for experiment number 11 together with modelled data

6.6 Conclusions from the experiments

Four experiments have resulted in a long time series of measured tracer concentrations in the sink reservoir. These are the experiments numbers 6, 8, 10 and 11 using crushed salt from the Gorleben salt mine. Additional experiments in the beginning of the project failed, predominantly due to experimental problems mainly arising from the necessity to use saturated sodium-chloride brines, which resulted in crystallisation and clogging of tubes and fittings or in the inner bores of the diffusion cell. The gradually enhanced experimental setup allows the realization of reliable diffusion experiments.

The porosity of the four samples investigated is either two or four percent. Within the measurements uncertainty, the permeability values determined for these samples are in the range expected of previous experiments as shown in figure 6.18. Therefore those four samples are considered to be representative for compacted crushed salt of the measured porosity.

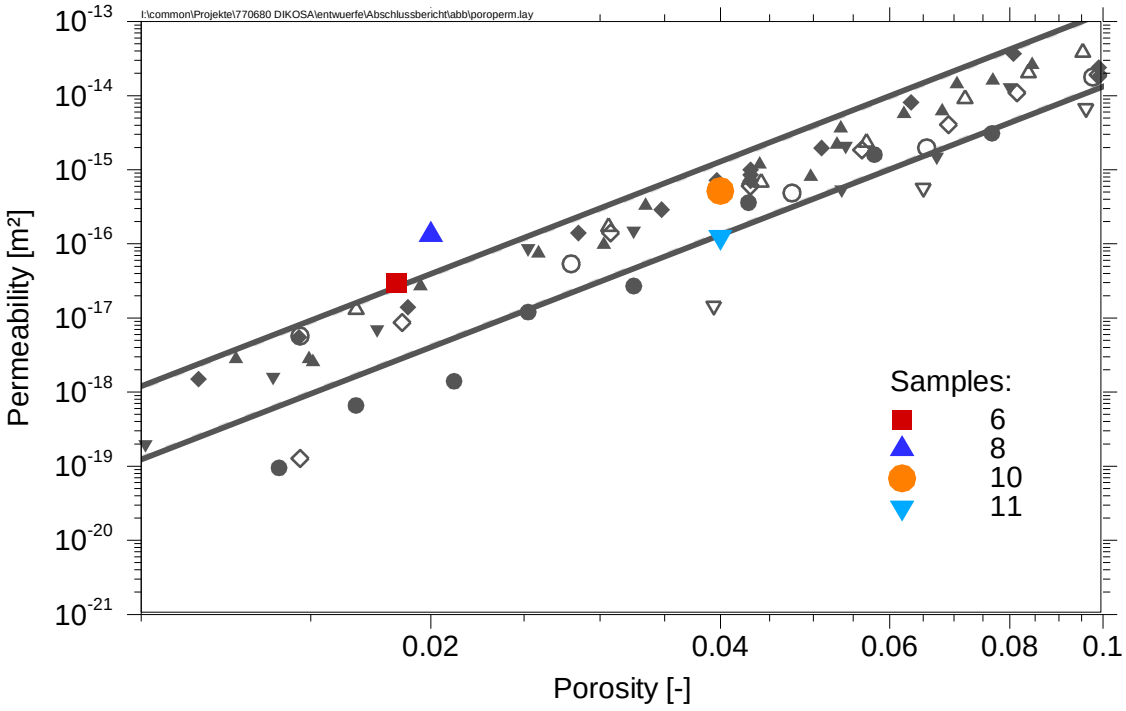

Fig. 6.18 Permeability of the DIKOSA samples compared to data presented in the project REPOPERM (in grey) /KRO 09/

For comparison, the results of the experiments 6, 8, 10 and 11 are plotted together in Fig. 6.19. Looking at the results obtained from the four experiments available for evaluation, it has to be concluded that all four experiments show a remarkable different be-

haviour and all yield unique concentration versus time plots. It has to be clearly said that the number of experiments is too small and the results are too different to allow reliable general conclusions. Nevertheless, a tentative explanation is proposed for the observations in the following, which however has to be regarded at least partly speculative.

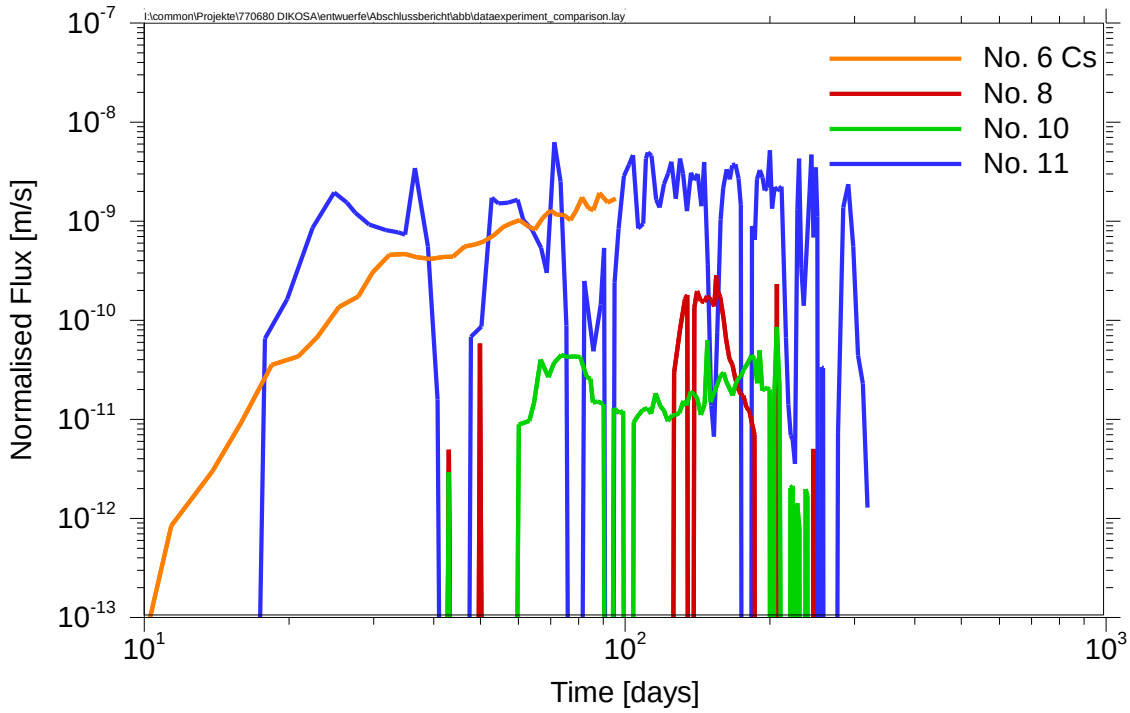

Fig. 6.19 Comparison of the result of experiments 6, 8, 10 and 11

The experiment 6 meets very well the expected behaviour for diffusion experiments. This experiment shows a constant increase of the caesium flux from the source to the sink reservoir, which within the uncertainty is in good agreement with the expected evolution from transport by diffusion. The effective diffusion coefficient calculated from this experiment indicates that the diffusion in the pore space occurs with the same diffusion coefficient as in free water. No significant effect of a tracer-matrix interaction – as it is known for example for anion exclusion in clays – can be noticed from the data. Unfortunately, experiment 6 was terminated prematurely before the steady-state was reached due to a clogging of the brine inlets of the diffusion cells due to crystallisation of NaCl, but the experimental duration was still long enough to confirm these statements. This experiment clearly shows that the diffusion of caesium in the pore water of compacted salt grit of a porosity of 2 % is not retarded compared to the diffusion in free water. The high diffusion coefficient measured cannot be explained by analytical or experimental artefacts. Accordingly, no effect can be expected for higher porosities, but

only for lower porosities. From this experiment alone it already can be concluded that modelling of diffusion of caesium in the pore space of compacted salt grit has to use the value of the diffusion coefficient of caesium in free water to be realistic.

The experiment showing results qualitatively closest to those of experiment 6 (porosity n = 2 %) is experiment number 11 (n = 4 %). Experiment 11 also yields tracer fluxes into the sink reservoir with a magnitude as expected from diffusion in the pore water with the same diffusion coefficient as in free water. On the other hand it shows an unexpected effect: a very rapid decrease und subsequent increase of the tracer flux. Inbetween the time of decrease and increase, the tracer flux was significantly lower for some time or not detectable at all. This behaviour is in disagreement to the typical results obtained from through-diffusion experiments with other porous media.

An even more pronounced effect of high fluctuations in the tracer flux was also observed in the experiments number 8 (n = 2 %) and 10 (n = 4 %). These two experiments show long time intervals during the experiment where no or only a small tracer flux to the sink reservoir is observed. The maximum flux observed in those two experiments is lower than that in experiments number 6 and 11, i.e. lower than the flux expected for pore diffusion like in free water. The observed effect seems to be independent from the initial physical porosity. The reason for this effect might be

1. that in contrast to experiment 6 the diffusion process in this case is affected by an interaction of the tracer and the salt or
2. that the pore space in those two samples is not fully connected or accessible for the diffusion process and therefore the porosity determining the effective diffusion coefficient is lower than the physical porosity calculated from the compaction process.

The latter explanation seems much more reasonable to us, because the tracer used was the same in all experiments and the temporal development of the measured concentration in the experiments 8 and 10 does not fit to the expected behaviour if lower diffusion coefficients would be responsible for the effect.

This does not explain the high fluctuation of the determined fluxes with measured concentrations in the sink reservoir even below the detection limit. This obviously contradicts the idea of a homogenous and temporal invariant porous medium. We interpret

those fluctuations with a continuous dissolution and recrystallization of the salt in the sample resulting in a continuous restructuring of the pore space.

Recrystallization of salt has been observed for rock salt samples and is reported in the literature. Olander and other authors studied the movement of fluid inclusions in rock salt due to dissolution and crystallization in a temperature gradient field e.g. /OLA 84/. But even without the presence of a temperature gradient, the movement of water in rock salt due to recrystallization has been reported /TER 05/, /URA 86/. However, to our knowledge there are no publications which report this effect for compacted crushed salt.

The following effect is assumed: The restructuring of the pore space seems to lead to closed areas of pore water in the sample which may open up again after some time. The recrystallization of the salt in the crushed salt sample can even lead to a completely closed pore space for some time. If parts or even all of the pore space are closed in a way that the diffusion front is not able to move forward anymore, but is still connected to the source reservoir it may lead to the effect that the tracer concentration in this area is increasing with time. When this area opens up again towards the sink reservoir this may lead to comparably fast increase and high fluxes to the sink reservoir, since the concentration gradient between the mentioned area and the sink reservoir is higher than expected in the normal case.

This behaviour is schematically illustrated in figure 6.20. The left picture (i) depicts the normal behaviour of diffusion in a porous medium. In the horizontal direction, a concentration profile establishes according to the diffusive front propagating through the sample with high concentrations at the boundary to the source reservoir (left hand side) and low concentrations at the sink reservoir (right hand side of the sample). In the vertical direction, the concentration is equally distributed all over the whole cross section of the sample. The middle picture (ii) shows the situation if part of the sample is isolated from the rest of the sample. This part is indicated by the red line. In this case, the concentration in the isolated part increases until the concentration at point (A) is equal to point (B), because there is no tracer flux from this part towards the sink. The flux to the sink is accordingly decreased by the same percentage as the proportion between the cross-section of the isolated part and the sample. The right picture (iii) shows the situation if the area opens up again towards the sink reservoir. In this case, the gradient between point (A) and the sink reservoir is higher than at a comparable point outside the isolated part of the sample, leading to an increased flux to the sink reservoir. A potential ad-

ditional diffusive flux in vertical direction from the previously isolated area is not depicted in (iii).

However it cannot be ruled out that these processes occur on the sample surface towards the source or sink reservoirs leading to a sealing of these surfaces and therefore have to be regarded as an experimental artefact. In that case, the effect would have to occur on the sink reservoir side of the sample, since if precipitation occurs resulting in a sealing of the sample inlet side, the distance for diffusion to the sink reservoir would be too long and the diffusive transport too slow, to result in such dramatic flux variations as observed in the experiments.

Permeability measurements have been repeated on the samples 8, 10 and 11 a second time after finishing the diffusion experiments. These measurements have shown no reduction in the permeability values compared to the initial measurements. This finding contradicts the possibility of a permanent blockage of the pore space. This behaviour also suggests the possibility of a precipitation of salt on the sink sample side which is removed during the permeability measurement.

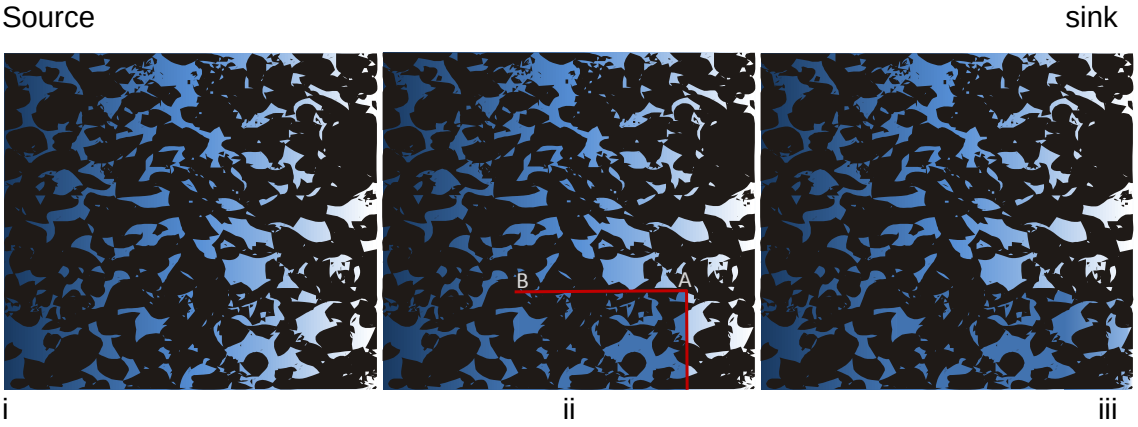

Fig. 6.20 Schematic illustration of diffusion in the pore space of compacted crushed salt

Very long time frames are regarded in long-term safety assessments. During such time frames, diffusive transport processes may dominate the radionuclide release from the containment-providing rock zone. The project DIKOSA was started to contribute to the answer of the question about how the diffusion of radionuclides takes place in the compacted backfill of a repository in salt. There have been new results achieved in DIKOSA which suggest that the diffusion in compacted crushed salt is not fully comparable to those in a homogeneous, temporally stable porous medium like sand or clay.

With results from four experiments, the existing data basis is however far too small to make reliable statements on how to consider diffusion in the compacted crushed salt in long-term safety assessment calculations in the future. The experiments suggest that the diffusion might be affected in a way that the diffusive radionuclide flux in the pore space of the compacted crushed salt is lower than in free water, but not necessarily by the reduction of the diffusion coefficient, but by the reduction of the accessible pore space. Long-term safety assessment calculations should continue to use the diffusion coefficient in free water to consider diffusion of radionuclides in the pore water of compacted crushed salt as long as no additional results are obtained. A larger number of experiments will be needed to improve the statements made. Additional experiments could be performed:

- to improve the data basis: this would need a larger numbers of experiments using the same tracer,
- to determine the effect of the species: this would need additional experiments with other tracers,
- to determine the long-term behaviour: this would need experiments for a much longer time span, to investigate if the recrystallization tends to close the pore space of the samples with time or if the pore space just restructures, but stays open.

As overall conclusion it has to be clearly stated that the results achieved in the experiments numbers 6 and 11 show that no reduction of the pore diffusion coefficient could be observed at a low porosity of 2 %. A potential long-term reduction of the diffusive flux due to structural changes in the pore space leading to a partial sealing of the pore space will be difficult to justify for the long-term. Therefore, the approach used in the long-term safety assessment so far remains valid: The diffusion of radionuclides in the pore space of compacted crushed salt occurs with the same diffusion coefficient as in free water. The diffusive flux however, is of course reduced linearly with the decreasing porosity due to the reduction of the effective cross-sectional area as given in equation 2.2 by Fick’s law for porous media.

7 Integration of the results in a safety assessment code

The integrated safety assessment code LOPOS (Loop structures in repositories) has been developed by GRS to simulate the one-dimensional, single-phase transport processes in the repository mine of a nuclear waste repository in salt /HIR 99/. A simulation includes the calculation of the inflow of brine from the overburden, through the mine to the emplaced waste, the mobilisation of the radionuclides from the waste matrix and the transport of the radionuclides through the repository mine up to the shaft top /REI 16/.

For modelling the transport in the repository mine, the mine is virtually broken down into segments, each representing parts of the mine. These segments are linked in all six directions in space to ring-shaped paths finally representing any potential structure of a repository mine. In each of the segments the relevant processes like convergence of the salt host rock, reduction of void spaces and compaction of the backfill are simulated. Different segment types exist for open or backfilled spaces, drift, seals, shafts, emplacement locations and more to represent the different processes that have to be accounted for.

The fluid pressure, brine flow and radionuclide transport are calculated simultaneously by a non-linear balance equation for all segments on the basis of the equation of continuity. In porous media like backfilled drifts, a flow according to the Darcy law is assumed, while in open spaces a flow according to the equation by Hagen-Poiseuille is modelled.

The radionuclide transport between the different segments is simulated by the transport equation according to the method of finite elements with variable time stepping. As transport mechanisms advection, dispersion and diffusion and if applicable convection are taken into account. The discretisation of time is controlled by stability criteria of the equation solver.

It was initially planned to further develop the LOPOS code, to consider the dependency of the diffusion coefficient of the crushed salt porosity in the calculation of the diffusive transport. At the current stage, the diffusive flux is directly proportional to the porosity of the crushed salt as described by Fick’s law, but the diffusion coefficient itself is independent from the porosity. Two steps were performed during the project to prepare the LOPOS code development:

1. **Analysis of the influence of the diffusion coefficient on the radionuclide transport:** Already with the current LOPOS version, the influence of the new results can be estimated by running several individual simulations for appropriate ranges of diffusion coefficients. Additionally, separate simulations may be run for different stable tracers of representative elements with a range of appropriate diffusion coefficients.

2. **Analysis of the LOPOS code:** The diffusion coefficient is used for the calculation of the radionuclide transport in different code subroutines. A detailed analysis of the code and the data structures was needed to plan the development work of the LOPOS code.

The following two subsections describe the two steps undertaken prior to the actual development work. Due to the experimental result which did not yield a direct relationship between the value of the diffusion coefficient and the porosity of the crushed salt, the implementation of such a relationship in the LOPOS code was not carried out: Long-term safety assessment calculations should use the diffusion coefficient in free water to consider diffusion of radionuclides in the pore water of compacted crushed salt as long as no additional results are obtained.

7.1 Analysis of the influence of the diffusion coefficient

Due to the complexity and large amount of work needed for the analysis of the influence of the diffusion coefficient value on the radionuclide transport out of a nuclear waste repository in salt, synergetic effects have been used and the work was conducted in cooperation with the project ISIBEL-II /BUH 16/. The project ISIBEL-II calculated integrated long-term safety assessment based on the preliminary safety assessment of the Gorleben site (VSG) /LAR 13/. The following chapter only summarized the most important results relevant for the topic under investigation here. A detailed description of the input data, model assumptions and of other results can be found in /BUH 16/.

The simulations have been performed with the code package RepoTREND (Transport and Retention of Non-decaying and Decaying contaminants in final Repositories) /REI 16/ from which the modules LOPOS and BioTREND have been used. The segment structure shown in figure 7.1 for the near-field is based on the one used in the project ISIBEL /BUH 08/ and was modified according to the repository concept devel-

oped in VSG /BOL 12/. The input data is also based on the VSG and is not listed in the following, but can be found in /BUH 16/.

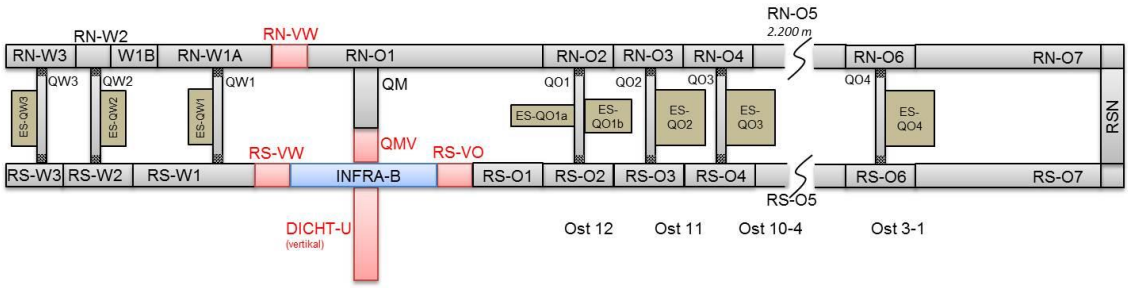

Fig. 7.1 Segment structure of the LOPOS model (not to scale)

Since the flow of brines grinds to a halt at late times, advective transport does not play a role on the long-term and the radionuclide transport is dominated by diffusion. The value of the diffusion coefficient therefore is expected to be of high relevance. In the reference case, a diffusion coefficient which is independent of the porosity of the crushed salt was used and a value of $1.5 \cdot 10^{-9}$ m^2/s was assumed, which is close to the expected value for caesium (see section 5.4.1). In the probabilistic simulations, a bandwidth of $1 \cdot 10^{-9}$ to $2 \cdot 10^{-9}$ m^2/s with a uniform probabilistic density function was considered to reflect the uncertainty. These values are in the range of the diffusion coefficients in free water and comply with the findings in the DIKOSA project and the statement given above that term safety assessment calculations must conservatively use the diffusion coefficient in free water to consider diffusion of radionuclides in the pore water of compacted until additional results are obtained. In the VSG project a lower value of $1 \cdot 10^{-10}$ m^2/s was used /LAR 13/. The results are presented as RGI-value (Radiologischer Geringfügigkeitsindex) /MOE 12/, which gives the ratio of the determined dose value compared to a regulatory limit.

The probabilistic simulation shows a variation of the calculated maximum RGI index of about one order of magnitude for the variation of the diffusion coefficient by a factor of two as can be seen from figure 7.2. The sensitivity analysis clearly shows that the diffusion coefficient is the most significant parameter for the RGI value as can be seen from the contribution to sample mean (CSM) plot shown in figure 7.3. A what-if case considering much lower diffusion coefficients confirm these findings. All these results clearly show the high relevance of the diffusion and thus the diffusion coefficient on the radionuclide transport and the need for the reduction of uncertainty of the diffusion coefficient.

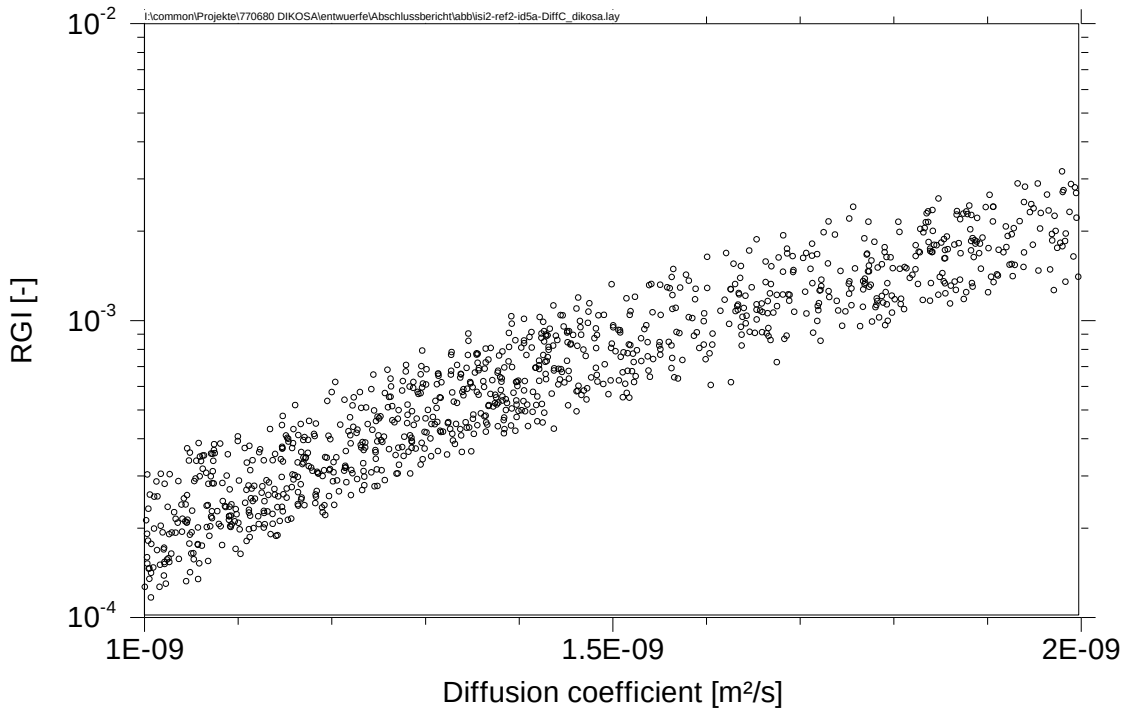

Fig. 7.2 Scatterplot for the variation of the RGI indicator in relation to the diffusion coefficient

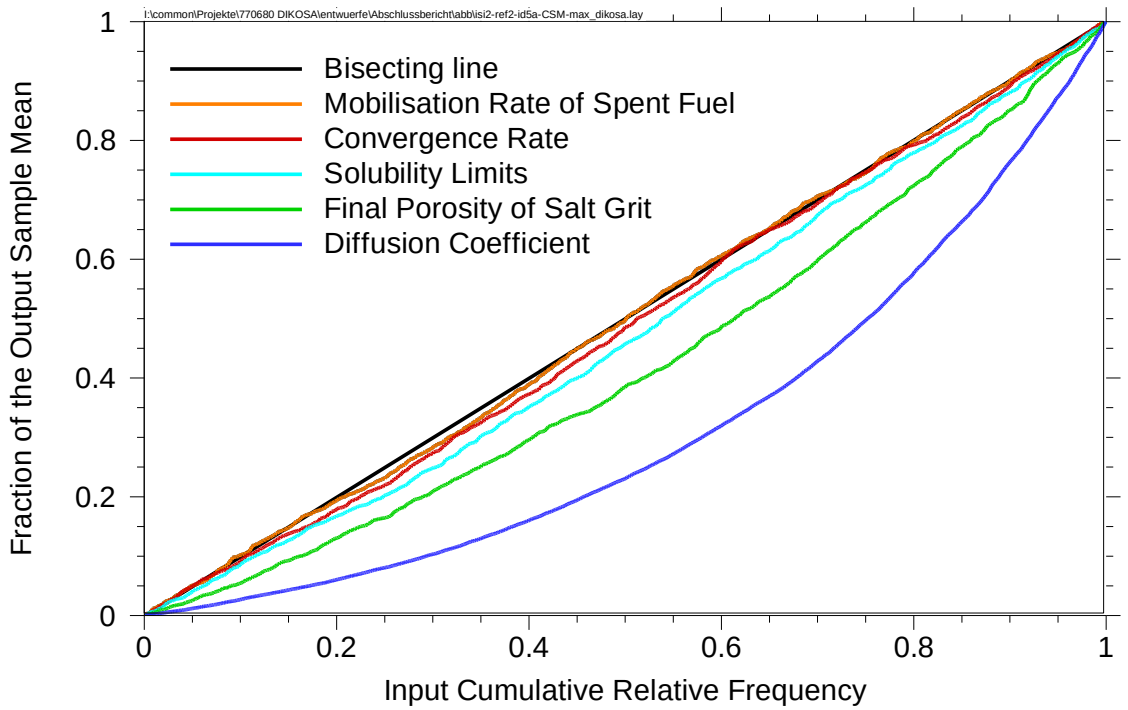

Fig. 7.3 Contribution of the different independent parameters to the sample mean (CSM)

7.2 Analysis of the LOPOS code

The current version of LOPOS was analysed to plan the development work to implement a porosity dependent diffusion behaviour. The diffusion coefficient is used in the simulation in two different respects: On the one hand it influences the radionuclide distribution within the segments, and on the other hand, it is used for calculating the transfer between the segments. These two effects are implemented in different routines in LOPOS, which has to be accounted for in the correct parameter description of all respective routines. At this stage, the diffusion coefficient is dependent on the temperature, but the same diffusion coefficient is used for all radionuclides and no dependence of the pore diffusion coefficient on the porosity of the backfill is regarded /HIR 99/.

An extension of the program code LOPOS in order to regard the varying diffusion coefficient would imply the need of additional input parameters. Therefore, not only the required changes to the code LOPOS, but also to the user interface XENIA /REI 16/ will be explained in the following.

The dependence of the diffusion coefficient on the porosity will be accounted for by a new routine. In a first step, the diffusion coefficient will be provided as a table with a varying number of parameter values. In between these points, LOPOS will interpolate the diffusion coefficient linearly, outside these points the nearest value will be used. The influence of the new implementation of the diffusion coefficient on time integration schemes needs to be considered.

The current computation procedure of the radionuclide transport in LOPOS is depicted in figure 7.4. The left column lists the involved variables and the right column lists the related computational steps of the routine *CLOPOS* as well as subsequently called routines labelled with (::). The variables are either valid only locally or available for each routine that uses the same *CommonBlock*. To some extend they allocate memory for each **n**uclide, each **s**egment and each spatial **d**irection (bold letters refer to the nomenclature in the following figures) already. The coloured arrows indicate whether the variables are read only (red) or are also being modified (green). Binoculars represent the link to the more detailed following figures (e. g. *Call LoSeg*).

The diffusion coefficient is currently stored in the field of element specific parameters *RBPY*. When the diffusion coefficient is element specific, the terms *RSLD*, *RSLT*, calculated by the routines *LOSLAD*, *LOSLAT*, and also the interim variable *RUSY* will be

element specific as well. The increase of their dimensionality has to be taken into account in all involved routines in order to also make the variables *RUNY*, *RONY* element specific.

Details of the computation in the routine *LoSeg* (figure 7.5) show that the increase in dimensionality of *RUSY* also impacts further interim variables *RISY*, *RIZY* and *RINY*. The variables of the *CommonBlock* are used in other routines as well, which are not shown here like the routines for the control output and initialization. The implementation of the dependence of the diffusion coefficient on the porosity and the respective element requires extensive changes of the codes in numerous computations, dimensions and transfer lists, namely by modifying the variables of the *CommonBlock*. An alternative approach to minimize the required changes would be to introduce new auxiliary variables. This way the computation procedure for *RUNY* shown in figure 7.4 will still consider the modified, element specific diffusion coefficient without running the risk of accidently skipping single interim variables. Disadvantages of this implementation would be the twofold computation of the variables and the lack of the possibility to write the newly introduced interim variables in any output file.

The local modification of the diffusion coefficient and its application for the computation of the radionuclide transport within the segments is finally depicted in figure 7.6.

The user interface XENIA requires the provision of a table of diffusion coefficients as a function of specific elements and porosities. The dimension of this table will persist, only the number of values will increase. Technically, the input of the element specific and porosity dependent diffusion coefficient may be realized like for other element specific parameters by the XENIA module *elementdata-NF* (nearfield). The number and the respected set of values may vary in the XENIA user interface. In LOPOS, this number is limited due to static variable allocation. The dynamic structure of the XENIA input mask is used to specify the parameters rather than using an external provision of data engaged for the geological temperature profiles input, e. g. The user may define an optional number of parameters of the same type. The measured diffusion coefficients will be employed for a number of future simulations. Thus it is favourable to store the data in a data base in order to avoid their repeated error-prone input. The universal diffusion coefficient used so far will be maintained for those radionuclides, which are not specifically listed in the data base. It will be ensured, that besides the new implementation of the diffusion coefficient, the conventional handling of the diffusion coefficient will also be still applicable.

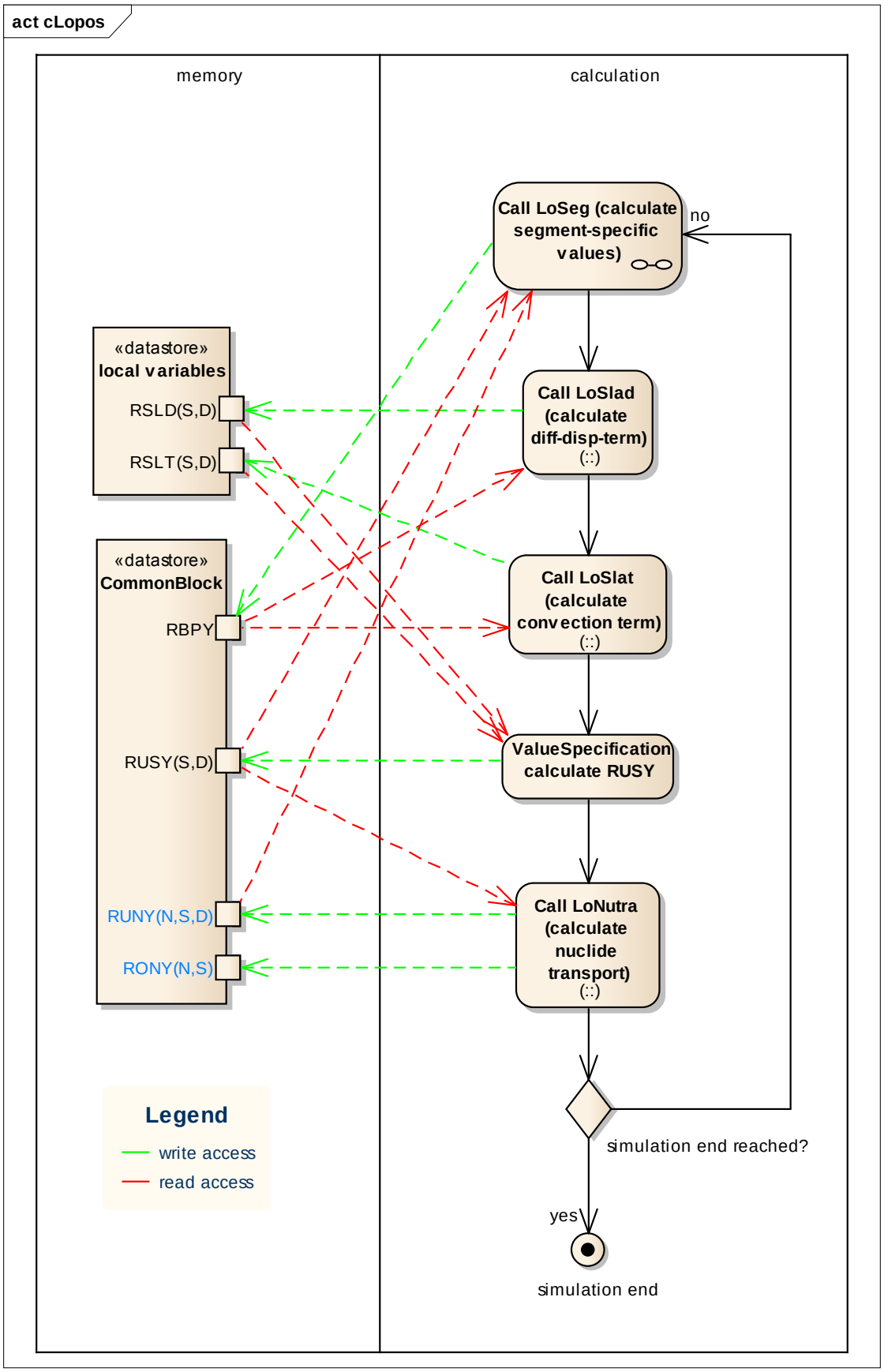

Fig. 7.4 Computation procedure for *RUNY* in the routine *CLOPOS*

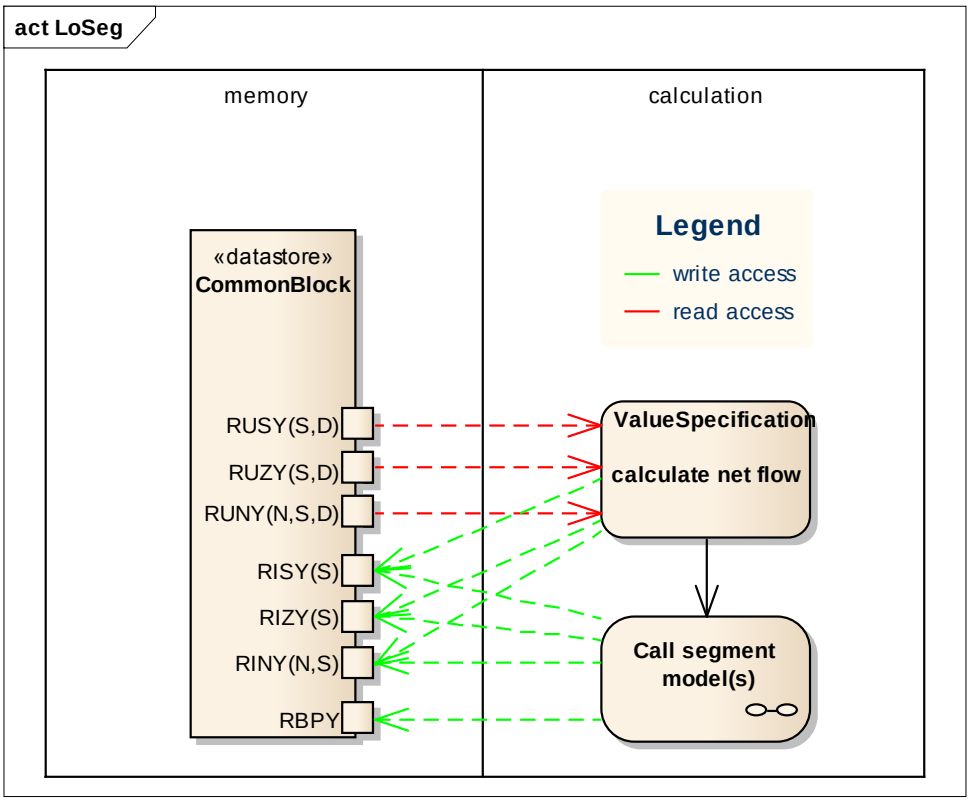

Fig. 7.5 Main computation procedure for *RUNY* in the routine *LOSEG*

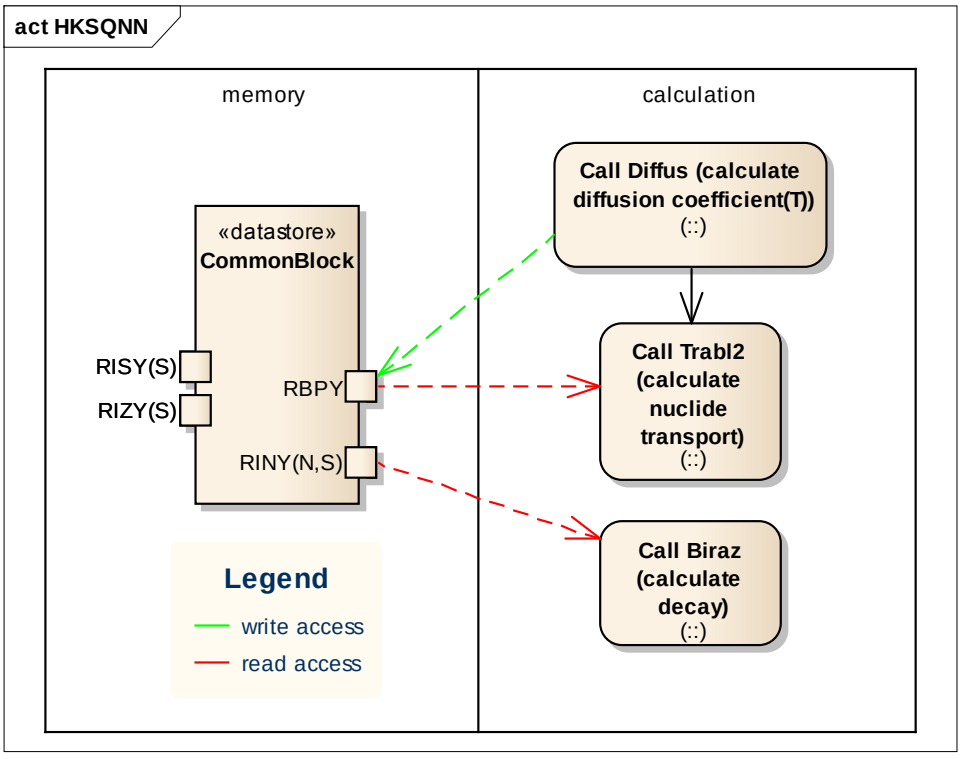

Fig. 7.6 Main computation procedure for *RUNY* in the segment model *HKSQNN*

8 Résumé

Recent safety assessments for high-level nuclear waste repositories in salt host rock have shown that in the reference case, with the proven integrity of the barriers, a contact of significant volumes of brine with the waste is generally to be expected only at such a point in time, when the convergence of the openings has already reached its final state /LAR 13/, /BUH 08/ and /BUH 16/. In this case, no flow of brines out of the repository by displacement from convergence occurs. Consequently, no advective transport of radionuclides in the brine occurs likewise and the diffusive transport process may dominate the radionuclide release from the containment-providing rock zone. Hence, the diffusion coefficient of the radionuclides in the pore water of the compacted crushed salt is the most sensitive parameter for the radionuclide flux from the repository.

In case of a repository in a salt formation, the medium in which the diffusive transport takes place is the crushed salt used as backfill in the drifts, as the host rock itself is impermeable. The crushed salt is emplaced with a porosity of 30 % or more and is compacted with time to a porosity in the range of 1 % or less by the convergence of the salt rock. The pore space is at least partially filled with saturated brine solution. So far, diffusion coefficients like in the free water have been applied for the diffusion in pore water in models for long-term safety assessments. This conservative assumption was used, since data for the diffusion coefficient of dissolved substances in crushed salt have been missing. Furthermore, the diffusion coefficient in the pore water was assumed to be constant and independent from the porosity of the crushed salt since this dependence was not investigated before.

This report for the first time presents measurements of diffusion coefficients of pollutants in the pore water of compacted crushed salt by through-diffusion experiments. Although this method is rather common, the use of salt and saturated saline solutions involved a number of difficulties which demanded for a further development of the method. This comprises the design and construction of the diffusion cells. To withstand the high pressures during the crushed salt compaction and corrosion potential of the saturated sodium chlorine brines, the cells were manufactured using titanium with a wall thickness of up to 50 mm, resulting in rather large and heavy cells of 35 kg.

The major issue working with salt and saturated brines was the effect of dissolution and precipitation. Precipitation of salts from the brine sometimes resulted in crystal growth

in tubes and in the cell and consequently resulted in the blocking of the brine flow. Dissolution can potentially result in alteration of the salt sample surface. Consequently, temperature control was established in the dedicated laboratory area resulting in a temperature variation less then ± 2 °C. Eventually, it is not sure whether the temperature stability was sufficient (see below) or whether better temperatures control is needed. This however, would need large costly boxes to be used.

All diffusion experiments were all carried out with caesium as tracer. In one of the experiments, additionally iodine and neodymium were used. Although many of the experiments failed due to experimental problems, the developed method has shown to be suitable to determine the diffusion coefficients. Four experiments have finally succeeded to result in long time series of a measured tracer concentration and yielded estimations of the diffusion coefficient of caesium in the pore water of the compacted crushed salt samples with a porosity of two and four percent respectively. The permeability values determined for these samples are in the expected range from previous experiments.

The results obtained from the four diffusion experiments show a remarkable different behaviour and all yield unique concentration versus time plots. One experiment shows a constant increase in the determined flux of caesium from the source to the sink reservoir, which within the measurement uncertainty is in good agreement with the expected evolution from transport by diffusion. The effective diffusion coefficient calculated from this experiment indicates that the diffusion in the pore space even at a low porosity of 2 % occurs as in free water. No significant effect of a tracer-matrix interaction – as it is known for example for anion exclusion in clays – can be noticed from the data. Likewise, no reduction of the pore diffusion coefficient can be expected for higher porosities, but only for lower porosities. From this experiment alone it can be concluded that modelling of diffusion of caesium in the pore space of compacted salt grit has to use the value of the diffusion coefficient of caesium in free water to be realistic.

The other three samples show an unexpected effect: A rapid decrease und subsequent increase of the tracer flux. Between the decreases and increases, the tracer flux determined was significantly lower or was even not detectable at all. Two experiments show long time intervals during the experiment with no or only a small tracer flux to the sink reservoir.

This behaviour is in disagreement with the typical results obtained from through-diffusion experiments with other porous media. It obviously contradicts the idea of a homogenous and temporally invariant porous medium. We interpret the fluctuations to result from a continuous dissolution and recrystallization of the salt in the sample accompanied by in a continuous restructuring of the pore space. It however cannot be fully ruled out that these processes occur on the sample surface and have to be regarded as an experimental artefact.

As overall conclusion it can be stated that the results achieved in the experiments suggest that no reduction of the pore diffusion coefficient occurs even at a low sample porosity of 2 %. A potential long-term reduction of the diffusive flux due to structural changes in the pore space leading to a partial sealing of the pore space might exist, but will be difficult to justify for the long-term. Therefore, the approach currently used in the long-term safety assessment to use a diffusion coefficient for free water for modelling pore diffusion in the pore water of crushed salt remains valid: The diffusive flux however, is reduced linearly with the decreasing porosity due to the reduction of the effective cross-sectional area according to Fick's law for porous media.

9 References

/DBE 08/ Überprüfung und Bewertung des Instrumentariums für eine sicherheitsanalytische Bewertung von Endlagern für HAW: ISIBEL. DBE-Tec, Bericht TEC-09-2008-AB, Peine, 2008.

/ALD 14/ Aldaba, D.; Glaus, M.; Leupin, O.; van Loon, L.R.; Vidal, M.; Rigol, A.: Suitability of various materials for porous filters in diffusion experiments. Radiochimica Acta, Vol. 102(8), pp. 723-730, 2014.

/BUH 08/ Buhmann, D., Mönig, J., Wolf, J.: Untersuchungen zur Ermittlung und Bewertung von Freisetzungsszenarien. Teilbericht zum Projekt ISIBEL: „Überprüfung und Bewertung des Instrumentariums für eine sicherheitliche Bewertung von Endlagern für HAW“. GRS-233, ISBN 978-3-939355-07-6, Gesellschaft für Anlagen- und Reaktorsicherheit (GRS) mbH. BMWi-FKZ 02E10055, Braunschweig, 2008.

/BUH 16/ Buhmann, D.; Laggiard, E.; Rübel, A.; Spießl,S.; Wolf, J.: Probabilistische Bewertung von Szenarien in Langzeitsicherheitsanalysen. BMWi-FKZ 02E10719, Gesellschaft für Anlagen- und Reaktorsicherheit (GRS) mbH, GRS-241, Braunschweig, 2016.

/BOL 12/ Bollingerfehr, W.; Filbert, W.; Dörr, S.; Herold, P.; Lerch, C.; Burgwinkel, P.; Charlier, F.; Thomauske, B.; Bracke, G.; Kilger, R.: Endlagerausklegung und –optimierung. Bericht zum Arbeitspaket 6. Vorläufige Sicherheitsanalyse für den Standort Gorleben. GRS-281, Gesellschaft für Anlagen- und Reaktorsicherheit, Köln, 2012.

/BOR 08/ Borkowski, M., Lucchini, J. F., Richmann, M. K., Reed, D. T. Actinide (III) Solubility in WIPP Brine: Data Summary and Recommendations. Report LA-UR 09-03222, Los Alamos National Laboratory, Los Alamos, NM, 2008.

/BOV 01/ Boving, T.B.; Grathwohl, P.: Tracer diffusion coefficients in sedimentary rocks: correlation to porosity and hydraulic conductivity. Journal of Contaminant Hydrology, Vol. 53(1-2), pp. 85-100, 2001.

/CHU 14/ Churakov, S.V.; Gimmi, T.; Unruh, T.; van Loon, L.R.; Juranyi, F.: Resolving diffusion in clay minerals at different time scales: Combination of experimental and modeling approaches. Applied Clay Science,Vol. 96, pp. 36-44, 2014.

/CRA 79/ Crank, J.: The Mathematics of Diffusion, Oxford University Press, Oxford, 1979.

/DIN 98/ DIN Deutsches Institut für Normung e. V.: DIN 18121-1: 1998-4. Baugrund, Untersuchung von Bodenproben - Wassergehalt - Teil 1: Bestimmung durch Ofentrocknung

/DIN 83/ DIN Deutsches Institut für Normung e. V.: DIN 18123: 1983-4. Baugrund, Untersuchung von Bodenproben – Bestimmung der Korngrößenverteilung

/DIN 04/ DIN Deutsches Institut für Normung e. V.: DIN 66137-2:2004-12. Bestimmung der Dichte fester Stoffe - Teil 2: Gaspyknometrie

/GEV 81/ Gevantman, L.H. (ed.): Physical Properties Data for Rock Salt. National Bureau of Standards Monograph 167, Washington, 1981.

/GLA 15/ Glaus, M.A.; Aertsens, M.; Maes, N.; van Laer, L.; van Loon, L.R.: Treatment of boundary conditions in through-diffusion: A case study of 85Sr2+ diffusion in compacted illite. Journal of Contaminant Hydrology, Vol. 177-178C, pp. 239-248, 2015.

/GRA 98/ Grathwohl, P.: Diffusion in Natural Porous Media, Contaminant Transport, Sorption/Desorption and Dissolution Kinetics. Kluwer Academic Publishers, 1998.

/HAR 96/ Hartikainen, J., Hartikainen, K., Hautojärvi, A., Kuoppamäki, K., Timmonen, J.: Helium gas methods for rock characteristics and matrix diffusion. POSIV A-96-22. Helsinki (Posiva Oy), 1996. p. 58.

/HER 11/ Herbert, H.-J.; Kasbohm, J.; Lan, N. T.; Meyer, L.; Thao, H. T. M.; Xie, M., Fe-Bentonite - Experiments and Modeling of the Interactions of Bentonites with Iron, BMWi-FKZ 02E10538, Gesellschaft für Anlagen- und Reaktorsicherheit (GRS) mbH, GRS-295, Braunschweig, 2011. p. 298.

/HIR 99/ Hirsekorn, R.-P.; Boese, B.; Buhmann, D.: LOPOS: Programm zur Berechnung der Schadstofffreisetzung aus netzwerkartigen Grubengebäuden. Gesellschaft für Anlagen- und Reaktorsicherheit (GRS) mbH, GRS-157, Braunschweig, Juni 1999.

/HU 08/ Hu, Q. H., Möri, A.: Radionuclide transport in fractured granite interface zones. Physics and Chemistry of the Earth 33 (2008) 1042–1049

/INF 11/ InfraServ Wiesbaden Technik GmbH & Co.KG, Angebot Nr. A-Mh-3000-110919 5 Titan-Messzellen, 13.07.2011

/JOS 60/ Jost, W.: Diffusion in solids, liquids and Gases. Academic Press, New York, 1960.

/KRO 09/ Kröhn, K.-P.; Stührenberg, D.; Herklotz, M.; Heemann, U.; Lerch, C.; Xie, M., Restporosität und -permeabilität von kompaktierendem Salzgrus-Versatz – REPOPERM Phase 1, BMWi-FKZ 02E10477, Gesellschaft für Anlagen- und Reaktorsicherheit (GRS) mbH, GRS-254, Braunschweig, 2009. p. 266.

/LAR 13/ Larue, J.; Baltes, B.; Fischer, H.; Frieling, G.; Kock, I.; Navarro, M.; Seher, H.: Radiologische Konsequenzenanalyse. Bericht zum Arbeitspaket 10. Vorläufige Sicherheitsanalyse für den Standort Gorleben. GRS-289, Gesellschaft für Anla-gen- und Reaktorsicherheit, Köln, 2013.

/LI 74/ Li, Y.-H., Gregory, S. Diffusion of ions in sea water and in deep-sea sediments. Geochimica et Cosmochimica Acta 38, 703-714, 1974.

/LID 05/ Lide, D. R., ed.. CRC Handbook of Chemistry and Physics (86th ed.). Boca Raton, CRC Press, 2005.

/LOO 03/ van Loon, L.R.; Soler, J.M.; Bradbury, M.H.: Diffusion of HTO, 36Cl− and 125I− in Opalinus Clay samples from Mont Terri. Journal of Contaminant Hydrology, Vol. 61(1-4), pp. 73-83, 2003.

/LOO 05/ van Loon, L.R.; Eikenberg, J.: A high-resolution abrasive method for determining diffusion profiles of sorbing radionuclides in dense argillaceous rocks. Applied Radiation and Isotopes, Vol. 63(1), pp. 11-21, 2005.

/LOO 15/ van Loon, L.R.; Mibus, J.: A modified version of Archie's law to estimate effective diffusion coefficients of radionuclides in argillaceous rocks and its application in safety analysis studies. Applied Geochemistry, Vol. 59, pp. 85–94, 2015.

/LUA 00/ Landesumweltamt Nordrhein-Westfalen: Empfehlungen für die Durchführung und Auswertung von Säulenversuchen gemäß Bundes-Bodenschutz- und Altlastenverordnung (BBodSchV). Merkblätter, Nr. 20. Essen (Landesumweltamt NRW), 2000.

/MOE 12/ Mönig, J.; Buhmann, D.; Rübel, A.; Wolf, J.; Baltes, B.; Fischer-Appelt, K.: Sicherheits- und Nachweiskonzept. Bericht zum Arbeitspaket 4. Vorläufige Sicherheitsanalyse für den Standort Gorleben. GRS-277, Gesellschaft für Anlagen- und Reaktorsicherheit, Köln, 2012.

/NAG 02/ Nagra: Projekt Opalinuston. Synthese der geowissenschaftlichen Untersuchungsergebnisse. Entsorgungsnachweis für abgebrannte Brennelemente, verglaste hochaktive sowie langlebige mittelaktive Abfälle. NTB-02-03, Nagra, Wettingen 2002

/OLA 84/ Olander, D.R.: A Study of Thermal-Gradient-Induced Migration of Brine Inclusions in Salt: Final Report. Office of Nuclear Waste Isolation, ONWI-538, Columbus, 1984.

/PAR 09/ Park, C.-K.; Baik, M.-H.: Diffusion of some chemical species through a granite considering their geochemical properties. Korean Journal of Chemical Engineering, Vol 26(5), pp. 1279-1285, 2009.

/PEA 99/ Pearson, F.J.: What is the porosity of a mudrock? in: Alpin, A.C.; Fleet, A.J.; Macquaker, J.H.S. (Editoren), Muds and Mudstones: Physical and Fluid Flow Properties. Geological Society, London, Special Publications, 158, pp. 9-11, 1999.

/REI 16/ Reiche, T.: RepoTREND – Das Programmpaket zur integrierten Langzeitsicherheitsanalyse von Endlagersystemen, GRS-413, Gesellschaft für Anlagen- und Reaktorsicherheit (GRS) mbH, Braunschweig, 2016

/RUE 02/ Rübel, A.; Sonntag, C.; Lippmann, J.; Pearson, F.J.; Gautschi, A.: Solute transport in formations of very low permeability: Profiles of stable isotopes and dissolved noble gas contents of pore water in the Opalinus Clay, Mont Terri, Switzerland. Geochimica et Cosmochimica Acta, Vol. 66, No.8, pp. 1311-1321, 2002.

/ROT 99/ Rothfuchs, T.; Feddersen, H.-K.; Kröhn, K.-P.; Miehe, R.; Wieczorek, K., The DEBORA-Project: Development of Borehole Seals for High Level Radioactive Waste – Phase 2, BMWi-FKZ 02E8715, Gesellschaft für Anlagen- und Reaktorsicherheit (GRS) mbH, GRS-161, Braunschweig, 1999. p. 109.

/SHA 91/ Shackelford, C.D.: Laboratory diffusion testing for waste disposal – A review. J. Contam. Hydrol., Vol. 7, pp. 177-217, 1991.

/SKA 83/ Skagius, K., Neretnieks, I.: Diffusion measurements in crystalline rocks. SKB 83-15. Stockholm (Royal Institute of Technology), 1983. p. 19.

/TAC 15/ Tachi, Y., Ebina, T., Takeda, C., Saito, T., Takahashi, H., Ohuchi, Y., Martin, A. J.: Matrix diffusion and sorption of Cs^+, Na^+, I^- and HTO in granodiorite: Laboratory-scale results and their extrapolation to the in situ condition. Journal of Contaminant Hydrology 179 (2015) 10–24

/TER 05/ Ter Heege, J.H.; De Bresser, J.H.P.; Spiers, C.J.: Rheological behaviour of synthetic rocksalt: the interplay between water, dynamic recrystallization and deformation mechanisms. Journal of Structural Geology 27, pp. 948–963, 2005.

/URA 86/ Urai, J.L.; Spiers, C.J.; Zwart, H.J.; Lister, G.S.: Weakening of rock salt by water during long-term creep. Nature, 324, pp. 554-557, 1986.

/VAL 96/ Valkiainen, M., Aalto, H., Lehikoinen, J., Uusheimo, K.: The effect of thickness in the through-diffusion experiment. Final report. Espoo (Technical Research Center of Finland (VTT)), 1996. p. 30.

/ZHA 04/ Zhang, C.-L.; Rothfuchs, T.; Moog, H. C.; Dittrich, J.; Müller, J. (2004): Thermo-Hydro-Mechanical and Geochemical Behaviour of the Callovo-

Oxfordian Argillite and the Opalinus Clay. GRS-202, Gesellschaft für Anlagen- und Reaktorsicherheit (GRS) mbH, Braunschweig, 2004.

List of figures

Fig. 3.1 Schematic illustration of a through-diffusion experiment 9

Fig. 3.2 Normalised concentration in a sample of 4 cm length for different times of a through-diffusion experiment ($D_a = 5 \cdot 10^{-11}$ m/s) 11

Fig. 3.3 Normalised flux out of a sample of 4 cm length of a through-diffusion experiment ($D_a = 5 \cdot 10^{-11}$ m/s) 11

Fig. 5.1 Construction design of the diffusion cells: General assembly drawing and exploded view, after /INF 11/ 21

Fig. 5.2 Photos of the different parts of the diffusion cell 24

Fig. 5.3 Detail view of the sleeve nut 25

Fig. 5.4 Detail view of milled surface in the top flange 25

Fig. 5.5 Grain size distribution of the Grasleben and Gorleben crushed salt used in this project compared to the grain size distribution of the Asse crushed salt used in /KRO 09/ 27

Fig. 5.6 XRD spectrum of the Gorleben crushed salt 28

Fig. 5.7 Chemical analysis of Grasleben and Gorleben brines 31

Fig. 5.8 Results of the tracer interaction pretests with the Grasleben brine and the synthetic brine 35

Fig. 6.1 Time-dependent flux (upper figure) and concentration of the tracer in the sink reservoir (lower figure) for sample lengths of 0.04 m (solid lines) and 0.08 m (dashed lines) for three different diffusion coefficients . 38

Fig. 6.2 Amsler hydraulic press for compaction of the samples 41

Fig. 6.3 Temporal evolution of the applied load of the uniaxial press and the calculated sample porosity for sample 6 42

Fig. 6.4 Exemplary curves for pressure and brine flux during permeability measurement 42

Fig. 6.5 Experimental setup during sample saturation and permeability measurement 43

Fig. 6.6 Schematic illustration of the diffusion experiment setup (not to scale) 44

Fig. 6.7 Photos of the diffusion experiment setup from front and above 46

Fig. 6.8 Temporal evolution of the room temperature of the lab for a one-year time period starting at 01.03.2015 47

Fig. 6.9 Temporal evolution of the pumping rate for the experiments 8, 10 and 11 47

Fig. 6.10 Sampling density for the experiments 8, 10 and 11 48

Fig. 6.11 Reproducibility of brine density measurement 50

Fig. 6.12 Reproducibility of concentration measurement 50

Fig. 6.13 Normalised Cs-flux measured for experiment number 6 together with modelled data 53

Fig. 6.14 Normalised iodine and selenium fluxes measured for experiment number 6 together with modelled data 53

Fig. 6.15 Normalised flux measured for experiment number 8 together with modelled data 54

Fig. 6.16 Normalised flux measured for experiment number 10 together with modelled data 55

Fig. 6.17 Normalised flux measured for experiment number 11 together with modelled data 56

Fig. 6.18 Permeability of the DIKOSA samples compared to data presented in the project REPOPERM /KRO 09/ 57

Fig. 6.19 Comparison of the result of experiments 6, 8, 10 and 11 58

Fig. 6.20 Schematic illustration of diffusion in the pore space of compacted crushed salt 61

Fig. 7.1 Segment structure of the LOPOS model (not to scale) 65

Fig. 7.2 Scatterplot for the variation of the RGI indicator in relation to the diffusion coefficient 66

Fig. 7.3 Contribution of the different independent parameters to the sample mean (CSM) 66

Fig. 7.4 Computation procedure for *RUNY* in the routine *CLOPOS* 69

Fig. 7.5 Main computation procedure for *RUNY* in the routine *LOSEG* 70

Fig. 7.6 Main computation procedure for *RUNY* in the segment model *HKSQNN* 70

Fig. A.1 Construction design of the diffusion cells: General assembly drawing and exploded view /INF 11/ 87

Fig. A.2 Pos. 1. of the diffusion cells. Positioning within diffusion cell given in the general assembly drawing in Fig. A.1 /INF 11/ 88

Fig. A.3 Pos. 2. of the diffusion cells. Positioning within diffusion cell given in the general assembly drawing in Fig. A.1 /INF 11/ 89

Fig. A.4 Pos. 4. of the diffusion cells. Positioning within diffusion cell given in the general assembly drawing in Fig. A.1 /INF 11/ 90

Fig. A.5 Pos. 3. of the diffusion cells. Positioning within diffusion cell given in the general assembly drawing in Fig. A.1 /INF 11/ 91

Fig. A.6 Pos. 5. of the diffusion cells. Positioning within diffusion cell given in the general assembly drawing in Fig. A.1 /INF 11/ 92

Fig. A.7 Pos. 10. of the diffusion cells. Positioning within diffusion cell given in the general assembly drawing in Fig. A.1 /INF 11/ 93

List of tables

Tab. 5.1 Results of the chemical analysis of the saturated Grasleben brine (<DL = below detection limit) 30

Tab. 5.2 Results of the chemical analysis of the saturated Gorleben brine 30

Tab. 5.3 Limits of determination for selected tracers (ICP-MS) 34

Tab. 5.4 Results of the tracer interaction pretest with the Grasleben brine 34

Tab. 5.5 Results of the tracer interaction pretest with the synthetic brine..... 35

Tab. 6.1 Overview of main sample properties..... 52

A. Construction design of the diffusion cells

The diffusion cells were designed and manufactured by the company *InfraServ Wiesbaden Technik GmbH & Co.KG* /INF 11/. The following constructional drawings were prepared by *InfraServ*.

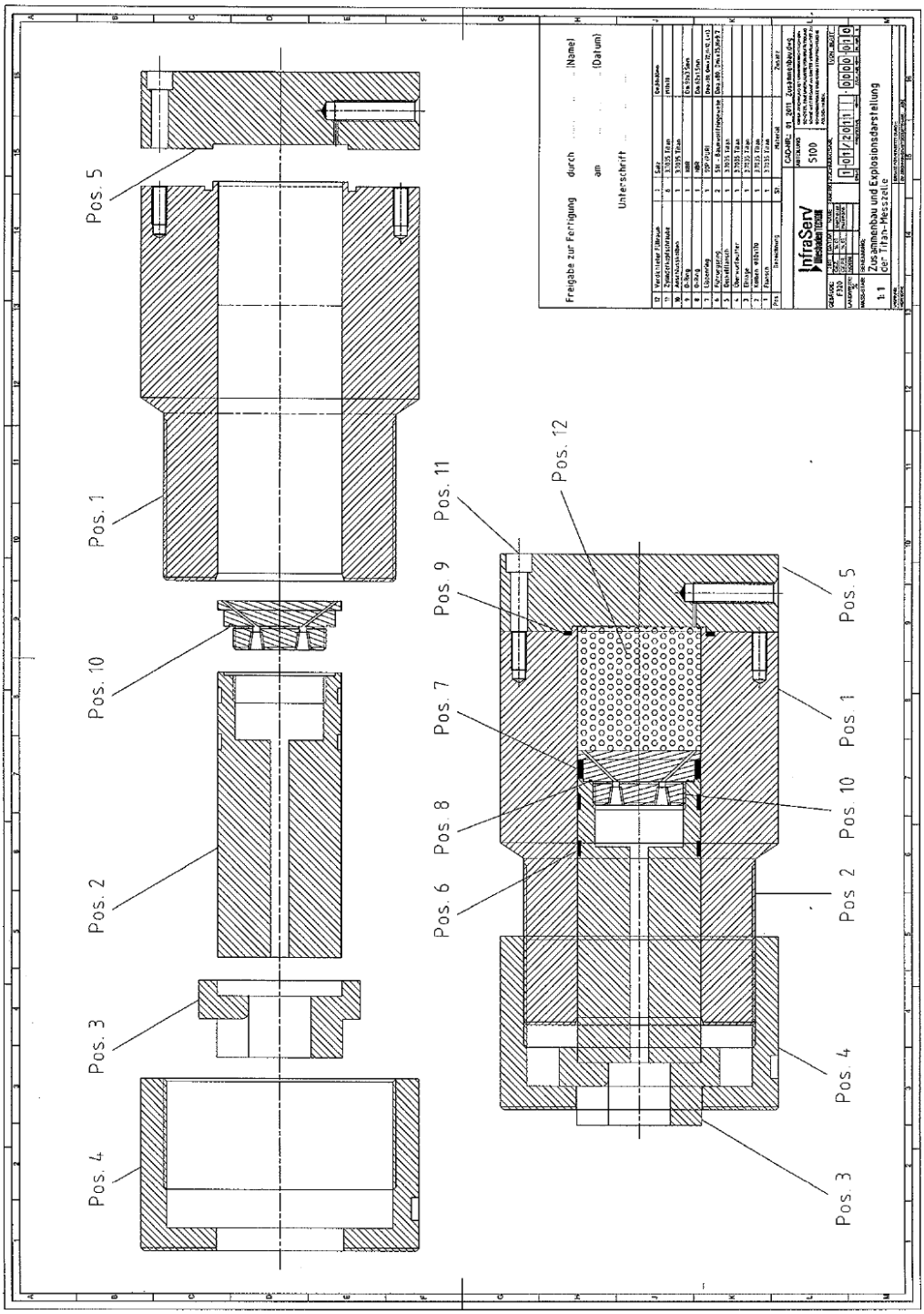

Fig. A.1 Construction design of the diffusion cells: General assembly drawing and exploded view /INF 11/

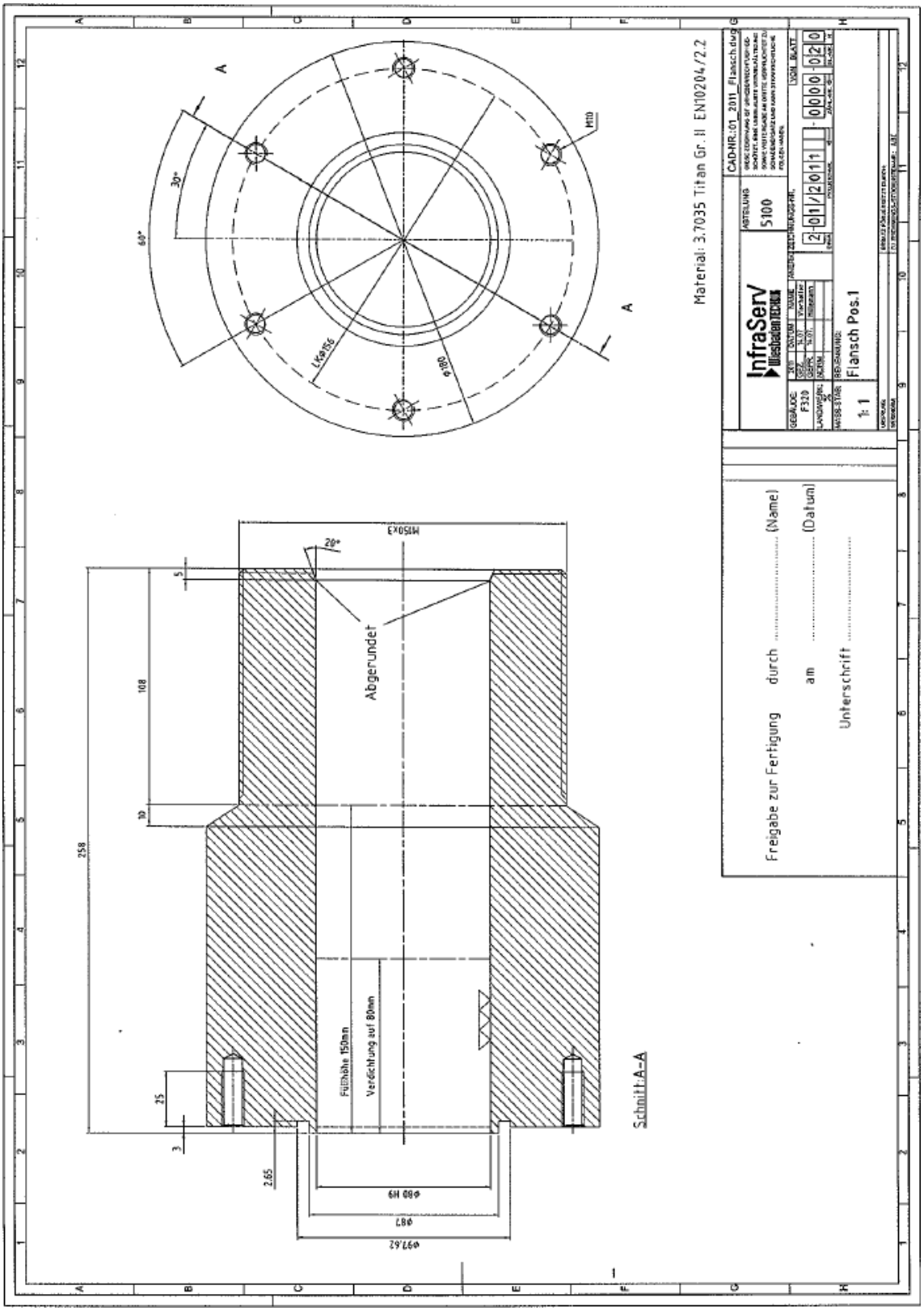

Fig. A.2 Pos. 1. of the diffusion cells. Positioning within diffusion cell given in the general assembly drawing in Fig. A.1 /INF 11/

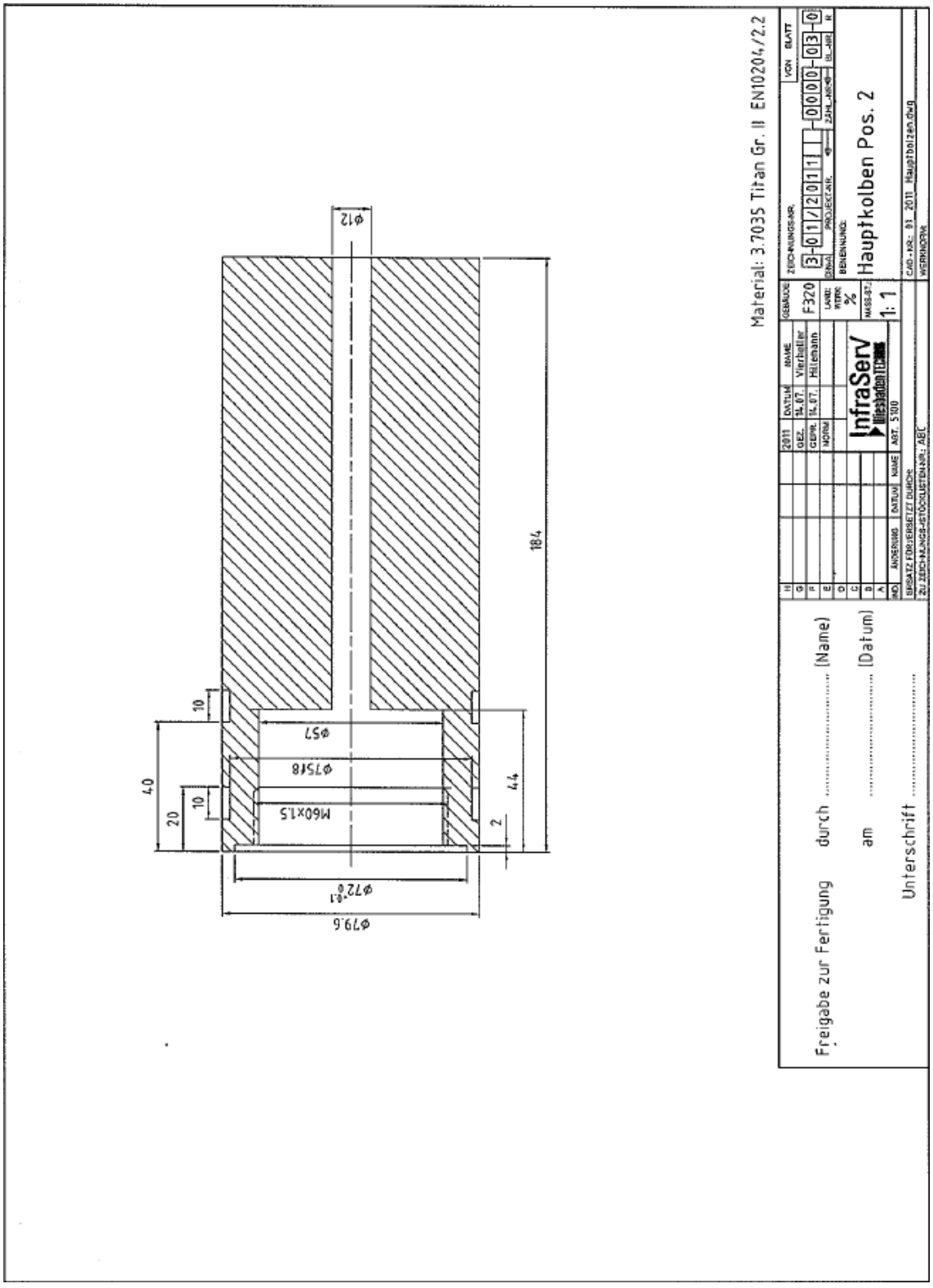

Fig. A.3 Pos. 2. of the diffusion cells. Positioning within diffusion cell given in the general assembly drawing in Fig. A.1 /INF 11/

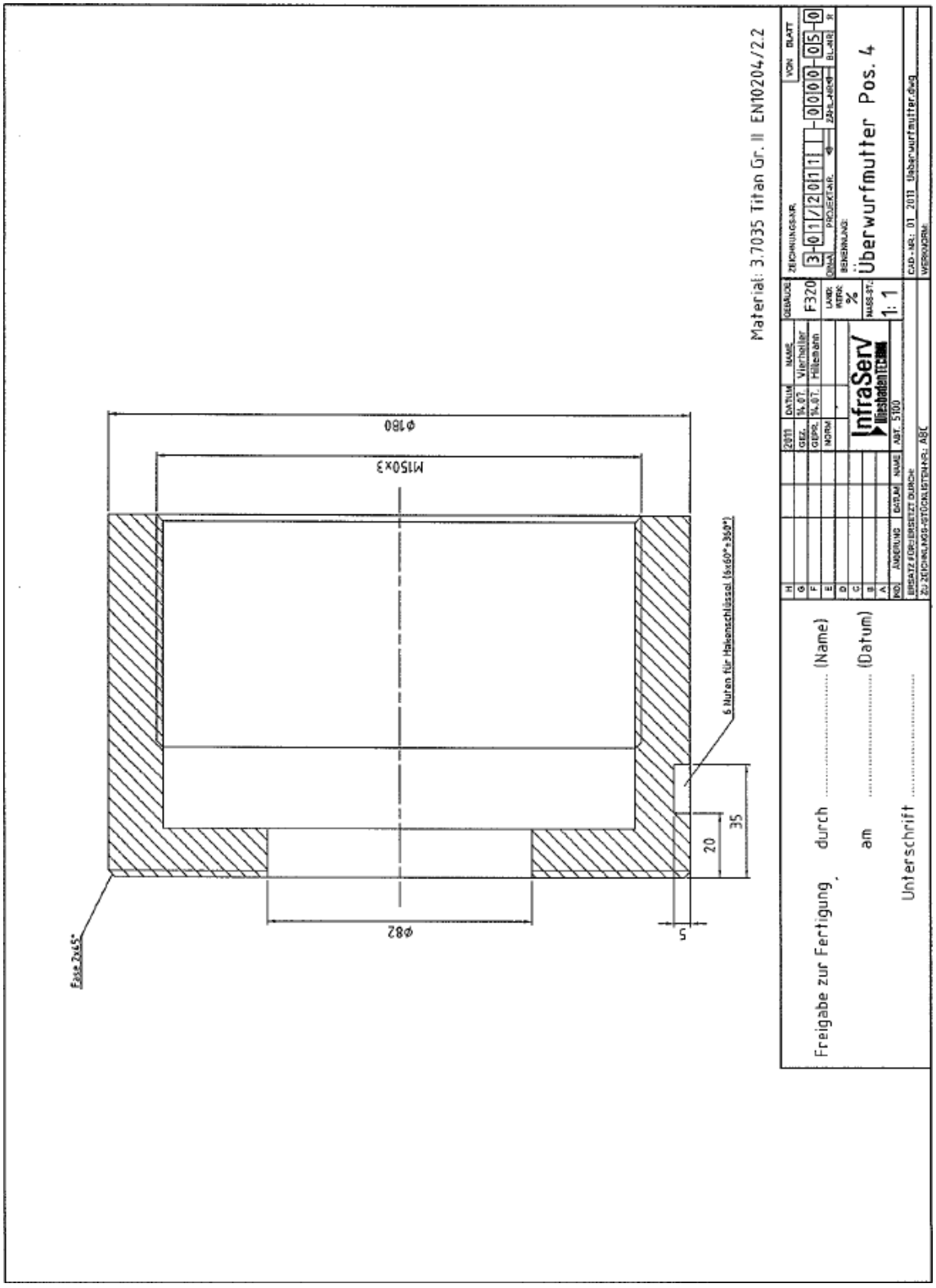

Fig. A.4 Pos. 4. of the diffusion cells. Positioning within diffusion cell given in the general assembly drawing in Fig. A.1 /INF 11/

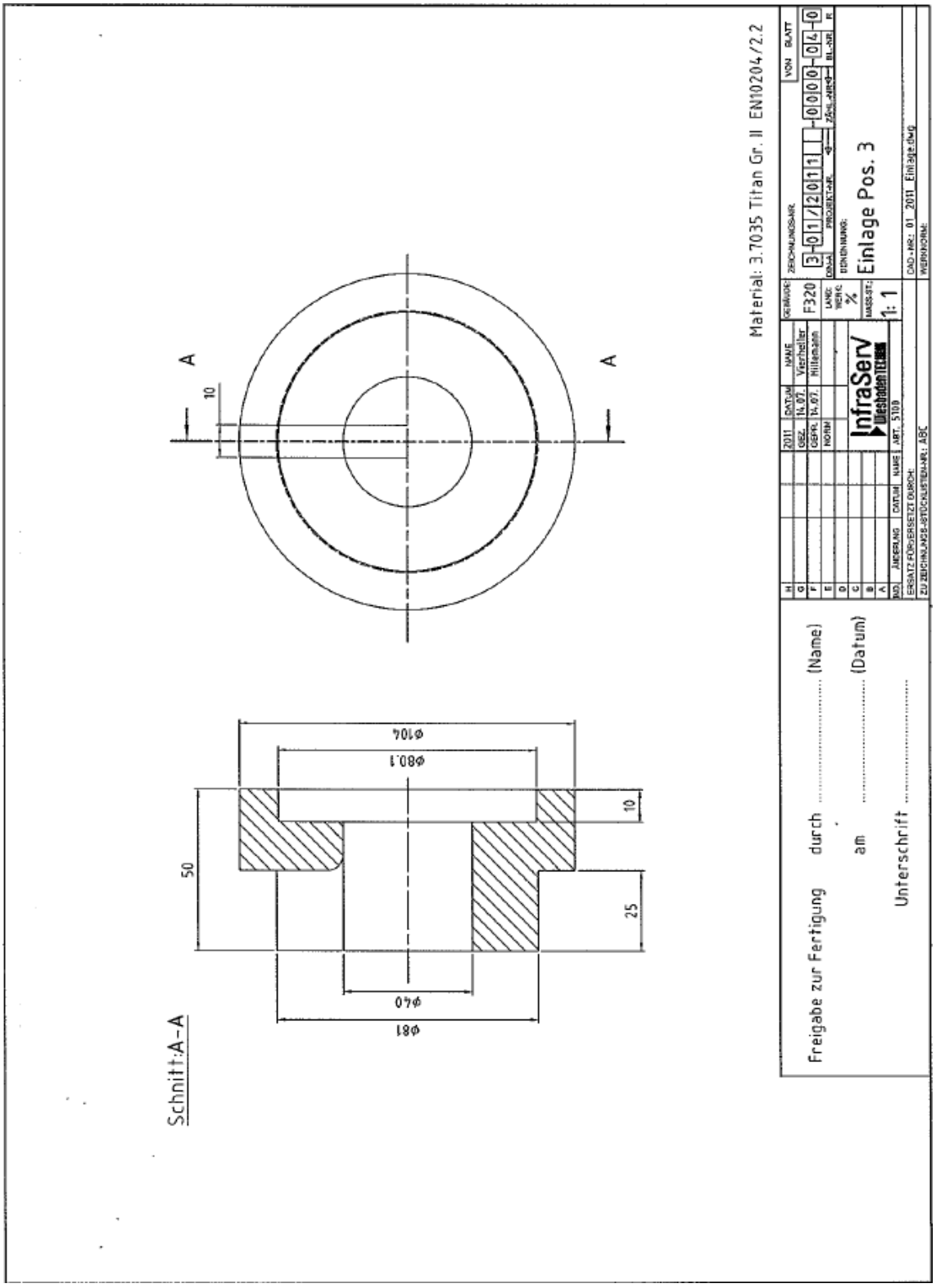

Fig. A.5 Pos. 3. of the diffusion cells. Positioning within diffusion cell given in the general assembly drawing in Fig. A.1 /INF 11/

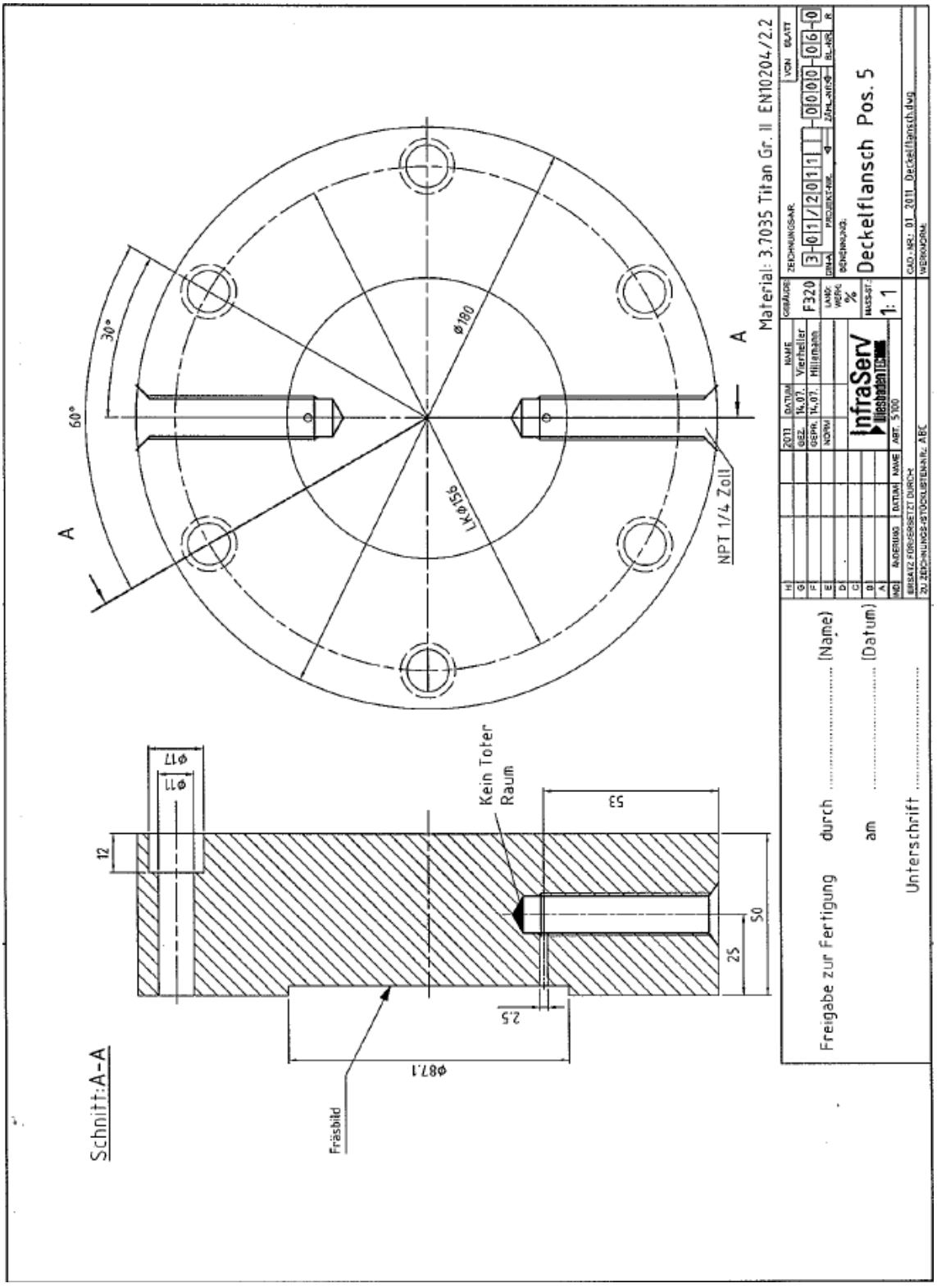

Fig. A.6 Pos. 5. of the diffusion cells. Positioning within diffusion cell given in the general assembly drawing in Fig. A.1 /INF 11/

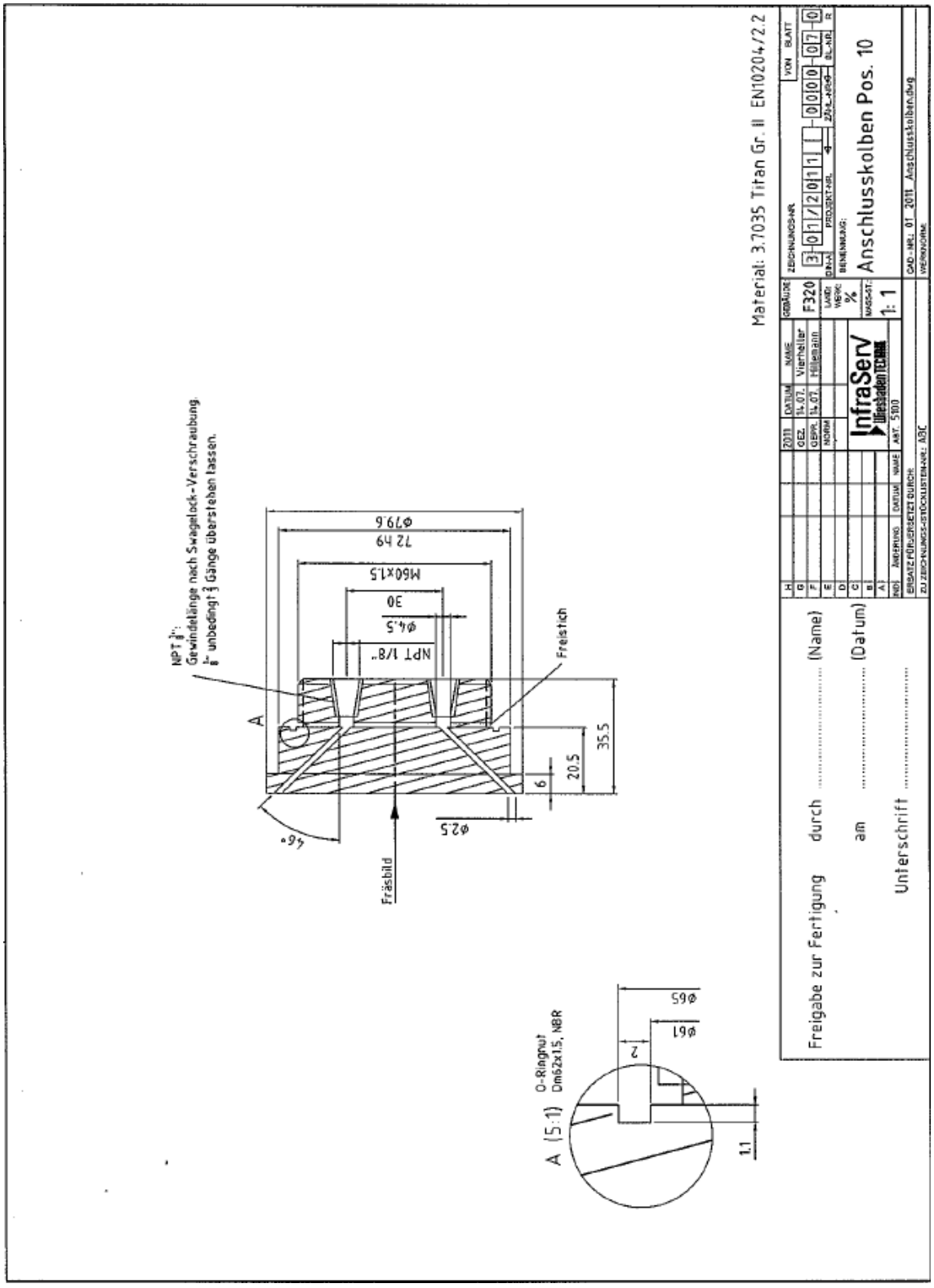

Fig. A.7 Pos. 10. of the diffusion cells. Positioning within diffusion cell given in the general assembly drawing in Fig. A.1 /INF 11/

Gesellschaft für Anlagen- und Reaktorsicherheit (GRS) gGmbH

Schwertnergasse 1
50667 Köln
Telefon +49 221 2068-0
Telefax +49 221 2068-888

Forschungszentrum
Boltzmannstraße 14
85748 Garching b. München
Telefon +49 89 32004-0
Telefax +49 89 32004-300

Kurfürstendamm 200
10719 Berlin
Telefon +49 30 88589-0
Telefax +49 30 88589-111

Theodor-Heuss-Straße 4
38122 Braunschweig
Telefon +49 531 8012-0
Telefax +49 531 8012-200

www.grs.de

ISBN 978-3-946607-03-8